A Chemical Mechanistic Approach to Understanding Cellular Selective Glycation

a dissertation submitted by

Vo Tri Tin Pham

in partial fulfillment for the degree of

Doctor of Philosophy in

Chemistry

Tufts University

May 2026

Advisor: Rebecca A. Scheck

Abstract

Glycation is a post-translational modification (PTM) that describes the spontaneous reaction of amino or guanidino groups on proteins with aldehydes or ketones on sugars and sugar-derived metabolites. This reaction produces a diverse set of modifications called advanced glycation end-products (AGEs) that are hallmarks of aging and disease. Approximately 40 AGEs have been identified to date, and many of these AGEs are reported as biologically relevant and implicated in many diseases. Unfortunately, there is not much known about the specific roles and the causal relationship that these AGEs have with these diseases due to a lack of understanding regarding their chemical mechanisms of formation and what features drive selective glycation. Past work in our lab has shown that primary sequence is the main driver for the propensity of a specific site to be glycated while secondary structure can influence the identity of AGEs that form. These studies also show that the surrounding chemical environment such as the presence of nearby polar, ionizable residues can enhance glycation while acidic residues can decrease glycation. In order to understand the causal relationship between AGEs and diseases, new chemical tools are needed for studying how and where certain AGEs can form on proteins in living cells in connection to diseases, thereby enabling studies of glycation as a functional PTM.

Argpyrimidine (APY) is a methylglyoxal-derived AGE that has been associated with multiple diseases. As APY forms without an enzyme, it remains exceptionally difficult to pinpoint where APY is likely to be found, both on individual proteins and in cells. In this thesis, we used a peptide model system and mass spectrometry analysis to investigate the chemical mechanism through which APY arises from methylglyoxal (MGO), a biologically relevant glycating agent. Consistent with other proposed APY formation mechanisms, our results identify AGE species with a mass change of [M+144], presumably including tetrahydropyrimidine

(THP), as a direct precursor to APY. However, our results rule out previously proposed reductone or oxidative decarboxylation mechanisms. Instead, we show that a formal oxidation step is not required, and that formate is released instead of CO_2. We further show the potential for a nearby residue such as Tyr to assist in the APY formation mechanism by acting as a general base. These experiments also reveal that phosphorylated Tyr or Ser residues can also promote equivalent levels of APY formation, despite introducing additional negative charges that we previously showed to impede glycation. Guided by these mechanistic insights and a newly defined role for phosphorylated residues on glycation substrates, we performed quantitative bottom-up proteomics analysis for MGO-treated cells. Gene ontology and functional annotation clustering analyses for APY-modified proteins suggested a correlation with phosphorylation-related terms (e.g. kinase activity or protein phosphorylation), which was validated using synthetic phosphopeptide substrates. Collectively, these data define a chemical mechanistic path to APY and suggest significant crosstalk between cellular phosphorylation and glycation events including APY formation. Finally, these results reveal to us that certain residues, including phosphorylated residues, can potentially bias the formation of select AGEs. This thesis work will provide valuable insights into the development of chemical and fluorescent tools that can be used to predict, sense, and study glycation events in living cells, improving our understanding of glycation biology.

Acknowledgement

First and foremost, I would like to thank my PI, Prof. Rebecca Scheck for her support and mentorship. This journey has not been easy, but Rebecca believed in me. She showed me the importance of perseverance and consistency and encouraged me to keep going. Rebecca has taught me many skills like how to make beautiful figures and communicate my research, but most importantly, I learned how to become a better scientist under her tutelage. Rebecca shows us (the Scheck lab) that our identity matters and always tries to foster an understanding and inclusive lab culture. As someone who constantly feel the pressure of standing out or fitting in, I have the great pleasure of just being myself in the lab doing science, and that means everything.

I would like to thank Prof. Luke Davis and Prof. Krishna Kumar for their guidance and helpful feedback throughout the many stages of my research. I am grateful to Prof. James Galligan at the University of Arizona for joining my thesis committee and for answering our proteomics questions. I would also like to thank our collaborators, Prof. Yu Zhang and Prof. Sam Thomas, for allowing me to use their instruments and lab space, and to Colin Lawler and Dr. Elisa Guzman for showing me how to perform unfamiliar experiments. I am also grateful to Prof. Joshua Kritzer for his support and advice since even before I joined Tufts and throughout my time here. In addition to the faculty, I am thankful for all the staff in the department. They are amazing, and their efforts in keeping the department running are well appreciated. Finally, I would like to thank Dr. Kristina Aikens and all of my GWC colleagues at the StAAR Center.

I couldn't ask for better Scheckmates. Nick and Brittany are my first friends here when we started in the lab together during Covid, and I always love talking to them just about anything. Special thanks to Dr. Suprama Datta, Amy Sterling, and Stefan Hansel for being great collaborators on my project. Jeremiah, Hannah, Ariana, Richard, and Niki make an amazing

cohort of graduate students in the lab, always buzzing with science or pop culture discussions. To our undergraduates, it is a pleasure to work alongside you, and I'm excited to see where you go next. Of course, I can't forget to thank Qing, Stefan, and Ben for being supportive of me and my project throughout, and Meghan, Joey, Caitlin, and Molly for getting me started in the lab.

I am grateful to all of my friends. To Minh and Nhi, you are my home away from home. To Siyuan and Phet, I hope we can go on many more trips to NYC Pride. Thank you to Tiffani for always lending an ear—a genuine empathetic listener and an ally. My friends and I have developed so many hobbies together: sewing classes, going karaoke, eating at new restaurants, and playing Pokemon Go. Special thanks to Nick, Edenilson, Siyuan, Tiffani, Manoj, Phet, Jonathan, Charles, and Rubiel for our little get-togethers throughout all these years and for putting up with my Halloween antics every October.

I cannot express enough gratitude to my father Tiến, my brother Trí, and my mother Tuyền, who unfortunately passed away in my second year of college, but who showed me tremendous grace and love that I will never forget. Con cảm ơn mẹ. Dù mẹ không thể dự lễ tốt nghiệp của con, con biết rằng mẹ luôn tự hào về hai anh em và luôn phù hộ cho tụi con. Con cảm ơn ba. Anh hai cảm ơn Trí. Con cảm ơn ngoại, dì Hai, dì Ba, cô Hai, chú Thủy, thím Ngọc, chị Xuân, anh Triết, Mi, Đa, Xumi, và cả nhà ở Việt Nam, dù xa mặt nhưng không bao giờ cách lòng và đã luôn đồng hành và ủng hộ con trên từng bước đi.

Most importantly, I would like to thank my husband, Charles, for your love and support. Charles puts up with all of my antics, drives me everywhere, and wait for me when I have to check on my experiments on the weekends. I love you. I couldn't have done this without you, and I am excited for our life together. Finally, I am grateful to Michelle and Russ, for welcoming me into the Healy family and for being such supportive and accepting parents.

Table of Contents

List of Figures

List of Tables

Copyright Notice and List of Copyrighted Materials

Work appearing in Chapter 1 is an adaptation of the publication in *Nature Chemical Biology*:

Martin, M. S.; Jacob-Dolan, J. W.; **Pham, V. T. T.**; Sjoblom, N. M.; Scheck, R. A. The Chemical Language of Protein Glycation. *Nat Chem Biol* **2025**, *21* (3), 324–336. https://doi.org/10.1038/s41589-024-01644-y.

Work appearing throughout Chapter 2-4 is an adaptation of the publication in *Journal of the American Chemical Society*:

Pham, V. T. T.; Datta, S.; Sterling, A. C.; Hansel, S. M.; Scheck, R. A. A Chemical Mechanistic Path Leads the Way to Cellular Argpyrimidine. *J. Am. Chem. Soc.* **2025**, *147* (42), 38055–38068. https://doi.org/10.1021/jacs.5c09369.

1. Chapter 1:

Introduction

1.1. The Chemistry of Glycation

1.1.1. Glycation is a Selective Post-Translational Modification

Post translational modifications (PTM) are biochemical modifications that occur on one or more amino acids on a protein after the protein has been translated by a ribosome. To date, approximately 70 PTMs have been reported, and out of this number, non-enzymatic PTMs account for 30% of the PTM landscape.[1,2] Enzymatic PTMs such as phosphorylation and methylation, etc. are highly regulated and selective, essential for cellular and protein function. On the other hand, there exist many PTMs that occur spontaneously and without an enzyme (i.e. non-enzymatic PTM), which are equally important to study because many are known to regulate certain biological pathways.[3–5]

Non-enzymatic PTMs can be broadly divided into oxidative stress and carbon stress. Classified under carbon stress, glycation (or non-enzymatic glycosylation) occurs via the Maillard reaction, in which sugars and protein amines react to form a Schiff base, which undergoes further conversion via an enaminol intermediate and rearranges into stable α-ketoamines. Specifically, Amadori[6] and Heyns[7] are two of the most well-defined rearrangement pathways, with Amadori products derived from aldose sugars, while Heyns from ketose sugars (**Figure 1.1**).[8] Notably, while most carbon stress reactions occur through acyl transfer from activated acyl-CoA donors or Michael-type addition to α,β-unsaturated species, glycation occurs via reaction between aldehydes or ketones of reducing sugars and amino or guanidino groups of Lys or Arg on proteins.[9,10] Unlike other carbon stress reactions that typically produce a single modification, glycation is unique in its ability to produce a diverse set of modifications called advance glycation end-products (AGEs). To date, approximately 40 modifications have been reported, with methylglyoxal-derived dihydroxyimidazolidine hemiacetal crosslink (MIDAL)

marking the latest reported AGE from Arg modification.[1,11] Although progress has been made in recent decades to identify and characterize these discrete AGEs, it is still difficult to grasp the full extent of the glycation chemistry and, consequently, its biology.

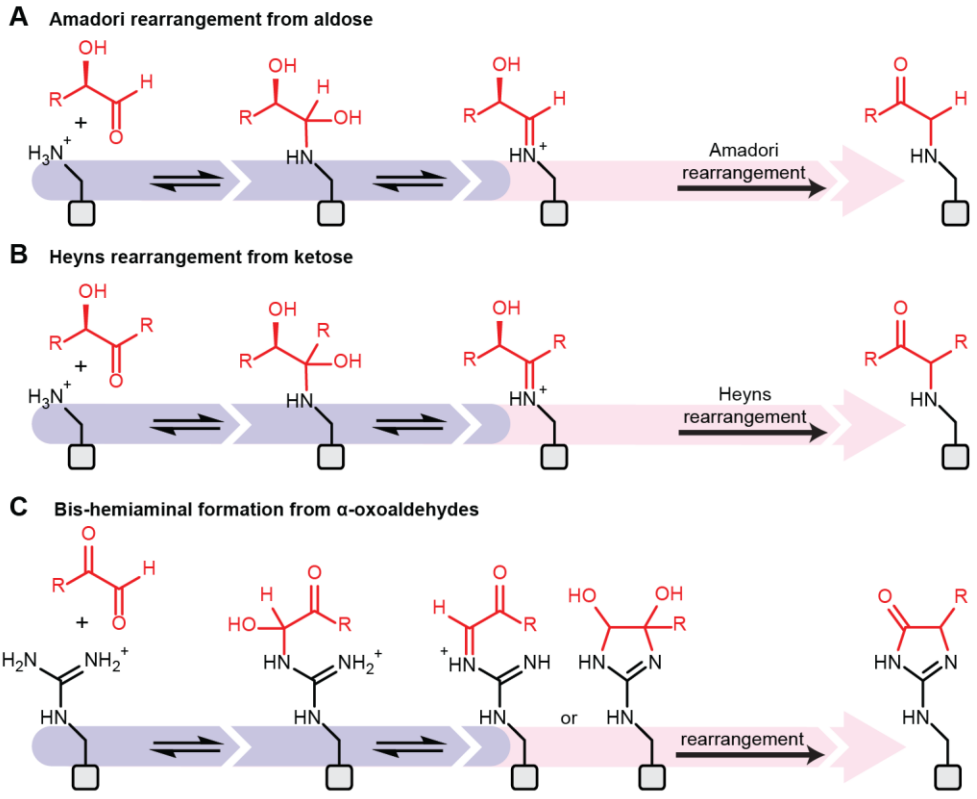

Figure 1.1. Mechanisms of Non-Enzymatic Glycation. Purple arrow represents rapid and reversible Schiff base formation. Pink arrow represents further reactions or rearrangement to yield stable AGEs. **(A)** Amadori rearrangement adducts derived from the reaction between amino groups on Lys and aldehyde of aldose sugars. **(B)** Heyns rearrangement adducts derived from the reaction between amino groups on Lys and aldehyde of ketose sugars. **(C)** AGEs derived from bis-hemiaminal formation between guanidino groups on Arg and α-oxoaldehydes.

Although the chemistry of glycation was first depicted as a "non-enzymatic browning" observed in food chemistry in 1912 when amino acids were heated with glucose[12,13], glycation is now expanded beyond the scope of its original definition to describe the spontaneous attachment of sugars and sugar derived metabolites to nucleophilic groups on proteins. Indeed, sugars and their derivatives, containing aldehydes and ketones, have been found to react to various extent

not only with amino and guanidino groups on lysine (Lys) and arginine (Arg)[1,14–19], but also with thiol group on cysteine (Cys)[20], and in some cases, N-terminal proline (Pro).[19] However, it is still most commonly observed via Lys and Arg modifications, with an estimated 1% of Lys and Arg residues reported to be glycated in physiological systems.[21]

1.1.2. Methylglyoxal is a Potent Glycating Agent

In general, electrophilic aldehydes and ketones on reducing sugars are susceptible to nucleophilic attack from protein amines. While glycation has been reported on reactions with hexose and pentose sugars such as glucose and ribose, they are relatively inert due to their low-energy hemiacetal configurations.[22] However, sugars in physiological systems can be fragmented and processed via multiple pathways, including glycolysis, fructolysis, the pentose phosphate pathway, and alcohol metabolism, to produce smaller metabolites. Unlike their parent monosaccharides, these metabolites, such as glyceraldehyde and acetaldehyde, do not cyclize yet still contain reactive aldehydes, allowing them to participate in glycation more readily. Notably, reactive dicarbonyls and physiological α-oxoaldehydes such as methylglyoxal (MGO), glyoxal, and 3-deoxyglucosone (3-DG) generated from glycolysis, lipid peroxidation, glucose auto-oxidation, and the polyol pathway, are among the most potent glycating agents. Indeed, MGO, a naturally occurring 1,2-dicarbonyl compound with enhanced electrophilicity, is one of the most prevalent and reactive glycating agents *in vivo*, making it a prime target for glycation studies.[23]

Although MGO can also be found via triosephosphate degradation, lipid peroxidation, acetone metabolism, and threonine catabolism, cellular MGO is mainly accumulated via glycolysis in glucose metabolism.[5,23] In short, during the fifth step of the 10-step glycolysis, dihydroxyacetone phosphate (DHAP) is converted to glyceraldehyde phosphate (GAP) in the presence of the catalyzing enzyme triose phosphate isomerase (TPI).[24,25] During this conversion,

the enzyme-stabilized enediol intermediate proceeds via protonation of the enediol in the enzyme active site to release GAP. In this manner, TPI suppresses an unwanted side reaction that can occur when this enediol intermediate spontaneously undergo phosphate elimination to yield MGO. Typical MGO concentrations in healthy mammalian cells have been reported to range from 1-5 μM and can sometimes rise above 300 μM.[26–28]

MGO is known to react preferentially and irreversibly with Arg residues to produce numerous advanced glycation end-products, including single addition, double addition, and crosslinking products.[1,19,20,29,30] Examples of MGO-derived single addition AGEs include the hydroimidazolone isomers (MGH-1,-2,-3), dihydroxyimidazolidine (MGH-DH), and carboxyethylarginine (CEA), whereas double addition AGEs include tetrahydropyrimidine (THP) and argpyrimidine (APY) (**Figure 1.2**). MGO-derived crosslinks have been reported to form between Arg and Lys such as methylglyoxal-derived imidazolium crosslink (MODIC)[30] and between Arg and Cys such as mercaptomethylimidazole crosslink (MICA).[20] Recent work in our lab has also revealed a newly characterized MGO-derived Arg-Arg crosslink called MIDAL.[29] Despite continuous efforts to identify new AGE structures, the chemical mechanistic formation of many MGO-derived AGEs remains elusive. As mentioned previously, glycation typically begins with nucleophilic attack on the aldehyde to form an imine or hemiaminal, which can undergo Amadori or Heyns rearrangement to form stable AGEs. However, α-oxoaldehydes like MGO lack an α-proton neighboring their aldehyde and cannot undergo Amadori rearrangement as a result. Instead, their initial steps likely involve the formation of a bis-hemiaminal (e.g. MGH-DH formation by MGO and Arg) (**Figure 1.1**). Generally, a lower pK_a and therefore greater nucleophilicity should be expected for a higher reactivity towards glycation. By this logic, one would expect Lys to be more susceptible to glycation compared to Arg. However,

glycation is influenced by many factors including the glycating agent used, its concentration, and the surrounding microenvironment. Therefore, despite having a higher pK_a, Arg has been found to be modified more than Lys by reactive 1,2-dicarbonyl glycating agents such as glyoxal and MGO.[19,31,32] Although MGO preferentially modifies Arg, the chemical rules that govern how and what AGE species are formed remain an enigma. Specifically, the sequence and structural features that drive AGE formation on proteins are still largely unexplored.

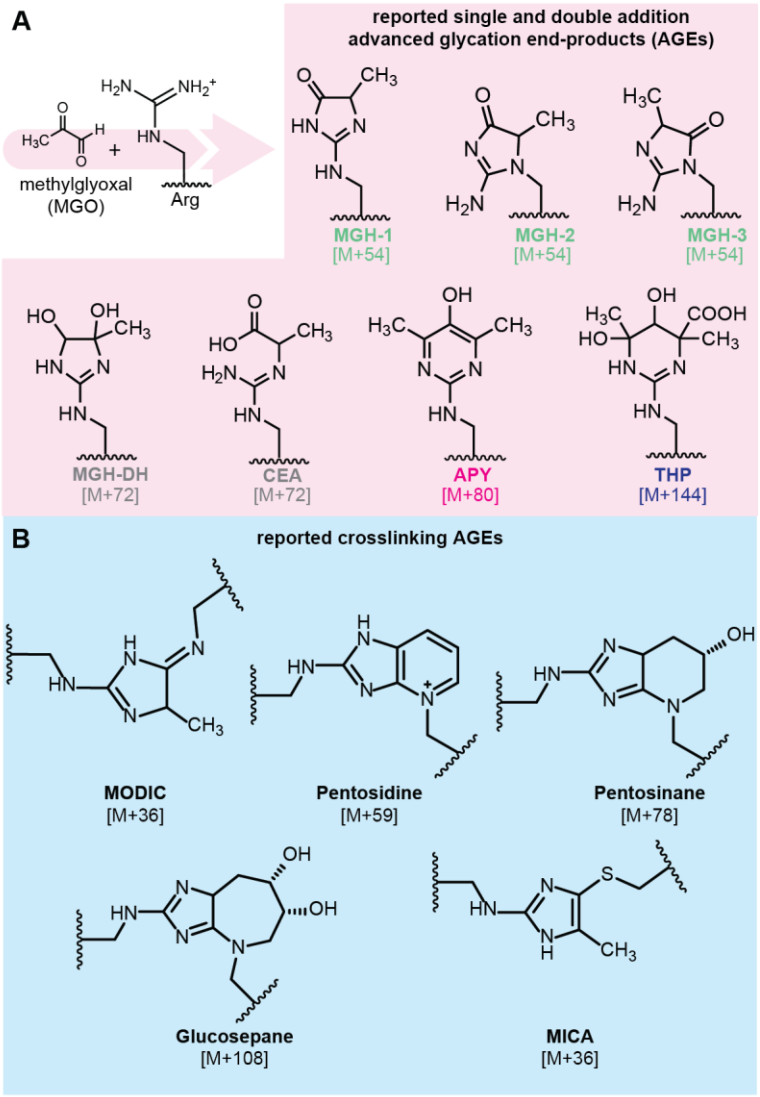

Figure 1.2. Examples of Reported AGEs. (A) MGO-derived single addition AGEs include the hydroimidazolone isomers (MGH-1,-2,-3), dihydroxyimidazolidine (MGH-DH), and carboxyethylarginine (CEA). Double addition AGEs include tetrahydropyrimidine (THP) and argpyrimidine (APY). **(B)** Crosslinking AGEs include methylglyoxal-derived imidazolium crosslink (MODIC), pentosidine, pentosinane, and glucosepane formed between Arg and Lys, and mercaptomethylimidazole crosslink (MICA) formed between Arg and Cys.

1.1.3. The Chemical Mechanistic Formation of AGEs are Poorly Understood

Although many AGEs have been structurally defined and characterized, their formation mechanisms remain poorly understood.[1] Many studies that identify AGE-modified proteins or metabolites in cellular samples have used a variety of glycating agents, including glucose or MGO, to induce glycation. However, glucose and other hexoses are readily processed and converted into other, potentially more reactive metabolites, like MGO.[33] This makes it difficult to correctly and explicitly define the specific glycating agents that lead to the formation of distinct AGEs in cellular studies. In some cases, this information can be straightforward by considering mass changes via LC-MS analysis.[1,19,31] For example, CEA [M+72] and THP [M+144] has mass changes that correspond to a single addition and double addition of MGO (mass of 72.06 Da), respectively, while MGH-1 [M+54] indicates a loss of water from a single addition of MGO. However, for other AGEs like APY [M+80], the mass change is not easily attributed to a gain or loss of water from MGO, leading to several proposed mechanisms that have not been validated.

As a result, most of the mechanistic studies to-date have been performed *in vitro*. Many of these studies have focused on the incubation of proteins or amino acid monomers with glycating agents for prolonged periods of time. This approach allows for straightforward purification and characterization of AGEs, but it often requires extremely high concentrations and/or incubation conditions that may not be biologically relevant. Recent efforts have focused on addressing this issue. For example, Spiegel and co-workers have circumvented this challenge by performing chemical synthesis of discrete AGE-modified amino acid derivatives.[34] Additionally, deRamon *et al.* used chemically synthesized pentosinane and pentosidine amino acid derivatives to demonstrate that pentosinane is substantially more stable at physiological pH than previously believed.[35] They further demonstrated that pentosinane's decomposition into

pentosidine is pH-dependent, suggesting that the detection of pentosidine may have been artifact from total acid hydrolysis, which was performed as part of a metabolomics workflow. This finding implies that future studies focused on pentosidine formation in cells are likely to be less relevant to genuine biology than those that focus on pentosinane. Taken together, it is clear that glycation papers with a focus on mechanism might reveal inconsistencies with earlier findings whose goals are to isolate and identify AGEs.

Despite considerable progress, mechanistic studies on amino acid monomers and derivatives cannot account for the contribution of the microenvironment surrounding glycation sites on proteins. Past works in our lab have found that certain amino acids, particularly Tyr, positioned near the glycation site can promote glycation, and specifically, the formation of MGH-1.[19,31] For instance, McEwen *et al.* used short, unstructured peptides to evaluate the sequence features that promote MGH-1 formation.[19] This work was the first to elucidate the mechanistic pathways connecting three distinct AGEs (MGH-DH, MGH-1, and CEA): MGH-DH rearranges to form MGH-1, and subsequent hydrolysis of MGH-1 yields CEA. Although CEA was a known hydrolysis product of MGH-3, it was previously suggested that MGH-1 was recalcitrant to hydrolysis. However, these prior studies were performed at high concentrations and/or using amino acids that overlooked this phenomenon. Nonetheless, this work suggests that the relative ratios of MGH-1 and CEA could be important to consider in the context of cellular studies that monitor AGEs as a function of time.

In general, there remain many open questions about AGE formation mechanisms. Particularly, argpyrimidine (APY) is one such AGE that has been the subject of several mechanistic studies without a clear resolution (**Figure 1.3**). Two separate studies hypothesized that APY is a degradation product of THP, as observed by the correlation between a decrease in

THP and an increase in APY over incubation time.[36,37] Another study proposed that MGH-3 was a precursor for APY, as observed by the disappearance of purified MGH-3 that corresponded with an appearance of APY.[37] Finally, a third study, which has become the most widely cited model for APY formation involves the formation of an intermediate reductone, 3-hydroxypentane-2,4-dione, derived from two molecules of MGO.[18] However, the proposed reductone formation mechanism involves several high activation barrier steps, including loss of a formyl anion. Because this reductone is prone to oxidation and fragmentation, this mechanistic study was performed by synthesizing a stable precursor to the reductone, 2,4-ethoxy-3-hydroxypentane-1,4-diene, and subjecting it to a highly acidic condition before starting the reaction with Arg monomer. As the free reductone was not isolated or experimentally confirmed in this study, it remains unclear if it is a plausible explanation for how APY form *in vivo*. Importantly, all three proposed mechanisms have suffered from a lack of validation of key mechanistic steps. Therefore, there may be other possibilities that drive APY formation under dynamic physiological conditions.

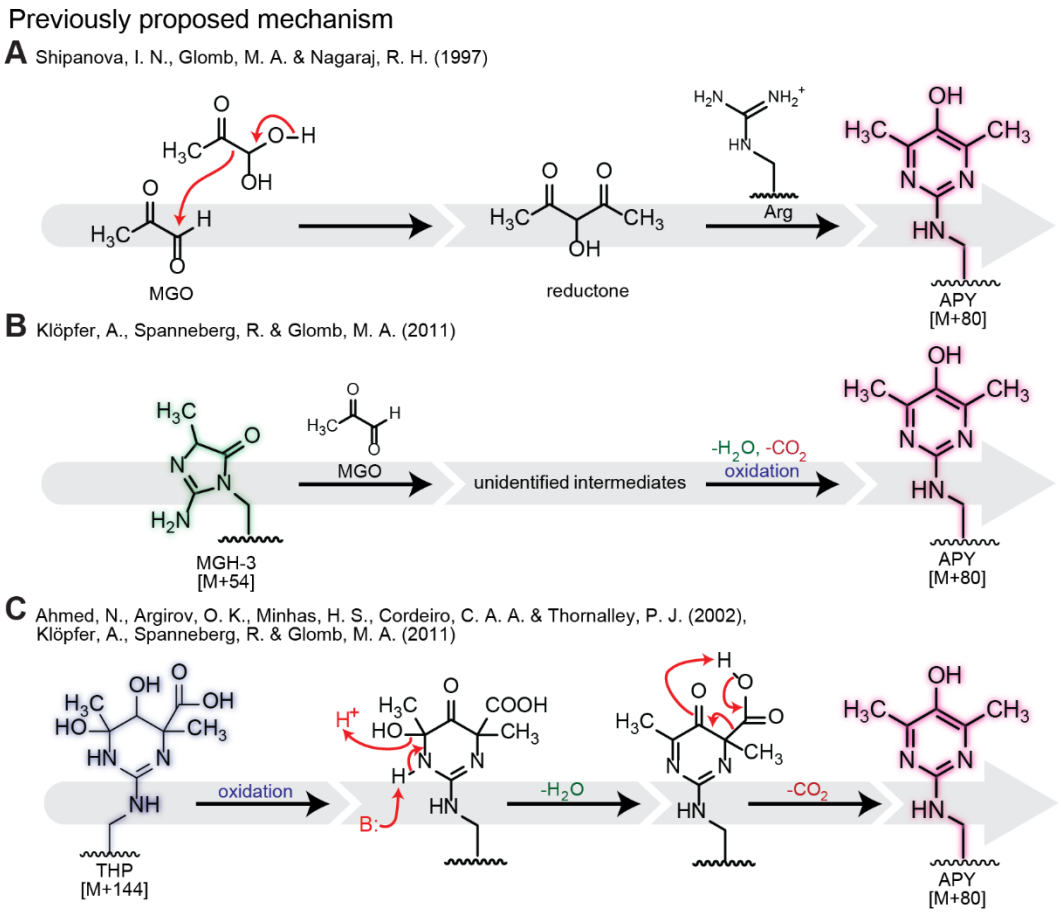

Figure 1.3. Previously Proposed APY Formation Mechanisms. Previously proposed mechanisms for APY formation from (**A**) reductone formation, (**B**) MGH-3 via oxidative decarboxylation, and (**C**) THP via oxidative decarboxylation.

Overall, how AGEs interconvert and under what conditions they are measured could easily impact the distribution of AGEs and the determination of the most prevalent AGE, as demonstrated by deRamon *et al.* and McEwen *et al.*[19,35] This could explain why multiple discrete AGEs, including MGH-1[16,38,39] and glucosepane,[40] etc. have been reported to be "the most abundant AGE" in different physiological systems. Thus, without proper chemical mechanistic knowledge, it remains difficult to comprehensively survey the landscape of AGE formation, glycation biology, and the causal relationship between AGEs and diseases.

1.2. The Biology of Glycation

1.2.1. AGE Formation and Disease Implications

Although glycation as a non-enzymatic reaction was first described in 1912 by the French chemist Louis-Camille Maillard, it was primarily studied through the lens of food chemistry as the "Maillard reaction".[12,13] It was not until 1955 that the first endogenous glycated protein, glycated hemoglobin HbA1c, was discovered as a protein modified by exposure to blood sugar in the human body.[41] This discovery has led to the current use of HbA1c as a biomarker for diagnosis of diabetes as HbA1c levels were found to be increased in individuals with diabetes. Since then, subsequent studies have provided increasingly more proof that implicate glycation and AGEs in aging and multiple diseases, including diabetes and cancer.[42–46]

The story of glycation and AGEs did not end there, however, as researchers shifted to identify and correlate increased levels of several AGEs with different diseases. Since it has been established that glycation occurs in the cell, MGO-derived AGEs have been of particular interest given the biological relevance of MGO as a toxic electrophilic metabolic byproduct.[5] Indeed, GLO I knockout (inhibition of MGO-detoxifying glyoxalase enzyme) has been reported to increase levels of MGO and MGO-derived adducts.[5,39] Several MGO-derived AGEs, such as MGH-1 and APY are hallmarks of aging and diseases, including diabetes, Alzheimer's disease, cardiovascular diseases, and cataractous lens formation.[15,42,44–49] However, with a few exceptions, many studies investigating the effects of glycation on biology rarely provided further validation beyond identification, leaving generalized guesses as to what features might promote selective glycation and what roles AGEs play in altering protein functions and cellular processes in connection to diseases.

Recent efforts in the field have pushed past individual instances of selective glycation and instead looked to investigate the role of AGEs in disease biology. Some AGEs, like the MGH isomers and CEA, have been shown to regulate chromatin architectures, influence histone-DNA interactions, and activate mitochondrial apoptosis.[39] Several reports have shown that accumulation of APY, a late-stage MGO-derived AGE, in different cell lines, such as human bronchial BEAS-2B cells, lens epithelial cells, human prostate cancer cells LNCaP, and periodontal ligament cells, can trigger mitochondrial apoptosis and regulate cell autophagy.[50–53] On heat shock proteins, APY has been shown to impair chaperone activity of Hsp27 and involve in silica-induced apoptosis in human bronchial cells via a mechanism involving Hsp70, JNK, and NF-κB pathways.[51,53,54] However, without fully knowing how AGEs form mechanistically, what features or conditions promote their formation, it remains difficult to understand why and when specific proteins are glycated and what effects they have on certain disease pathways.

1.2.2. "Readers, Writers, and Erasers" of Non-enzymatic Glycation

In general, PTMs are part of a tightly regulated signaling networks of enzymes that are maintained by protein "writers" that install, "readers" that recognize, or "erasers" that remove the modification (**Figure 1.4**). For instance, phosphorylation is installed by kinases and removed by phosphatases. However, this paradigm does not comprehensively describe every PTM. Indeed, glycation is a non-enzymatic PTM whose "writer" does not exist, meaning there is no enzyme that install the modification. Instead, it is a spontaneous, yet selective, covalent reaction between nucleophilic amino acid side chains with sugars and sugar-derived metabolites that affords the modification. Therefore, glycation, without a "writer" enzyme, has historically been thought of as random cellular damage that occurs over time and/or through disrupted metabolism.[5,21,55] As a result, reports on how and to what extent selective glycation is formed

have afforded multiple hypotheses, including solvent accessible surface area,[32,56] Arg or Lys pKa,[32,57,58] and charged neighboring residues.[57–62] However, not all have been experimentally confirmed. For MGO-derived glycation, our lab has begun to develop methods to validate generalizable features that influence AGE formation. Using a combinatorial peptide library and purified proteins, we observed that glycation is unlikely to be influenced by Arg or Lys pKa pertubations or solvent surface exposure but the presence of nearby polar or ionizable groups greatly influences glycation selectivity. Sjoblom *et al.* and McEwen *et al.* showed that the propensity for glycation is mainly influenced by the primary sequence while secondary structure and spatial alignment can define the set of heterogenous AGEs that form.[19,31] Still, in a complex cellular milieu where competing electrophilic metabolites can act glycating agents and in the absence of a "writer" enzyme, it remains a challenge to predict and modulate glycation events without knowing exactly what features influence selective glycation.

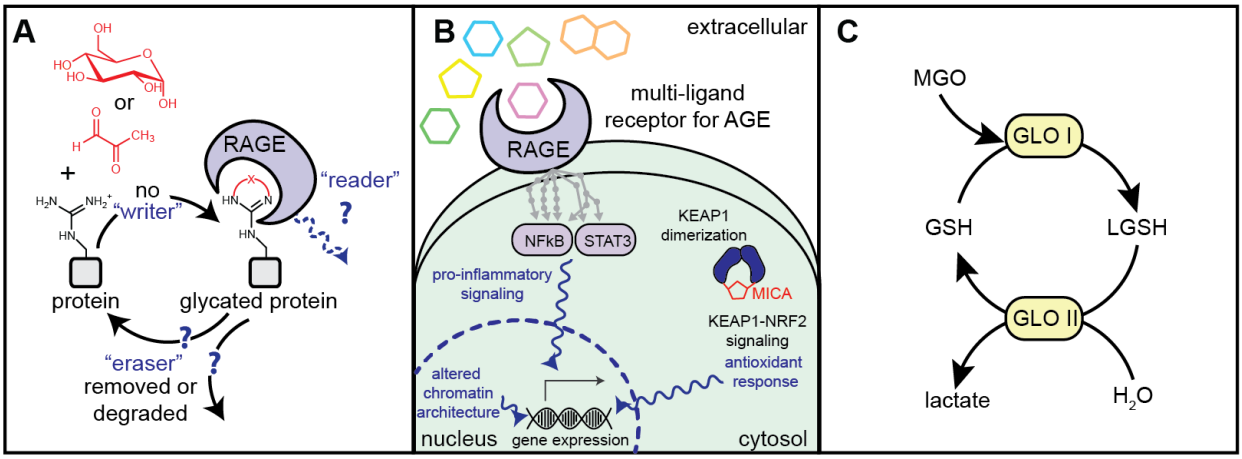

Figure 1.4. An Overview of the "Writer", "Reader", "Eraser" Paradigm in Glycation and the Biological Relevance of Glycation. (**A**) Glycation is a non-enzymatic PTM whose "writer" does not exist. Most of the signaling pathways attributed to AGEs have been studied through the glycation "reader", a cell surface receptor for AGE (RAGE). The existence of a deglycase (enzyme that removes AGEs) in human remains controversial. (**B**) Activation of RAGE results in the activation of pro-inflammatory signaling cascades, which in turn increase RAGE transcription, resulting in oxidative stress and a positive feedback loop of inflammatory response. Additionally, increased MGO levels disrupt global histone enzymatic PTM levels by altering chromatin architecture, while the formation of MICA on KEAP1 causes dimerization and releases the NRF2 transcription factor, activating an antioxidant response. (**C**) The glyoxalase enzymes detoxify MGO by converting it into D-lactate.

Since there is a gap in our understanding of how selective glycation is installed, most of the signaling pathways attributed to AGEs have been studied through the glycation "reader", a cell surface receptor for AGE (RAGE). Although this multi-ligand RAGE recognizes extracellular AGE-modified proteins, it is nonspecific as it has been reported that RAGE also recognizes extracellular polyanionic species unrelated to glycation.[63] RAGE is expressed in different cell types, including vascular endothelial cells, glomerular and aveolar epithelial cells, monocytes, granulocytes, and immune cells.[63–65] Moreover, activation of RAGE results in the activation of pro-inflammatory signaling cascades, including NADPH oxidase, JAK-STAT, MAPK, and ERK1/2, and the release of cytokines and chemokines.[63,64,66] These signaling pathways in turn increase RAGE transcription, which results in oxidative stress and a positive feedback loop of inflammatory response involving cell proliferation, migration, and undesired survival. Recent reports have further expanded on the role of AGEs in intracellular signaling by

looking at how certain glycated proteins exhibit altered structures and functions due to AGE installation. For example, histone glycation by MGO on intact chromatin was found to be at levels comparable to those of other native Lys and Arg modifications, such as acetylation and methylation.[67] While under hyperglycemic conditions, a significant increase in CEA formation was observed. Additionally, accumulation of MGH-1 and CEA have been found to disrupt the formation of canonical PTMs found on H2B, leading to altered global RNA transcription, and exposure of H3 and H4 to increased MGO levels also results in disruption of global histone enzymatic PTM levels.[39] Furthermore, the formation of MGO-derived crosslink MICA on KEAP1 has been reported to release the NRF2 transcription factor, activating a cytoprotective antioxidant response in IMR32 cells.[20] Taken together, these examples make an important case for investigating signaling response as a result of discrete AGE formation instead of treating all AGEs as one whole damage product.

Despite the ubiquitous nature of protein glycation, MGO is recognized as a toxic compound in our body, which has developed an efficient pathway to detoxify MGO. Glyoxalase I and II (GLO I and II) are two enzymes involved in detoxifying reactive dicarbonyls such as MGO to prevent AGE formation by converting them into D-lactate. Specifically, the hemithioacetal adduct of MGO and a catalytic amount of reduced glutathione (GSH) is isomerized into *S*-D-lactoylglutathione (LGSH) in the presence of the catalytic GLO I enzyme. GLO II further catalyzes the hydrolysis of LGSH into D-lactate and returns GSH to the GLO I-catalyzed reaction.[1,5,23,68] In addition, aldo-keto reductases (AKRs) and aldehyde dehydrogenases (ALDHs) have also been reported to have a minor role in MGO metabolism.[5]

Besides these enzymes, it remains contentious whether a deglycase (enzyme that removes AGEs) exists in human. Although certain enzymes like fructosamine-3-kinase (FN3K) and

amadoriases selectively remove fructoselysine in fungi and bacteria, a human deglycase that broadly removes AGEs have not been reported.[69–71] Indeed, the Parkinson-associated protein DJ-1 was proven to be an antagonist, rather than a deglycase like previously thought,[67,72,73] by converting MGO to lactate and decreasing the concentration of MGO available for glycation, consistent with glyoxalase activity.[74–76] A recent study done in our lab has clarified that DJ-1 cannot remove already installed AGEs, even early adducts like MGH-DH, by showing that only co-incubating DJ-1 and MGO decrease AGE levels, but subsequent treatment of DJ-1 did not.[77] Similarly, the protein arginine deaminase 4 (PAD4) has been shown to prevent AGE formation on histone arginines by converting Arg into citrulline.[78] While providing unique evidence for crosstalk between glycation and other modifications such as citrullination, this study, along with past DJ-1 studies, did not report which AGE structure, if any, would be the target for deglycase activity. As the reaction between MGO and Arg produces a diverse pool of AGEs, considering each AGE as a separate target is of imminent importance in glycation research.

1.3. Strategies to Study Selective Non-Enzymatic Glycation

1.3.1. Analytical Methods to Study AGEs

As glycation occurs through a multi-step process and can install multiple AGEs on a single Arg site, the ability to distinguish between heterogenous adducts is critical to understanding how these AGEs form and what effects they have on downstream signaling networks. For this reason, the majority of early glycation research focused on the identification and characterization of a specific, singular AGE. Structural confirmation of these AGEs was subsequently performed by comparing to synthetic AGE standards or HPLC assays and/or NMR. However, experimental conditions used in these studies were inconsistent due to the identity and

varied concentrations of glycating agents, prolonged incubation time, differences in pH and temperatures, and/or enrichment protocols unsuitable for capturing AGEs.

Given the dynamic chemistry and interconverting nature of AGEs, it is critical to assess conditions used to prepare and analyze AGEs. Many early AGE studies in food chemistry relied on total acid hydrolysis to process their samples and break them down to detect AGEs on the amino acid level. However, total acid hydrolysis requires high concentration of acid and elevated temperature, leading to degradation of AGEs and/or further reactions. For instance, it has been reported that acid hydrolysis can degrade AGEs like pyrraline, APY, MGH-1, glyoxal-derived dihydroxyimidazolidine (GH-DH), glyoxal-derived hydroimidazolone-1 (GH-1), carboxymethylarginine (CMA), and even some crosslinking AGEs such as 2-(2-furoyl)-4(5)-(2-furanyl)-1H-imidazole (FFI), pentosinane, pentosidine, glyoxal lysine amidine (GALA), and glyoxal lysine amide (GOLA).[36,79–81] Specifically, FFI has been found to be an artifact of ammonia and furosine, which are by-products of acid-hydrolyzed glycated proteins.[82] Pentosinane has also been reported to readily convert into pentosidine under mildly basic, strongly acidic or O_2-saturated conditions.[35] As a result, sample preparation protocols for AGEs require careful consideration of their structures and chemistry, which might have been underappreciated in early food science and biochemistry reports. Moreover, studies with a focus on identifying and cataloguing AGEs often involve long incubation periods (sometimes weeks to months) or long-lived proteins such as collagen and lens crystallins.[43] Therefore, AGEs that have been reported thus far might be biased towards those that are more stable or prone to accumulation over time.

AGEs can also be analyzed using antibody-based methods, such as Western blotting and immunoassay. However, these antibodies are often non-specific, as their epitopes, binding

affinity, or cross-reactivity data compared to other structurally similar AGEs remain unknown.[83] As a result, many immunological studies tend to treat AGE detection broadly, i.e. as a sum, rather than a specific AGE species with resolved structure.

Similarly, early detection of AGEs carried out using HPLC equipped with a fluorescence detector used measurement of fluorescence as an indication of AGE presence. Given the abundance of molecules in biological samples, background fluorescence can complicate quantification without proper controls or internal standards. For instance, pentosidine has been detected in human urine and plasma samples using HPLC with a fluorescent detector set at excitation and emission wavelengths of 328 and 378 nm, respectively.[84] However, APY has also been reported to fluoresce within this range, with excitation and emission wavelengths at 320 and 385 nm, respectively.[18] Indeed, this range of fluorescence has been used routinely to detect and quantify fluorescent AGEs in biological samples. This approach, though less common in recent years, has left many unanswered questions about the links between disease biology and the identity of AGEs.

Thanks to the continued advances in mass spectrometry (MS) instrumentation and techniques, most recent AGE studies have employed the use of LC-MS and LC-MS/MS to decipher mass adducts and site information. Further, there is an increased interest in using Orbitrap MS with high mass resolution in addition to the more traditional quadrupole time-of-flight (QTOF) MS to perform discovery proteomics of cellular glycation. Each technique has its own pros and cons. For instance, proteomics or metabolomics studies using cells treated with glycating agents are well-suited for identifying AGE-modified proteins and broadly mapping AGEs to cellular functions or compartments. In addition to treatment with glycating agents, cell-based studies are also often performed by inhibition of glyoxalase enzymes or induction of

hyperglycemia through high glycemic index diets. However, along with the highly demanding and complex nature of cell-based experiments and instrumental operation, it is difficult to identify treatment conditions that work. For instance, increased MGO concentrations and prolonged incubation have been found to decrease cell viability.[85] Moreover, intrinsic levels of glycating agents can also complicate analysis, as cells contain a multitude of biologically relevant aldehydes. Each of these can act as a glycating agent, influencing AGE distributions at a single site or at various, distinct sites, thereby obscuring information about chemical features that affect selective AGE formation. Further, proteomics studies also struggle with obtaining quantitative data and offering information on spatial effects important to selective glycation. While quantitative data can be obtained using stable isotope (SILAC) or tandem mass tag (TMT) labeling techniques, which are cost prohibitive and require advanced technical knowledge, information on spatial effects cannot be accessed due to the breakdown of proteins into primary sequences. In this regard, experiments on the protein and peptide levels are better matches for the investigation of chemical attributes that directly template selectivity of preferential AGE formation.

While intact LC-MS analysis is useful for quantifying overall total glycation levels on a protein, MS/MS analysis of digested protein samples is necessary for elucidating site information. With the help of MS as an analytical tool, our lab has employed both top-down and bottom-up approaches to cataloguing AGEs. For example, a top-down approach consists of intact analysis of purified proteins treated with glycating agents, followed by digestion into peptides. After comparing overall glycation on a panel of purified proteins, Sjoblom *et al*. performed digestion of these MGO-modified proteins to catalogue AGE distributions with respect to Arg residues on which heterogenous AGEs formed and followed up with studies on glycated

synthetic peptides.[31] On the other hand, McEwen *et al*. started with a combinatorial peptide library to identify consensus sequence characteristics that promote MGH-1 formation and subsequently performed cell-based experiments, expressing GFP variants with the hit sequence fused C-terminally, to confirm MGH-1 formation on full-length proteins.[19] Both approaches have led to many important findings, including the identification of generalizable chemical features that can be broadly applied to modulate the extent of MGO-derived AGEs and bias certain AGEs to form.

1.3.2. An Unmet Need for Tools to Study Glycation

Despite recent advancements in the field, glycation studies lack many necessary tools that can transform how we study AGEs. As mentioned above, one of the challenges in studying glycation stems from the difficulty in detecting or capturing AGEs. Antibodies have been widely implemented to detect certain AGEs, especially in immunohistochemistry in disease-related studies. However, many commercially available antibodies have later been found to be nonspecific, and in many cases, the exact epitope remains unknown.[19,46,48,67] This is because AGE antibodies are traditionally obtained against AGE antigens that were generated by reacting the chosen glycating agent with a protein (usually albumin). For example, APY has been implicated in many diseases, such as brunescent cataractous lens, filial amyloidotic polyneuropathy, and human cancer by studies done with extensive use of APY antibodies.[45–48,50,51,86–88] However, Sudnitsyna & Gusev have demonstrated that further experimental validation to these conclusions would have been beneficial, since it turned out that some of the APY antibodies used were found to recognize not only APY but also similar MGO-derived AGEs and their epitopes, leading to the false assumption that APY was detected on the small heat shock protein HspB1.[89] Although such antibodies could be subjected to greater

characterization by comparing their binding against unmodified proteins or glycated proteins using other glycating agents, they suffer from nonspecific binding owing to the myriad of distinct, sometimes structurally similar, AGEs that can form. Thanks to recent advancements in the field, there have been reports of antibodies that are well characterized with structurally known epitopes. The Spiegel lab has reported the generation and characterization of the first specific antibodies against each of the three MGH-1,2,3 isomers using chemically synthesized, homogeneous materials as the immunizing antigen.[90] They have similarly reported an anti-glucosepane antibody based on the total synthesis of glucosepane.[91] Collectively, the development of these antibodies shows the importance of antibodies that are well-characterized and can distinguish between different AGE structures.

In the absence of widely available antibodies for studying glycation, some have turned to the use of boronate affinity chromatography (BAC) to detect and enrich AGEs. This technique capitalizes on the binding of cis-diol groups on glycated proteins to the boronate affinity matrix. BAC has been widely used to capture AGEs on hemoglobin and albumin[92,93]. However, as BAC exhibits strong binding to cis-1,2-diols, a functional group more prevalent on sugars than other glycating agents like MGO, BAC is unable to capture prevalent and highly relevant AGEs like the MGH isomers or CEL/CEA. Moreover, BAC can only reveal the general quantification of glycation on proteins when compared to non-glycated controls, making it difficult to ascertain which AGEs are present, their structural information, and composition. Nowadays, BAC is typically used as an enrichment tool for glycated proteins and often coupled with MS that allows researchers to perform follow-up experiments to better deduce information about AGEs in the proteome. However, due to the binding chemistry of BAC, these studies are still likely unable to capture a significant portion of the glycated proteome.

Many recent glycation studies have turned their attention to identifying AGEs as part of metabolomics or proteomics workflows. Metabolomics workflow often comprises cell culture, protein extraction, enzymatic digestion, followed by analysis by LC-MS/MS. Even though a metabolomics approach is helpful in measuring AGE levels broadly and identifying AGEs in samples *in vivo*, it does not necessarily provide information about glycation as a functional PTM. This is because sample preparation for metabolomics leaves free amino acid in place of protein, so sequence information is lost, leaving unanswered the effects of the microenvironment surrounding the glycation site on AGE formation. In turn, this approach also leaves behind key details on mechanistic information. On the other hand, proteomics analysis is also apt for AGE identification, but it might not be as comprehensive as intended, especially for distinguishing isomers that have identical mass changes, such as MGH-1, -2, and -3 or MGH-DH and CEA. Metabolomics approach can overcome this challenge by introducing authentic AGE standards. Importantly, both approaches suffer from a lack of enrichment methods for capturing AGEs, as BAC cannot reliably capture all AGEs and most antibodies are non-specific. Therefore, experiments using unenriched cell lysates often result in a limited set of AGEs that can impede further functional annotation analysis due to a small sample size which significantly decreases the statistical power of connected biological relevance.

Recent efforts in addressing the enrichment problem have seen the development of several clickable chemical probes and quantitative workflows. These include an azidoribose probe to identify multiple targets of ribose on histone glycation,[94] an alkynyl-MGO probe to pinpoint AGEs on serum and blood proteins,[95,96] an MGO pulse followed by iodoacetamide alkyne (IA) chase workflow to profile glycated Cys forming hemithioacetals or MICA,[97] and another method based on impaired gel mobility of crosslinked proteins to identify crosslinking AGEs.[98]

Nevertheless, these studies only marked the beginning of the expansion of our glycation toolbox. The continued development of antibodies, chemical probes, enrichment protocols, and strategies to understand selective glycation will undoubtedly contribute to our knowledge of how AGEs form and what causal relationships they have with biological processes and diseases.

1.4. Leveraging Chemical Features of Selective Glycation to Expand the Toolbox

1.4.1. The Microenvironment Effect on Glycation

Currently, the lack of knowledge on chemical rules that govern how glycation is installed at a selective site remains a major roadblock for understanding how AGEs form. Past glycation literature has focused on evidence of *in vitro* selective glycation,[18,47,99,100] while proteomics studies have further catalogued instances of cellular glycation.[62,101–105] However, these studies, which also used inconsistent reaction conditions, only provided isolated examples of glycation on selected proteins, instead of a comprehensive understanding of how selective glycation occurs on a molecular level. There is no current consensus on how and what variable elements control selective AGE formation surrounding the glycation site. Our lab has centered our approach to understanding selective glycation on the molecular level by investigating the effects of the local microenvironment such as primary sequence identity and secondary structure on specific AGE formation. The ability to predict and/or control what AGEs form and to what extent is imperative to developing new tools that can assist in the study of glycation biology.

A previous study in our lab has determined several key generalizable features that influence MGO-derived glycation via mass-spectrometry (MS) analysis. Sjoblom *et al.* systematically screened a panel of purified proteins against MGO as the glycating agent *in vitro* and found that the amount of modification did not correlate with the total number of nucleophilic residues, the number of Lys or Arg, or isoelectric point (pI) of the intact protein.[31] Although

increasing MGO concentrations resulted in an increase in AGE levels in digested protein data, concentration did not influence site-selectivity of glycation. Similarly, Arg pK_a perturbations did not affect glycation, instead the presence of polar or ionizable groups was shown to drive the formation of stable adducts by promoting rate-determining rearrangements of AGEs. Indeed, when categorized by the extent of glycation, the presence of Tyr was revealed to be critical in promoting glycation, consistent with previous findings.[32] Replacing the Tyr with Phe in follow-up peptide experiments also revealed that the hydroxyl group is more important to this promotion than the aromatic ring. Conversely, clustered negative charges were shown to decrease overall glycation, contrary to previous reports.[62,106,107] However, by comparing glycated native proteins to their denatured counterparts, Sjoblom *et al.* also found that primary sequence is the main driver for the extent of selective glycation, while the surrounding structure influences the identity of AGEs that form. This could explain why multiple negative charges have been shown to decrease glycation in some studies yet increase in others.[19,31,108,109]

Building upon this understanding of how primary sequence and secondary structure influence selective glycation, our lab further investigated the formation of several discreet AGEs. Past mechanistic studies have focused mainly on single amino acid derivatives and/or monomers, obscuring the effects of long- or medium-range interactions that can bias the formation of certain AGEs.[18,37,100,110,111] This lack of information inhibits our understanding of how AGEs are assembled in a complex cellular milieu where sequence and structure become important. McEwen *et al.* used a bottom-up approach to study selective glycation by performing a combinatorial one-bead-one-compound peptide library to select for “hits” that promote the formation of MGH-1, a biologically relevant MGO-derived AGE and the most stable of the three MGH isomers.[19] This study focused on uncovering the effects of long- and medium-range

interactions on the formation of MGH-1. Perhaps unsurprisingly, the role of Tyr was corroborated in this study to play a vital role as a general base in the preferential formation of MGH-1 by eliminating water from MGH-DH to produce MGH-1. In particular, Tyr in the +2 position from the central Arg was shown to have a cooperative effect with Glu in the -2 position to favor MGH-1, as point mutation at these positions resulted in significant changes in glycation. Most importantly, through a series of time-course and dilution experiments on point-mutated short peptides *in vitro*, McEwen *et al.* revealed key mechanistic steps connecting MGH-DH to the formation of MGH-1. Follow-up studies done on purified MGH-1-containing peptides showed that MGH-1 can further hydrolyze to yield CEA. Through these findings, our lab was the first to reveal the mechanistic connection between several AGEs, including MGH-DH, MGH-1, and CEA. McEwen *et al.* also showed that the primary sequence effects of polar/ionizable groups on short, unstructured peptides can be translated into specific placements of these residues on fully folded proteins to mimic the microenvironment effects and potentially influence glycation surrounding the central Arg.

To understand the effects of secondary structure and other properties of full-length, folded proteins on site-selectivity of glycation, Martin *et al.* developed a unique tool called "dialAGE" that allows for site-specific modulation of protein glycation.[109] The target of this research was the small protein ubiquitin (Ub), whose structure and disease relevance is well understood. While the seven Lys residues on Ub have been the focus of many past studies due to polyubiquitin chain formation, disassembly, and quality control, Ub also possesses four Arg residues (R42, R54, R72, and R74) that can influence these elements.[112–115] Select point mutations were introduced on Ub, specifically at Q49, a residue located within 5Å of the guanidinium sidechain of R42 in a nearby β-strand. Specifically, dialAGE variants of Q49Y and

Q49E were prepared by replacing Gln with Tyr and Glu, respectively, based on the hypothesis that a nearby Tyr promotes while Glu decreases glycation as confirmed on short peptides in previous *in vitro* studies in our lab. Using MS analysis on intact and digested Ub variants, Martin *et al.* found that the introduced mutations resulted in the expected modulation of overall Ub glycation levels for both dialAGE^{R42} and dialAGE^{R54}, while only dialAGE^{R42} produced a consistently site-specific effect. With the help of molecular dynamics simulations, it was revealed that Q49Y mutation likely resulted in lengthening the distance between R42 and site 49, allowing more space for MGO to access R42 and positioning Tyr to aid glycation. In contrast, Q49E mutation potentially acted as an electrostatic trap, reducing glycation at R42. Overall, these experiments not only confirmed the importance of the local microenvironment effects on glycation but also revealed that these effects can be used to modulate glycation on full-length, folded proteins. This knowledge will be extremely beneficial for future research in developing tools to study glycation biology and elucidate its role as a functional PTM.

1.4.2. Leveraging Known AGE Formation Features to Develop Chemical Tools for Site-specific Labeling of Arginine

APY is an autofluorescent AGE that has been found in glycation *in vivo*. APY has been implicated in many diseases such as brunescent cataractous lens, filial amyloidotic polyneuropathy, and human cancer.[47,48,88,116] Specifically, APY has been found to accumulate more in the nuclear region of the aging lens in brunescent cataractous lens compared to that of healthy lens.[48] MGO concentration in human lenses has also been found to be at least 20 times higher than in human plasma, and previous studies have successfully detected APY in lens proteins as a result of MGO modification of Arg. On the other hand, protein glycation has also been found in amyloid diseases such as Alzheimer's disease and filial amyloidotic

polyneuropathy (FAP), an amyloid disease that affects both the peripheral and autosomal nervous systems.[88] FAP has also been associated with APY formation, which was chromatically identified from amyloid deposits from FAP patients. In human cancer, tumors have been found to have an increased uptake of glucose and glycolysis, resulting in an increase in AGE formation.[116,117] In the same study, APY has also been detected in human cancer tissues by expression in different types of tumors by immunohistochemistry.

In the glycation literature and associated disease studies, APY has been identified mainly via immunoreactivity detection of its antibody visualized using sodium dodecyl sulfate–polyacrylamide gel electrophoresis (SDS PAGE) and western blot, or HPLC equipped with a fluorescence detector.[14,51,88,116,118,119] APY is an autofluorescent AGE, so it can easily be detected using its fluorescent properties. However, since the chemical mechanism of APY formation is still not fully understood, scientists have struggled to produce APY in experimentally convenient quantities on peptides and proteins. Therefore, APY fluorescence has been used mainly to detect its presence in processed biological samples collected from patient tissues.

Even though there are many studies that use fluorescence HPLC to detect APY in biological samples, APY has not traditionally been thought of as a potential fluorescent label. Bhattacherjee, Dhara, and Chakraborti have started to explore this idea by synthesizing an APY tagged nanoparticle to study drug delivery via the cell surface RAGE.[120] In this study, Bhattacherjee and coworkers were able to visualize the fluorescence of their APY tag on the surface of the cells using fluorescent microscopy. However, one significant drawback that prevents the widespread development of an APY fluorescent tag in live cells is that its excitation and emission are too low for the majority of current commercial microscopy systems. Specifically, common optical filters used for excitation in the near-UV (on the shortest end of the

visible spectrum) typically start in the 320-400 nm range. With APY's $\lambda_{ex,\ max}$ at 320 nm, these filters are unsuitable for observing APY fluorescence, whereas specialized filters are costly. Two or three photon microscopy could potentially help solve this problem. Given the inverse relationship between photon energy and wavelength, in two photon microscopy, APY could be excited at 640 nm. However, this value still lies on the lower end of the two photon excitation limit, as well as these microscopic systems are expensive and technically demanding, so there have been no reports of using it for APY fluorescence. Moreover, the development of many fluorescent tags relies on reports of quantum yield calculation (the ratio of the number of photons emitted to that of photons absorbed, valued between 0 and 1) to quantify how "bright" a fluorophore is. For reference, the enhanced green fluorescent protein (eGFP) commonly used as a fluorophore in biological samples has a quantum yield of 0.60 in physiological pH.[121] The quantum yield for APY has not been reported, making it difficult to assess its potential as a fluorescent tag. Nevertheless, the ability to develop a fluorescent tool is highly important in tracking cellular glycation events *in vivo*. Since our lab has accumulated increasing knowledge of predicting the extent of site-selective MGO-derived AGE formation based on primary sequence and secondary structure, we are optimistic that we will be able to leverage this knowledge for the near-future development of an APY fluorescent tag on a shirt peptide, whether by itself on conjugated with other molecules for enhanced fluorescence. Still, the first step is to understand its chemical mechanistic formation, which remains elusive and unvalidated in the current glycation literature.

1.5. Conclusions

Currently, there is a lack of tools to study the biology of glycation in living systems. Because glycation is non-enzymatic (lacks a "writer" enzyme), AGEs cannot be studied using

enzymes like other types of PTMs. Enzymes consist of unique and precise arrangements of amino acid side chains within the enzyme active sites, facilitating the site-specific modification of native side chains by priming the local microenvironment for catalysis. However, because enzymatic active sites do not apply to glycation, little is known about the effects of the local environment on the site-specific side-chain modification of Arg. Recent studies in our lab have shown that primary sequence plays a key role in governing the likelihood of glycation at a specific site, whereas secondary structure sculpts the identity of AGEs that form. We have begun to leverage this knowledge to define chemical mechanistic pathways of several interconnected MGO-derived AGEs, including MGH-DH, MGH-1, and CEA, and identified sequence features that bias MGH-1 formation.

Argpyrimidine (APY) is an autofluorescent AGE that has been associated with multiple diseases, yet unfortunately, there is not much known about the specific roles and the causal relationship APY has with these diseases due to a lack of understanding regarding its chemical mechanism. In order to understand this cause-and-effect relationship, new chemical tools are needed for studying how and where APY form, both on proteins and in cells, in connection to these diseases. Additionally, as informed by previous research in our lab, information on the influence of the surrounding environment such as the identity of nearby residues is essential to predicting AGE distribution and controlling the extent of its accumulation *in vivo*. In the cellular context, sugars can be fragmented into various metabolites with active aldehydes and ketones that participate in AGE formation, making it difficult to discern which glycating agents are responsible for the AGEs formed. Understanding the chemical mechanism behind APY formation will help pinpoint the conditions and locations in cells where APY is more likely to accumulate and predict strategies to modulate APY formation on proteins. Given its unique

fluorescent characteristics, the chemical mechanistic pathway of APY formation is important for developing novel chemical tools to predict and/or control selective AGE formation in cells and potentially discovering new fluorescent sensor to track the formation of AGEs in diseases.

In the following work, by harnessing the rules that govern regioselectivity of a native Arg modification, our studies reveal key features that promote APY formation on short peptides. We further identify conditions at which APY can be observed as a predominant adduct, which has not been reported to our knowledge. Our experiments below provide concrete chemical evidence of APY formation mechanism that is likely to occur under physiological conditions, reconciling past mechanistic hypotheses. Additionally, we demonstrate that APY, as a late-stage AGE, is also connected to other MGO-derived AGEs in the AGE maturation process and is more stable than previously thought. In our proteomic analysis of MGO-treated cells, for the first time, we establish a potential connection between cellular APY formation and another prevalent PTM that is phosphorylation. We further show that phosphorylated residues can promote equivalent levels of glycation despite introducing extra negative charges that have been previously shown to impede glycation and even bias the formation of certain AGEs. Collectively, these findings will provide necessary mechanistic and biological insights to inform future research on developing potential chemical and fluorescent tools that can be used to predict, sense, and study glycation events in living cells.

2. Chapter 2:

In vitro Peptide Studies to Enhance AGE Formation

2.1. Introduction

Argpyrimidine (APY) is one of a group of nearly 40 protein post-translational modifications (PTMs) known as advanced glycation end-products (AGEs).1–3 AGEs are hallmarks of aging and disease that form non-enzymatically on Lys, the N-terminus, or—in the case of APY—on Arg residues.1–3 Despite a relatively high pKa, the Arg guanidino group reacts selectively with α-oxoaldehydes such as the biological glycating agent methylglyoxal (MGO), forming multiple AGEs.4–6 In addition to APY, these include the methylglyoxal-derived hydroimidazolone isomers (MGH-1, -2, & -3), dihydroxyimidazolidine (MGH-DH), carboxyethylarginine (CEA), and tetrahydropyrimidine (THP) (**Figure 2.1**). Although there is accumulating evidence that certain AGEs, especially the MGH isomers and CEA, lead to specific biological consequences,[5,20,39,67,122,123] far less is known about the biology of APY. Several reports have correlated APY with cellular processes like apoptosis, autophagy, or chaperone activity, and a few have shown its association with diseases like brunescent cataractous lens, filial amyloidotic polyneuropathy, or cancer.[45,47,48,50,51,86–88,116] Still, there are virtually no causal connections that link APY to specific biological consequences.

These open questions persist because APY has been notoriously difficult to track due to a lack of highly specific tools and an unknown mechanism of formation. Given that APY requires more than a single MGO molecule to form, it could be particularly relevant under hyperglycemic conditions. Additionally, it has been proposed that APY formation also depends on oxidative stress, suggesting that it could be a critical link between glycation and other cellular stresses.[88,124,125] It is therefore essential to understand APY's formation mechanism to pinpoint the features that influence its formation and the locations—both on proteins and in cells—where APY is more likely to accumulate.

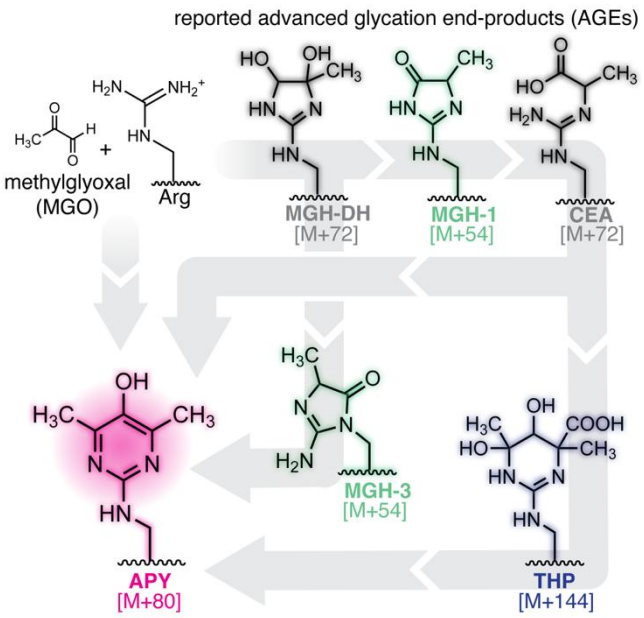

Figure 2.1. Overview of MGO-derived AGEs. In addition to APY, these include the methylglyoxal-derived hydroimidazolone isomers (MGH-1, -2, & -3), dihydroxyimidazolidine (MGH-DH), carboxyethylarginine (CEA), and tetrahydropyrimidine (THP). Several possible pathways for APY formation have been previously proposed (gray arrows).

Previous work in our lab has shown that specific Arg-derived AGEs depend not only on MGO concentrations, but also the surrounding chemical microenvironment.[19,31,109] We have shown that several of these Arg-derived AGEs are mechanistically connected and can interconvert.4 In this chapter, we use a peptide model system to determine chemical features that favor APY formation. Through *in vitro* glycation experiments performed on short peptides, we determine that APY formation does not depend on the initial MGO concentration. Instead, we confirm that [M+144] species, presumably including tetrahydropyrimidine (THP), are a direct precursor to APY.

Furthermore, forming APY in experimentally convenient quantities has been a consistent challenge in glycation studies, as previous protocols have incubated proteins or Arg monomer with MGO for two weeks or longer.[18,37] We report herein that we have identified a condition under which APY becomes the predominant AGE. We also show that although APY is generated

more slowly than other AGEs, it is also quite stable once formed. Together, these findings can greatly facilitate the observation of APY on short peptides and its purification for future studies.

2.2. Results

2.2.1. Determining [M+144] AGEs as a Precursor to APY

Although APY requires two molecules of MGO (72.02 Da), its mass change ([M+80]) does not clearly match with an obvious mechanism involving loss or gain of water, as is the case for other AGEs like MGHs, MGH-DH, or CEA.[19] This has made it particularly challenging to define the APY formation mechanism.[18,37,100] Prior work from our lab and others' points to tetrahydropyrimidine (THP, [M+144]) as a possible precursor to APY.[19,37,100] Specifically, we found that by observing AGE distributions for up to 4 weeks of incubation with MGO, there was an inversely proportional relationship between APY and [M+144] species over time.[19] We therefore initiated this study with the same hit sequence from our prior study (Ac-LESRHYA, peptide **1**) that was selected from a one-bead one-compound peptide library for its ability to form MGH-1.[19] We treated peptide **1** (1 mM) with two equivalents (2 mM) of MGO, expecting that APY levels would increase at higher MGO concentrations. However, little to no APY was observed (< 3% APY), even after 72 hours of treatment, despite total glycation nearing 100% after 48 h, as assessed by liquid chromatography-mass spectrometry (LC-MS) (**Figure 2.2 A, B**).

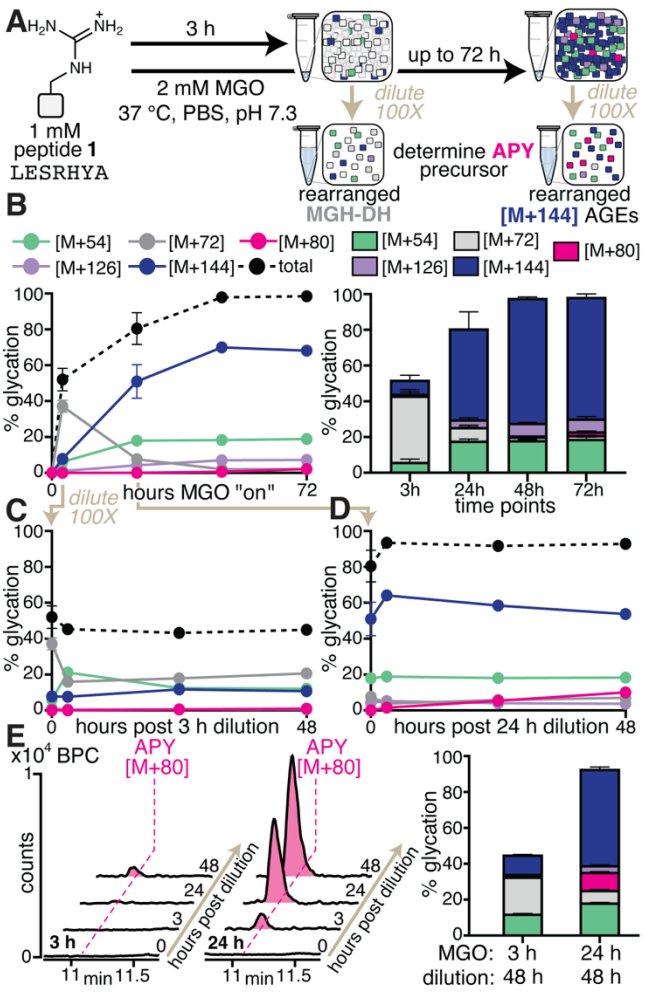

Figure 2.2. [M+144] AGEs are a Precursor to APY. (A) General scheme showing the experimental setup used to determine the APY precursor. **(B)** Peptide **1** (1 mM) was treated with 2 mM MGO and incubated for up to 72 h (labeled as "hours MGO "on"), as shown in a time course (left) and stacked bar graph (right) showing AGE distributions. **(C)** After 3 h, (when MGH-DH became the predominant adduct) or **(D)** after 24 h (when [M+144] species become the predominant AGEs), the reaction was diluted 100X in the same buffer and incubated for additional 48 h post dilution ("hours post dilution"). Since dilution markedly slows MGO addition, this protocol diminishes new AGE formation on already glycated peptides, enabling the clear observation of rearrangements between AGEs. **(E)** Representative base peak chromatograms (BPC) (left) and bar graph (right) for peptide **1** at several post dilution time points (n≥3 for all reactions). Please note that not all error bars are visible, as many are smaller than the size of the symbol. A significant increase in APY [M+80] (magenta) levels was observed at 48 h post dilution of the 24 h time point when compared to that of the 3 h timepoint. These results suggest that [M+144] species (blue), and not MGH-DH (gray), is a precursor for APY.

In addition to peptide **1**, we also evaluated two additional peptide sequences, both from lens crystallin, that we previously identified as APY-modified using MGO-treated proteins in vitro (**Figure 2.3**).[31] In these studies, all three peptides were identified with APY formation upon treatment with MGO. Though APY formation requires two MGO, increasing initial MGO

concentrations did not increase APY levels even after 48 hours of incubation. Even when increasing MGO concentrations to 3 mM, there was little to no (< 3%) APY after 48 hours across all three peptides, signifying that APY formation is largely independent of initial MGO concentrations, despite requiring two MGO equivalents to form.

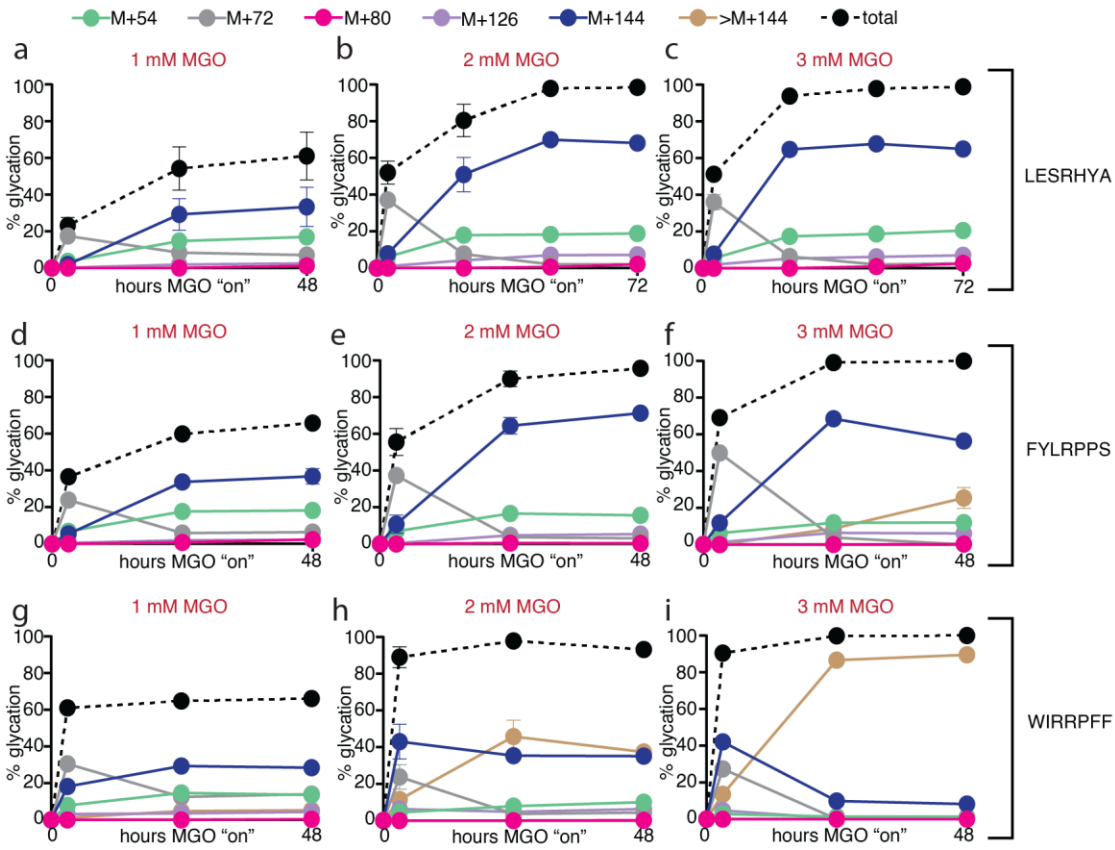

Figure 2.3. Peptide Glycation for Previously-Identified APY-modified Protein Sequences. (a), (b) & (c) Distribution of AGEs on MGO-treated peptide **1** at 1 mM, 2 mM, and 3 mM MGO concentrations after 3 h, 24 h, 48 h, or 72 h ($n \geq 3$). **(d), (e) & (f)** Distribution of AGEs on MGO-treated peptide Ac-FYLRPPS at 1 mM, 2 mM, and 3 mM MGO concentrations after 3 h, 24 h, and 48 h ($n \geq 3$). **(g), (h) & (i)** Distribution of AGEs on MGO-treated peptide Ac-WIRRPFF at 1 mM, 2 mM, and 3 mM MGO concentrations after 3 h, 24 h, and 48 h ($n = 2$ for 48 h time point, $n = 3$ for all other time points). These peptides were chosen because they have been identified as APY-modified based on previous work done in our lab.4,9 Specifically, peptide Ac-LESRHYA was identified via a one-bead-one-compound combinatorial peptide library and selected for its ability to form MGH-1. Peptides Ac-FYLRPPS and Ac-WIRRPFF, both from lens crystallin, were identified by *in vitro* glycation of proteins.

Nonetheless, the major difference in AGE distribution at 3 and 24 h allowed us to test the hypothesis that [M+144] AGEs (likely including THP) are a precursor to APY. To do so, we incubated peptide **1** with 2 mM MGO for either 3 h or 24 h. After this initial incubation, we

diluted the reaction mixture 100X in the same buffer and compared the resulting AGE distributions at several post-dilution time points (**Figure 2.2 C—E**). Since dilution markedly slows MGO addition, this protocol diminishes new AGE formation on already glycated peptides, thereby enabling the clear observation of rearrangements between AGEs. At 3 h, MGH-DH (37.1 ± 3.4 %) was the predominant AGE, but at 24 h, multiple [M+144] species (51.0 ± 9.4 %) became the predominant AGEs. While dilution of the 3 h incubation did not yield any APY even at 48 h post dilution (**Figure 2.2 C, E**), we observed a substantial increase in [M+80] levels when the 24 h incubation was diluted, reaching 10.0 ± 0.3% APY after 48 h post dilution (**Figure 2.2 D, E**). These data confirmed the hypothesis that [M+144] AGEs are a precursor to APY.

2.2.2. Enhancing APY Formation

Despite defining [M+144] as an intermediate along the APY formation pathway, persistent low levels of APY remained a consistent technical challenge. Seeking to increase APY levels, we conducted a temperature scan in which we incubated peptide **1** with 2 mM MGO for 24 hours, using temperatures ranging from 37–70 °C (**Figure 2.4**). We found that between 37 °C and 45 °C, there was hardly any change in the AGE distribution. Across the entire range of temperatures used, other AGEs, like MGH-1 and CEA, stayed fairly constant, with only slight increases at higher temperatures. However, at 55 °C, we began to observe a notable increase in APY that was concomitant with reduced [M+144] levels. APY levels peaked at 60 °C (53.1 ± 12.1 %), becoming the predominant AGE in just 24 hours (**Figure 2.4 A, B**). Importantly, these findings not only identify conditions at which APY can become a major AGE, but they also suggest that the rearrangement of [M+144] into APY likely involves a high energy activation barrier that can be overcome by the addition of heat.

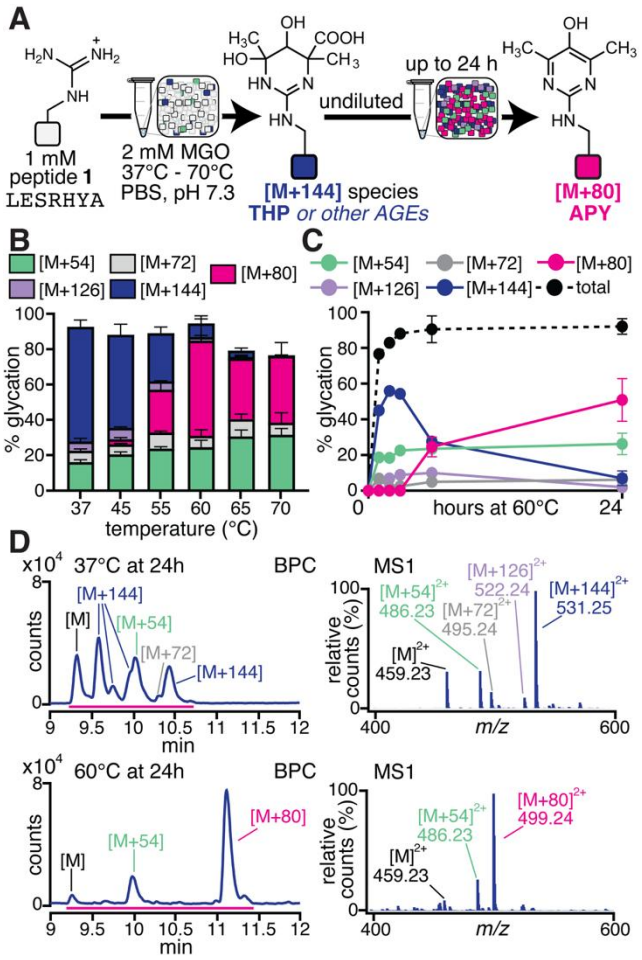

Figure 2.4. APY is a Stable AGE. (A) General scheme depicting treatment of peptide **1** with 2 mM MGO over a range of temperatures from 37 °C to 60 °C. The reaction was incubated for 24 h undiluted, and AGE distributions were assessed *via* LC-MS analysis. **(B)** Stacked bar graph showing AGE distributions for peptide **1** treated with MGO for 24 h at 37 °C, 45 °C, 55 °C, 60 °C, 65 °C, and 70 °C. **(C)** Time course of peptide **1** glycation reactions at 60 °C, extended over several time points (1 h, 2 h, 3 h, 6 h, and 24 h) (n≥3 for all reactions). **(D)** Representative BPCs and MS1 spectra for the glycation reaction of peptide **1** after 24 h incubation at 37 °C (top) and 60 °C (bottom).

2.2.3. Confirming [M+144] Species as a Precursor to APY

To further investigate the relationship between APY and [M+144], we extended the reaction at 60 °C across multiple time points. At 60 °C, the reaction quickly reached 88.1 ± 1.9% total glycation in only 3 h. From this, we conclude that most of the free MGO is quickly consumed, producing [M+144] as the major early AGEs (54.3 ± 1.8% of total glycation) (**Figure 2.4 C**). APY levels began to increase after 2 h of incubation, with a precipitous increase (from

0.0 % to 24.5 ± 5.5 %) between 3 and 6 h. During this same time frame, a concomitant, proportional decrease in [M+144] levels was observed, providing unambiguous assignment of [M+144] as a precursor to APY. We note that we consistently observed up to four different [M+144] species with distinct retention times (**Figure 2.4 & Figure 2.5**). To our knowledge, THP is the only [M+144] AGE that has been reported.[14] While it is possible that THP diastereomers may have different retention times, we also suspect that these discrete [M+144] adducts could also represent other intermediate structures or other double addition adducts (see also **Figure 3.1**). Notably, all of the [M+144] species we observed appear to mature into APY, since each one decreased at the same rate as APY levels increased (**Figure 2.5**). For this reason, we report all [M+144] species totaled together, represented as a combined [M+144].

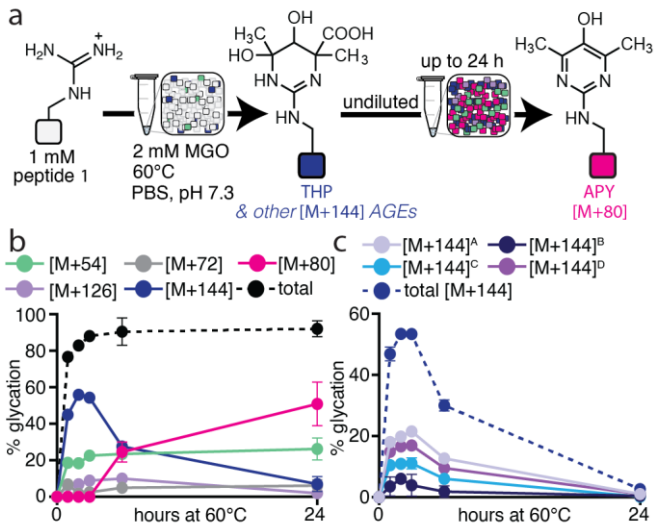

Figure 2.5. All [M+144] Species mature into APY over Time. General scheme describing the experimental procedure of glycation reactions on MGO-treated peptide **1** 60 °C (20 mM PBS, pH 7.3). Time points were taken at 0 h, 1 h, 2 h, 3 h, 6 h, and 24 h to monitor changes in AGE distributions (n ≥ 3). **(b)** Distribution of AGEs on MGO-treated peptide **1**, also shown in **Figure 2.4**. **(c)** Distribution of all [M+144] AGEs observed on MGO-treated peptide **1**. We consistently observed up to four different [M+144] species with distinct retention times. To our knowledge, THP is the only [M+144] AGE that has been reported.[14] However, all of the [M+144] species we observed appear to mature into APY, since each one decreased as APY levels increased. Therefore, we report [M+144] as a total sum of all [M+144] AGEs.

2.2.4. APY Formation is Dependent on Primary Sequence

Comparison of the AGE distributions at 37 °C and 60 °C revealed APY is a stable AGE. After heating at 60 °C for 24 h, only MGH-1 and APY remained in appreciable quantities, while other AGEs, like CEA and [M+144] species including THP, disappeared, presumably due to rearrangements into MGH-1 and APY (**Figure 2.4 D**). We have also shown that while elevated temperatures increase APY levels at earlier time points, APY formation is still dependent on the sequence identity (**Figure 2.6**). Since clustered negative charges have been reported to impede glycation, it was important to confirm that this also included APY formation. Ac-LDDREDA was identified as a negative hit sequence from a previous combinatorial peptide library for MGH-1 formation and was not known to form APY.[19] Expectedly, overall glycation levels were seen to decrease for the sequence Ac-LDDREDA compared to those of peptide **1**. Although APY levels increased as temperature increased for both sequences, we found that APY was not formed until higher temperatures for Ac-LDDREDA.

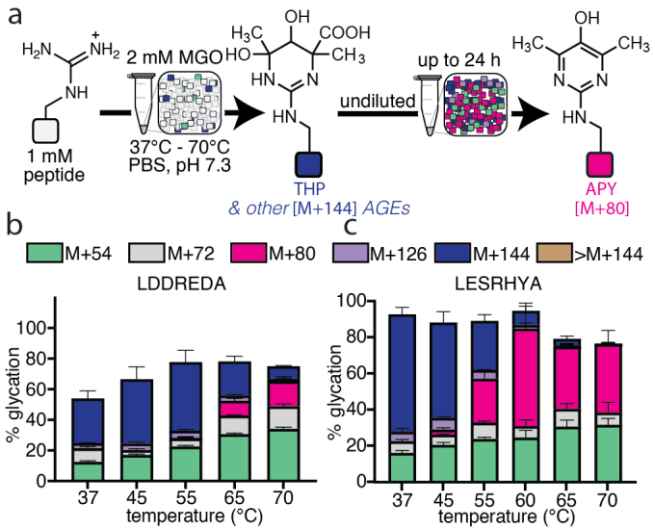

Figure 2.6. APY Formation can be Affected by the Surrounding Sequence. (a) General scheme describing the temperature scan conducted for 24 h peptide glycation reactions performed at 37 °C, 45 °C, 55 °C, 65 °C, or 70 °C (n ≥ 3 for all reactions). **(b)** Distribution of AGEs on MGO-treated peptide LDDREDA after 24 h. **(c)** Distribution of AGEs on MGO-treated peptide Ac-LESRHYA after 24 h, also shown in **Figure 2.4.**

2.2.5. APY is Stable on a Short Peptide

Thanks to high levels of APY observed, we also conducted stability studies for purified APY on peptide **1** (peptide $\mathbf{1}^{\mathbf{APY}}$) and showed that APY on a short peptide is stable, exhibiting minimal decay for up to a week at physiological conditions (**Figure 2.7**). APY has been reported to be unstable at pH 7.4 and 37 °C, having a short lifetime (1.7 days), which was extended to 9.3 days in the presence of the metal-ion chelator DETAPAC.[100] However, our extensive peptide studies using peptide **1** suggested that APY is more stable than previously reported. To further confirm its stability, we purified APY-modified peptide **1** (peptide $\mathbf{1}^{\mathbf{APY}}$) to conduct stability studies in PBS with pH 7.3, 8, and 9. We found that APY was much more stable than previously thought, exhibiting a steady but slow decay even after 7 days of incubation in PBS pH 7.3 at 37 °C, without any metal-ion chelator. As pH increased, APY decayed faster, and a mass adduct [M+54] with the same retention time as that of MGH-1 was observed. The difference in results of APY stability could be due to the effects of the microenvironment surrounding the APY site on a short peptide, which was not present in previous studies using monomeric APY. Together, our results confirmed that APY−or AGE overall−formation and stability are greatly influenced by the surrounding amino acids of the glycated site, thereby suggesting that glycation studies done on peptides or proteins can offer different insights into the behaviors of AGEs that are more likely to be observed in a cellular context.

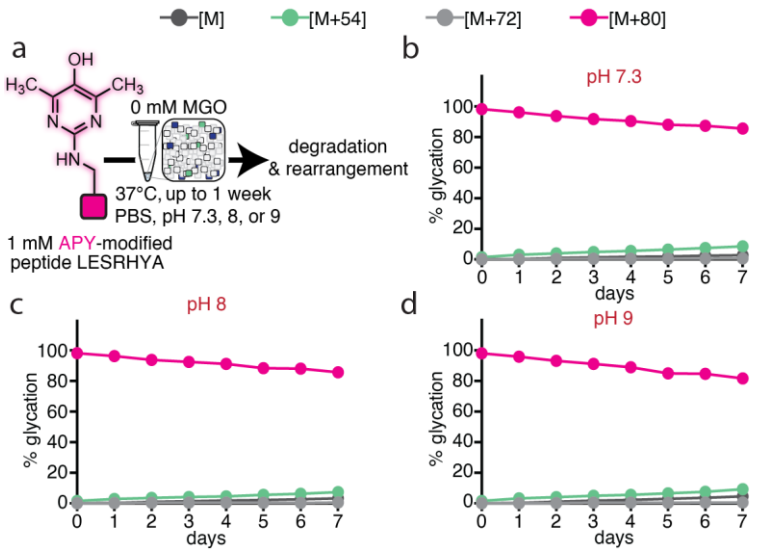

Figure 2.7. APY on a Short Peptide is Stable under Physiological Conditions. Purified APY-modified peptide **1** (peptide $\mathbf{1}^{\mathbf{APY}}$) was obtained to conduct stability studies in PBS with **(b)** pH 7.3, **(c)** pH 8, and **(d)** pH 9 ($n \geq 3$ for all reactions).

2.3. Discussion

Herein we have used a peptide model system to determine [M+144] species as a precursor to APY formation. We built upon a previous study done in our lab that identified peptide **1** as a sequence capable of forming APY after 48 h of incubation, although minimally. The most cited proposed mechanism for APY includes the formation of a reductone from MGO, indicating that APY is dependent on the initial MGO concentration.[18] However, our results from incubating peptide **1** and other peptides identified from previous studies in our lab with increasing MGO concentrations show that APY formation is independent of the initial MGO concentration, despite requiring two MGO equivalents to form. Instead, utilizing a dilution protocol, we identified [M+144] species as a precursor to APY.

As mentioned, we consistently observed up to four species of [M+144] with distinct retention times, yet only one species has been characterized via NMR with structural confirmation.[14] Interestingly, we have not been able to find any other instance in the literature

that mentions the identification of multiple [M+144] species as a result of MGO modification, as all mentions of [M+144] assume that it must be THP. This is likely a result of glycation reactions done on Arg monomer, leaving out critical medium- and long-range interactions observed with the surrounding sequence that can influence the formation of other [M+144] species and/or intermediates. Although we cannot conclude that a singular, specific [M+144] species is a direct precursor to APY, we do not rule out the possibility that other [M+144] species may represent diastereomers, intermediates, or unknown double addition adducts. However, given that all [M+144] species matured into APY at similar rates as observed via LC-MS, we unambiguously show that [M+144] species, collectively, are responsible for APY formation in our system.

Although appreciated for its unique fluorescence properties,[18,37,126] APY has been difficult to study as it was not previously known how to produce it in experimentally convenient quantities from the reaction of Arg and MGO.[51,87,88] Our results indicate that APY formation depends surprisingly little on initial MGO concentrations, and instead greatly depends on other factors, including sequence identity and temperature, each of which can help to overcome a relatively high energy rate determining step. Through these studies, we discover that APY is quite stable and identify *in vitro* conditions under which APY becomes the predominant AGE, which to our knowledge, has not been previously reported. These findings alone provide an important technical advance that will greatly facilitate future studies on APY.

2.4. Materials and Methods

2.4.1. General Materials

All chemical reagents and solvents were of analytical grade, obtained from commercial suppliers, and used without further purification, unless otherwise noted. Methylglyoxal (MGO)

(40% w/v in water) was purchased from MilliporeSigma (M0252). Water used in glycation experiments was distilled and deionized using an Arium Pro purification system (Sartorius). All statistical analysis was conducted using Prism GraphPad.

2.4.2. Peptide Synthesis

Peptides were synthesized using standard Fmoc-based solid phase peptide synthesis on Trityl chloride resin (200 mesh, 1.6 mmol/g loading, Novabiochem®) or Fmoc-Ala-Wang resin (100-200 mesh, 0.64 mmol/g loading, Creosalus Inc.), typically on a 100 µmol scale in a 3 mL polypropylene fritted syringe. For Trityl chloride resin only, C-terminal amino acids (5 equiv., 500 µmol) were coupled overnight in a solution of 10 equiv. (1 mmol) N,N-diisopropylethylamine (DIEA) in 3 mL dimethylformamide (DMF). The next day, the resin was washed and capped with a solution (3 mL) of DMF:MeOH:DIEA (17:2:1 by volume) for 1 hour before further deprotection and coupling steps. C-terminal coupling and resin capping was not required when using Fmoc-Ala-Wang resin. Fmoc deprotection was accomplished using 20% piperidine in DMF (3 mL, 3 x 5 min), followed by washing steps with DMF (3 mL, 4 x 1 min). Amino acid couplings were completed by incubation of amino acid (5 equiv. relative to resin loading) with O-(benzotriazole-1-yl)-N,N,N’,N’-tetramethyluronium hexafluorophosphate (HBTU, 5 equiv.) and DIEA (10 equiv.) in 1-2 mL of DMF for 45-90 min. All peptides were N-terminally acetylated following deprotection of the last amino acid coupling via incubation with acetic anhydride (4 equiv.) and DIEA (3 equiv.) in 1-2 mL DMF for 2 hours. Following the final acetylation step, peptides were washed with DMF (3 mL, 4 x 1 min), followed by dichloromethane (DCM) (3 mL, 2 x 1 min, then 2 x 15 min), and stored under vacuum desiccation until ready for side-chain deprotection and cleavage. The side chain protecting groups used were as follows: Glu (tBu), His (Trt), Lys (Boc), pSer (Bzl), pTyr (Bzl), Trp (Boc),

and Tyr (tBu). Side-chain deprotection and peptide cleavage was completed by incubation with trifluoroacetic acid (TFA), triisopropylsilane (TIPS), and water (95:2.5:2.5 by volume) in 4 mL of acid solution per resin for 2 hours. The resulting crude peptide was dried under constant air flow and then dissolved in 1-3 mL of a water/acetonitrile mixture based on solubility, prior to purification.

2.4.3. Peptide Purification

All peptides were purified using a semi-preparative Agilent 1260 Infinity LC system equipped with an Agilent ZORBAX SB-C18 column (9.4 × 250 mm, 5 μm particle size). The mobile phase contained water (A) and acetonitrile (B) with 0.1% TFA. Crude peptide solutions were eluted with a gradient of 5% B to 40% B over 20 min and a flow rate of 3.0 mL/min. Absorbance at 215 and 280 nm was used to observe desired peptide peaks, which were then eluted and collected using an automated fraction collector. APY-specific absorbance could be detected using its characteristic absorbance at 320 nm.[18,37,126] Collected fractions were assessed for purity using matrix-assisted laser desorption/ionization time-of-flight (MALDI-TOF) mass spectrometry (Bruker) and/or an Agilent 6530 quadrupole time-of-fight (Q-TOF) mass spectrometer (Agilent). Pure fractions were combined and lyophilized. Peptide stock solutions were prepared at 20 mM concentrations in DMF.

2.4.4. MALDI Mass Spectrometry

0.5 μL of each peptide collected fraction were co-crystallized onto a ground steel plate with 0.9 μL of saturated solutions of α-cyano-4hydroxycinnamic acid in 50% acetonitrile, 50% water with 0.1% trifluoroacetic acid.

2.4.5. Liquid Chromatography-Mass Spectrometry Analysis and Quantification

Reversed-phase liquid chromatography and mass spectrometry (LC-MS) was performed using an Agilent 1260 LC system coupled to an Agilent 6530 Accurate Mass Q-TOF. The mobile phase contained water (A) and acetonitrile (B) with 0.1% formic acid. Peptide glycation reactions were injected onto an AdvanceBio Peptide 2.7 μm column (2.1 × 150 mm, Agilent) with the following method with a flow rate of 0.4 mL/min: isocratic at 5% B between 0.00-1.75 min, gradient change from 5% B to 40% B between 1.75-16.00 min, gradient change from 40% B to 100% B between 16.00-20.00 min, isocratic column washing at 100% B between 20.00-23.00 min, and re-equilibration at 5% B between 23.01-30.00 min. Peptide data were quantified using peak volumes determined by Agilent MassHunter Qualitative Analysis and the MassHunter Molecular Feature Extractor based on cumulative MS ion counts for 'volumes' observed for any and all charge states associated with a particular ion.

Percent glycation was quantified according to the formula:

$$\%\ glycation = \frac{volume\ of\ AGE\ modified\ peptide}{total\ volume\ of\ both\ modified\ and\ unmodified\ peptide}$$

2.4.6. Peptide Glycation Protocol

Peptide glycation reactions were carried out in Eppendorf tubes with a final volume of 50 μL. 10 mM MGO stocks were prepared by adding 15.38 μL commercial MGO solution (40% w/v) into 10 mL of ultrapure water and stored at 4°C for up to one week. 100 mM PBS stocks (pH 7.3) were prepared using BupH Phosphate Buffer Saline packs according to instructions provided by Thermo Scientific (28372). Typically, a peptide in vitro glycation reaction contained 27.5 μL of ultrapure water, 10 μL of 10 mM MGO stock in water (2 mM final concentration), 10

μL of 100 mM PBS stock in water (20 mM final concentration), and 2.5 μL of 20 mM peptide stock solution in DMF (1 mM final concentration). Tubes were capped, briefly spun using a benchtop microcentrifuge, and incubated in a 37°C water bath for up to 24 h or up to 6 weeks depending on the experiment. After incubation, reactions were diluted 100X with ultrapure water and 500 mM Tris Buffer pH 7.4 (5 mM final concentration) to quench the reaction and then subjected to LC-MS analysis.

2.4.7. Peptide Glycation at Elevated Temperatures

Peptide glycation reactions were carried out according to the general glycation protocol for final concentrations. During screening, reactions were assembled in PCR tubes and incubated in a thermocycler (Biorad) using a temperature gradient so that each temperature is set for each row (37 °C, 45 °C, 55 °C, 60 °C, 65 °C, and 70 °C). Subsequently, glycation reactions were performed at 37 °C and 60°C with incubation in water baths.

2.4.8. Preparation of APY-Modified Peptide 1

APY-modified peptide **1** (peptide $\mathbf{1}^{\mathbf{APY}}$) was prepared by incubation of 200 μL of 20 mM peptide **1** stock in DMF with 400 μL of 10 mM MGO stock in ultrapure water and 400 μL of 100 mM PBS stock in ultrapure water (pH 7.3) at 60 °C for 24 hours. Under this condition, APY was the predominant adduct (roughly 50% yield by LC-MS) and was purified by semi-preparative HPLC system as described above using a gradient of 5% to 50% acetonitrile (B) in water (A) over 14.25 min at 3.0 mL/min. Collected fractions were characterized by MALDI-TOF, pooled, lyophilized, and assessed for purity by LC-MS prior to further experiments. The identity of peptide $\mathbf{1}^{\mathbf{APY}}$ was confirmed by its characteristic absorbance at 320 nm and fluorescence excitation and emission at 320 nm and 385 nm, respectively.

2.4.9. General Protocol for Dilution Experiments

For dilutions experiments described in **Figure 2.2.**, peptides (1 mM) were incubated with MGO (2 mM) as described above. At time points of interest (typically 3 h and/or 24 h), an aliquot of the reaction mixture (10 µL) was diluted into 990 µL 20 mM PBS (pH 7.3, 100X dilution), briefly spun using a benchtop microcentrifuge, and further incubated in a 37 °C water bath for up to 48 additional hours. The resulting diluted reaction mixture was subjected to LC-MS analysis without any further dilution or purification.

3. Chapter 3:

Mechanistic Studies of AGE Formation

3.1. Introduction

Glycation describes the reaction between nucleophilic residues with sugars and sugar derived metabolites. Despite having a higher pK_a, Arg has been found to be modified more than Lys by reactive 1,2-dicarbonyls such as glyoxal and methylglyoxal (MGO) as glycating agents.[127,128] In particular, the reaction between Arg and MGO is known to produce numerous AGEs with distinct mass changes and/or isomeric AGEs at a given time points. Unlike AGEs like MGH-DH and CEA with a mass shift of [+72] associated with a single addition of MGO or MGH-1 with a single addition and a loss of water [+54], APY is a double addition product of Arg and 2 molecules of MGO. However, its mass change [+80] is not obvious and cannot easily be attributed to a loss or gain of water from 2 MGO molecules, which has led to several proposed mechanisms, including a reaction with Arg via MGO-derived reductone formation and THP and MGH-3 rearrangements via oxidative decarboxylation.[18,36,37] However, these reports focused on APY identification by comparison of synthetic APY samples formed under forcing reaction conditions to those found on MGO-treated proteins. Without any validation, these proposed mechanisms appear more consistent with synthetic approaches involving high-energy pathways that might not apply under physiological conditions.

Past work in our lab has shown that formation of specific AGEs depends largely on the primary sequence, which influences the surrounding chemical environment via the presence of nearby basic or acidic residues.[19,31,109] We have shown that several Arg-derived AGEs from MGO modification, like MGH-1, MGH-DH, and CEA, are mechanistically connected and can interconvert.[19] In particular, the presence of a nearby Tyr facilitates the elimination of MGH-DH to form MGH-1, and Tyr and Glu in the +2 and -2 positions, respectively, surrounding the central Arg exhibit a cooperative effect that bias MGH-1 formation. Besides recent efforts in our lab to

elucidate the mechanistic connection between these AGEs on a maturation pathway, virtually no other MGO-derived AGEs have been reported to interconvert with known chemical mechanistic information, despite the dynamic nature of glycation.

In this chapter, we build upon the peptide model system discussed in **Chapter 2** to determine sequence features that favor APY formation. We herein propose a new APY formation mechanism from [M+144] rearrangement that involves an initial retro-aldol step, ultimately generating formate as a byproduct, rather than an oxidative decarboxylation. Additionally, we show that CEA and [M+144] species can share a similar mechanistic pathway that leads to APY. We further demonstrate that the presence of a nearby Tyr can facilitate APY formation. Finally, our results reveal that phosphorylated Tyr or Ser residues can also facilitate APY formation, despite adding substantial negative charges that we have previously shown to inhibit glycation.[1,19,31]

3.2. Results

3.2.1. Reductone Formation and MGH-3 are not Precursors to APY

To begin, we sought to understand possible mechanisms through which this rearrangement could take place. The most cited APY formation mechanism involves the generation of a reductone from two MGO, which then reacts with Arg to form APY (**Figure 1.3**).[18] In this model, preincubation of MGO alone would be expected to generate the reductone, consequently leading to faster APY formation once added to peptide. We found that preincubation, even at strongly acidic pH and elevated temperatures, did not promote any change in AGE distributions or further APY formation upon addition to peptide **1**, indicating that APY is unlikely to be formed *via* the reaction between Arg and an MGO reductone (**Figures 3.1 & 3.2**).

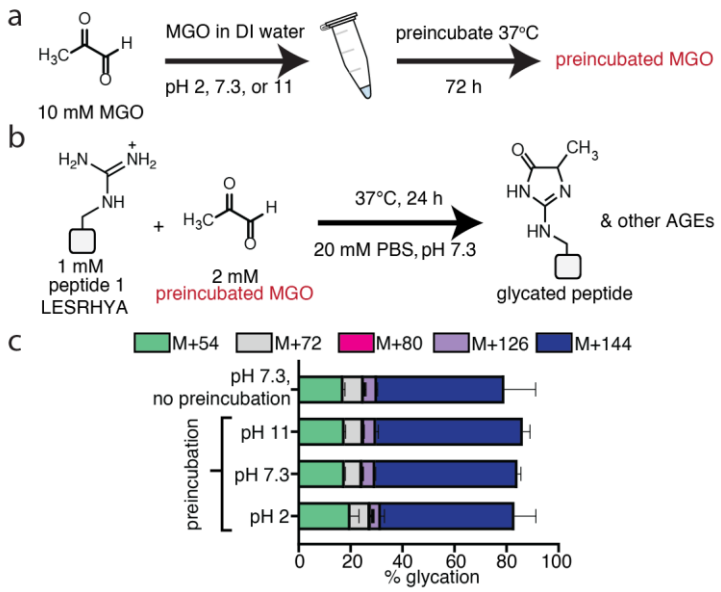

Figure 3.1. MGO Preincubation at Different pH does not generate APY. We preincubated MGO to see if this would facilitate APY formation by generating reductone prior to reaction with peptide. General scheme describing **(a)** the preincubation of MGO in ultrapure water at 37 °C, with pH adjusted to 2, 7.3, or 11, and **(b)** peptide glycation reactions using preincubated MGO. **(c)** Distribution of AGEs on MGO-treated peptide **1** after 24 h of incubation (n = 3). A control sample, labeled "no preincubation", was also performed for comparison.

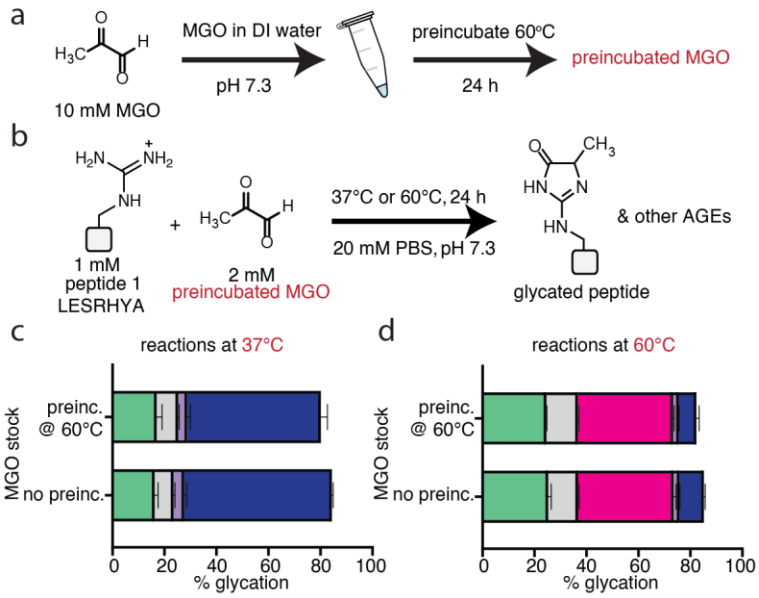

Figure 3.2. MGO Preincubation at Elevated Temperatures does not produce APY. As the formation of the previously proposed reductone intermediate could also be dependent on temperature, we preincubated MGO at an elevated temperature. General scheme describing **(a)** the preincubation of MGO in ultrapure water at 60 °C, in neutral pH and **(b)** peptide glycation reactions using preincubated MGO. **(c)** Distribution of AGEs on MGO-treated peptide **1** after 24 h of incubation at 37 °C (n = 3). **(d)** Distribution of AGEs on MGO-treated peptide **1** after 24 h of incubation at 60 °C (n = 3). In both conditions, a control sample, labelled "no preinc.", was also performed for comparison.

Additionally, we did not observe any evidence of reductone formation by NMR (**Figure 3.3**). These results are therefore inconsistent with reductone formation as a plausible model for APY formation in physiological conditions.

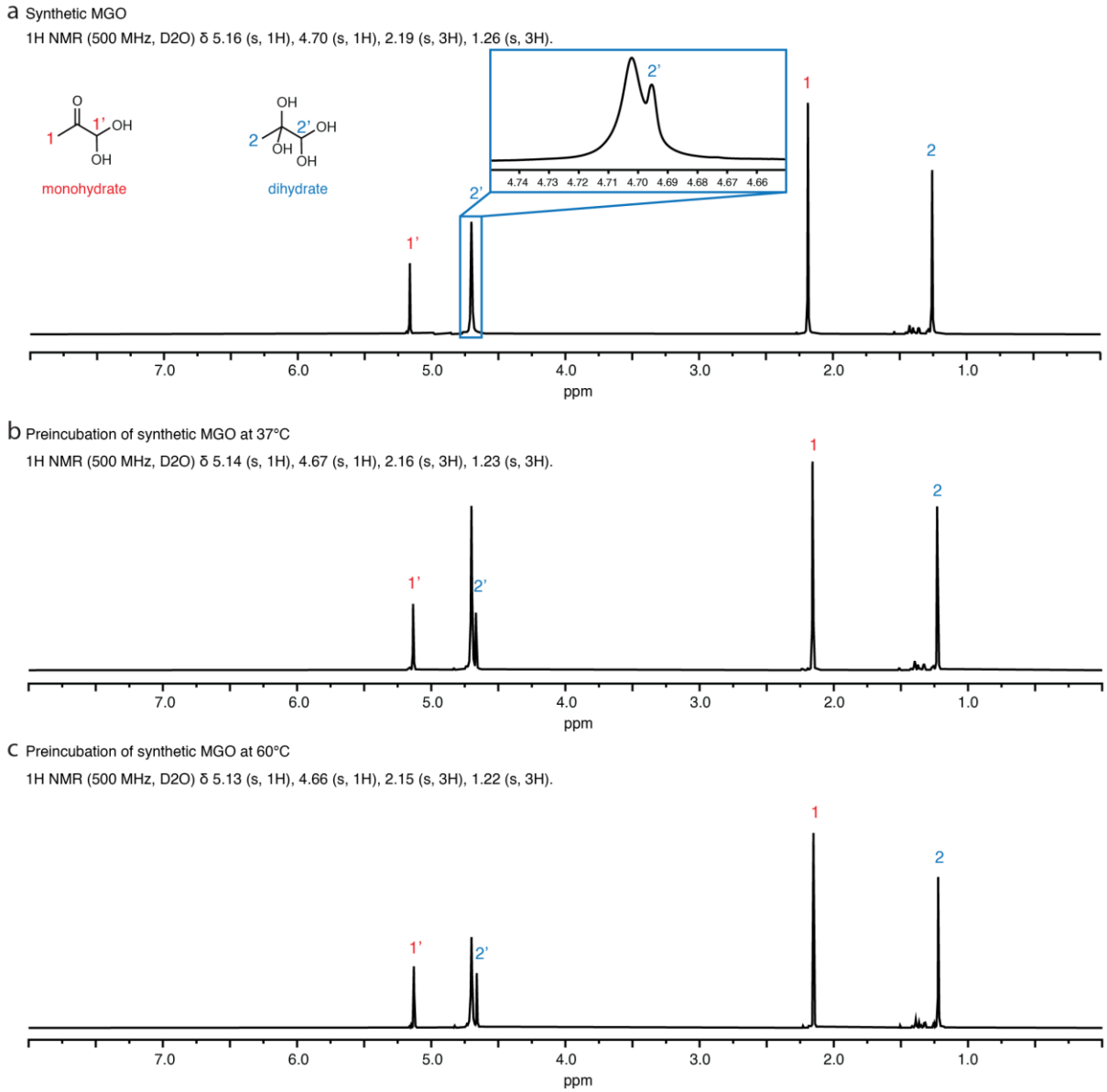

Figure 3.3. NMR Spectra do not show Reductone Formation by MGO Preincubation. (a) NMR spectrum of a fresh stock of synthetic MGO. **(b)** NMR spectrum of synthetic MGO following preincubation at 37 °C for 72 h. **(c)** NMR spectrum of synthetic MGO following preincubation protocol at 60 °C for 72 h. The peak with a shift of 4.7 corresponds to the solvent peak, sometimes not entirely resolvable with the aldehyde proton (labeled as "**2'**") peak of the dihydrate form. Monohydrate (red) and dihydrate (blue) forms of MGO were observed. A cluster of baseline peaks around 1.5 ppm region have been reported as a result of MGO polymerization.[129] Importantly, in both forms, the integration of the aldehyde proton (1H) peak (**1'** or **2'**) is one-third of that of the methyl proton (3H) peak (**1**, **2**). This would not be the case for the MGO reductone. The NMR spectra were observed to be identical before and after incubation, indicating no reductone formation.

Another proposed mechanism suggests that MGH-3 rearranges to form APY, presumably through oxidative decarboxylation.[37] However, our previous work shows that peptide **1** preferentially forms the MGH-1 isomer as confirmed by NMR, which we also confirmed in this study by matching the retention time (**Table 6.1**). As peptide **1** still forms APY, this suggests that MGH-3 is not a prerequisite for APY formation.[19]

3.2.2. THP does not rearrange into APY via Oxidative Decarboxylation

Previous proposals have hypothesized that THP rearranges to APY through a pathway involving oxidation, followed by decarboxylation and then dehydration (**Figure 1.3**).[37,100] To evaluate the feasibility of an oxidative decarboxylation from [M+144], we first sought to understand whether APY could form under O_2-free conditions. We scrupulously degassed all reaction components and used a glovebox to assemble and seal glycation reactions inside an N_2 sparged (O_2 < 4 ppm) scintillation vial that was further sealed prior to incubation (**Figure 3.4**). At 37 °C, despite slightly lowered overall glycation, AGE distributions remained unchanged when comparing O2-free samples to control samples. However, at 60 °C, virtually no difference in APY levels was observed between samples. Importantly, the resulting APY levels observed in both conditions were identical in the presence or absence of oxygen. Together, these data showed that APY formation from [M+144] rearrangement was not dependent on the presence of oxygen, suggesting that a formal oxidation step may not be required.

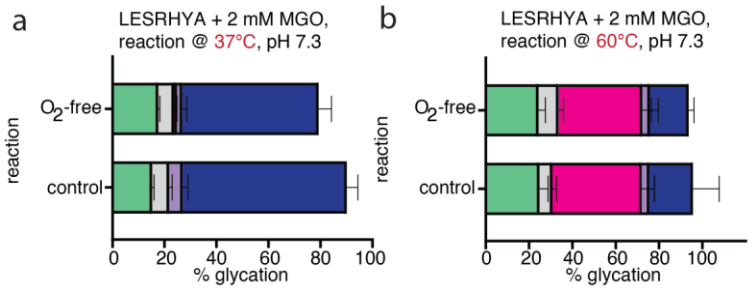

Figure 3.4. Oxygen is Not Required to Form APY. To investigate the role of oxygen in APY formation from THP and other [M+144] AGEs, we conducted glycation reactions with peptide **1** in the presence (control) or absence (O_2-free) of oxygen. Control samples followed our standard glycation protocols, without any degassing steps. **(a)** Distribution of AGEs on MGO-treated peptide **1** after 24 h of incubation at 37 °C (n = 3). **(b)** Distribution of AGEs on MGO-treated peptide **1** after 24 h of incubation at 60 °C (n = 3), showing virtually no difference in APY levels observed between samples.

However, our studies were performed using commercial sources of MGO, which may contain impurities. To see if any potential impurities were contributing to APY formation, we synthesized MGO using an established Riley oxidation protocol (**Figure 3.5**).[130] We found that there was no difference in APY formation between a freshly synthesized stock of MGO and commercial MGO. We also evaluated the role of buffer and salt concentrations and found negligible differences in APY levels (**Figure 3.6**).

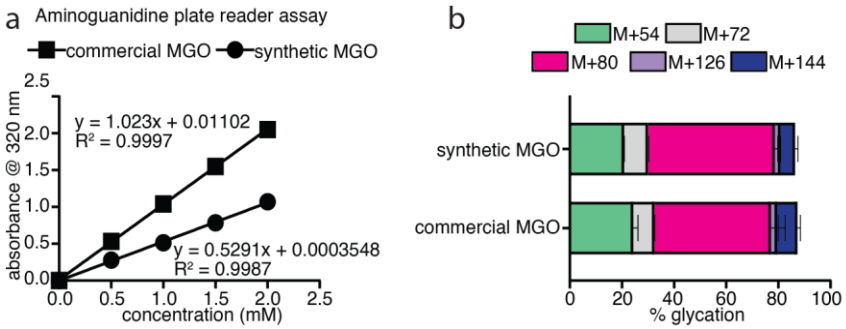

Figure 3.5. Synthetic and Commercial MGO Sources both generate APY. As our glycation reactions used commercial MGO, which may contain impurities, we aimed to investigate whether APY formation was affected by the use of commercial MGO compared to a freshly synthesized stock of MGO. **(a)** Following the successful synthesis of MGO, an aminoguanidine assay was performed to correct for any differences in MGO concentrations between the two sources using the slope of the calibration curve. **(b)** Distribution of AGEs on MGO-treated peptide **1** after 24 h of incubation at 60 °C (n = 3). These results showed no differences in APY levels or AGE distributions between samples, confirming that APY formation remained unaffected by either source of MGO used.

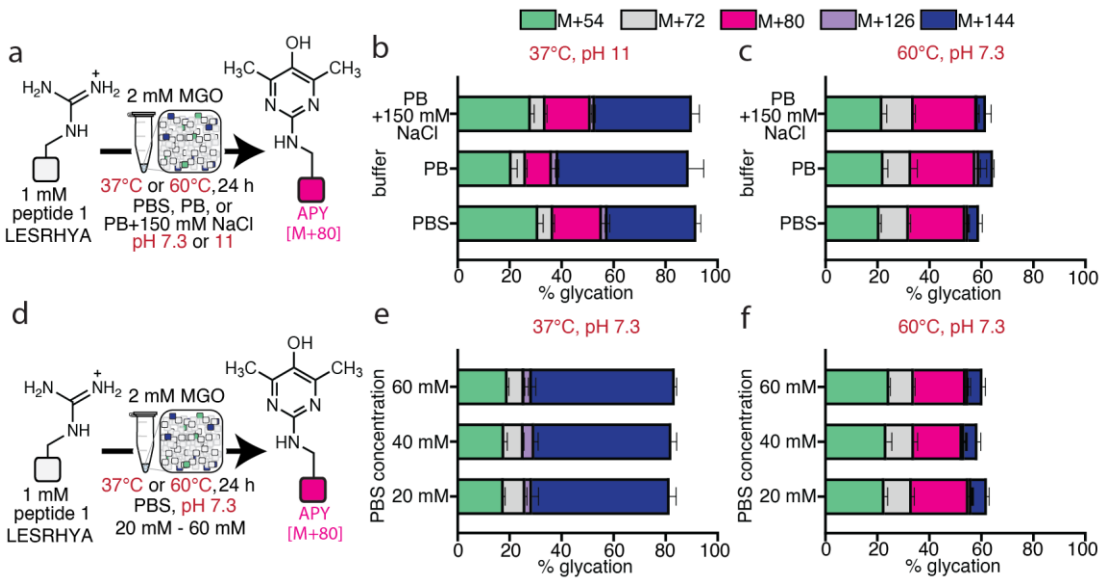

Figure 3.6. Phosphate Buffer and Salt Concentrations do not impact APY formation. To evaluate how phosphate concentration and buffer salts affected APY formation, we performed a series of controls using peptide **1**. **(a)** General scheme describing glycation reactions of peptide **1** using differently prepared buffers (24 h incubation, 37 °C or 60 °C, pH 7.3). Buffers used included a commercial phosphate buffered saline (PBS, which contained 100 mM sodium phosphate and 150 mM sodium chloride), phosphate buffer (PB) which was prepared in-house by adding calculated amounts of monobasic monohydrate and dibasic sodium phosphate in ultrapure water, and phosphate buffer with 150 mM NaCl (PB + 150 mM NaCl). **(b)** Distribution of AGEs on MGO-treated peptide **1** after 24 h of incubation at 37 °C (n = 3). **(c)** Distribution of AGEs on MGO-treated peptide **1** after 24 h of incubation at 60 °C (n = 3). **(d)** General scheme describing glycation of peptide **1** at standard reaction conditions using PBS at varied concentrations of 20 mM, 40 mM, and 60 mM. **(e)** Distribution of AGEs on MGO-treated peptide **1** after 24 h of incubation at 37 °C (n = 3). **(c)** Distribution of AGEs on MGO-treated peptide **1** after 24 h of incubation at 60 °C (n = 3). These results demonstrate that salt and buffer concentration had hardly any effects on APY formation.

3.2.3. A Proposed Mechanism for APY Formation *via* Retro-Aldol Reactions

As we could not attribute the source of oxidation required in the previously proposed mechanism, we considered other potential mechanisms in which THP—or other [M+144] species—could rearrange to form APY. Beginning from THP, we identified a possible pathway (**Figure 3.7**) in which initial deprotonation of the hydroxyl group at C5 promotes a retro-aldol ring opening (**Figure 3.7**, *blue path)*. Next, hydration of the aldehyde followed by deprotonation generates a geminal enediol at C5, followed by subsequent ring closure and another dehydration and retro-aldol step to generate the pyrimidine ring (**Figure 3.7**, *pink path*). This proposed mechanism generates formic acid as a byproduct.

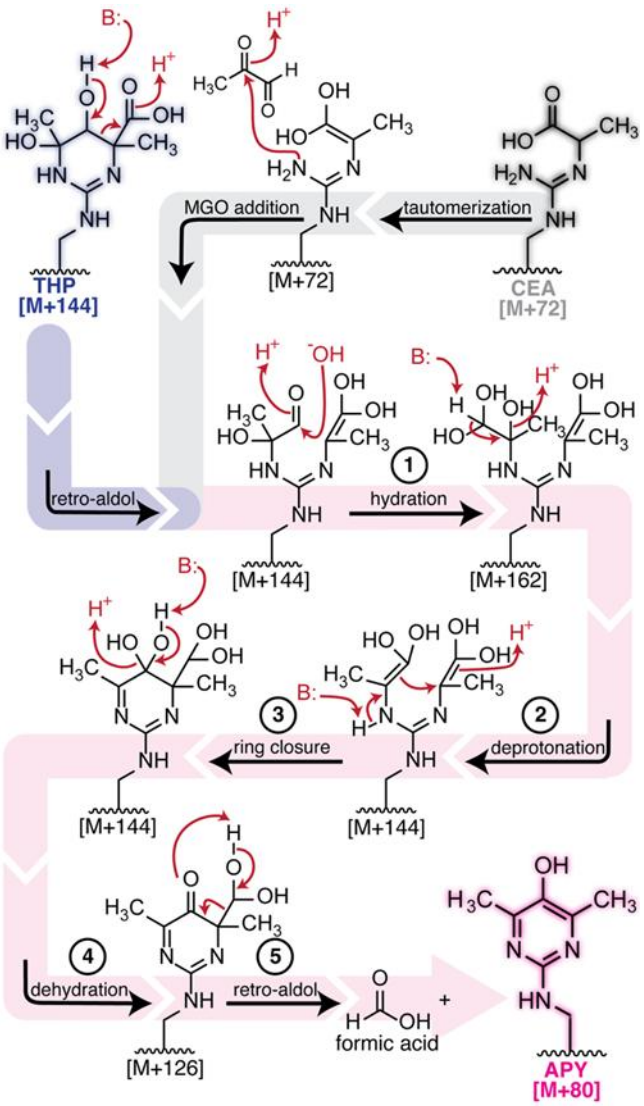

Figure 3.7. Proposed Mechanism for APY Formation. We propose that THP can rearrange into APY *via* a retro-aldol step (*blue path*), followed by hydration **(1)**, then deprotonation **(2)** and ring closure **(3)**, another dehydration step **(4)**, and finally a retro-aldol step **(5)** that also releases formic acid as a byproduct (*pink path*). Alternatively, it is likely that other [M+144] species could also rearrange into APY. Here we propose an alternate pathway, beginning from CEA (*gray path*), which involves tautomerization and addition of a second MGO equivalent to reach a common [M+144] intermediate along the APY formation pathway.

Supporting this proposal, we used an enzyme coupled assay to detect formic acid in reactions of peptide **1** with 2 mM MGO after 24 h (**Figure 3.8**). Our results indicate that formic acid is a byproduct of APY formation, as more formic acid was detected as APY formed on peptide **1** under our standard glycation conditions. However, we also found that formic acid generation is not necessarily exclusive to APY, since we also detected formic acid when MGO

was incubated with another sequence, (Ac-LDDREDA), that exhibited no detectable APY formation.

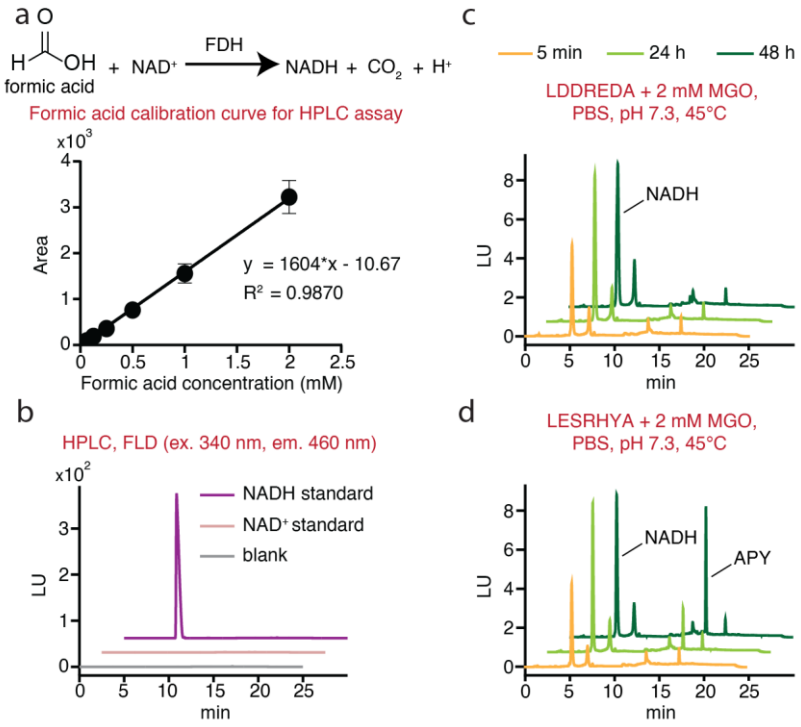

Figure 3.8. Detection of Formic Acid during Glycation Reactions. Our proposed mechanism shows formic acid as a byproduct of [M+144] rearrangement. Therefore, we aimed to identify formic acid using a formic acid assay kit purchased from Megazyme. Briefly, formate dehydrogenase (FDH) was used to detect formic acid in samples by converting NAD^+ to NADH, the fluorescence wavelengths of which was measured using HPLC equipped with a fluorescence detector (ex = 340 nm, em = 460 nm).[131] **(a)** General scheme depicting the assay design, and the calibration curve obtained using a formic acid standard (n = 3). **(b)** HPLC chromatogram of the working assay using NADH and NAD^+ standards, showing NADH fluorescence signal (ex = 340 nm, em = 460 nm) that was not observed in the NAD^+ sample. The retention time of NADH was observed around 5 min. **(c) & (d)** HPLC chromatograms of MGO-treated peptide LDDREDA (upper right) and peptide **1** (lower right) under standard glycation reaction conditions (24 h incubation, 45 °C, pH 7.3). 45 °C was chosen as the reaction temperature because at this temperature, we expected peptide **1** to produce observable APY signals, hence NADH signals, while this would not be the case for peptide LDDREDA. While higher concentration of formic acid was detected in 24 h reactions of peptide **1** with 2 mM MGO, similar concentrations of formic acid were observed when compared between peptide **1** and LDDREDA which had significantly less APY under the same condition. These results indicate that while formic acid may be a byproduct of our proposed mechanism, it is likely not exclusive to APY formation.

3.2.4. CEA might be a Precursor to APY

Just like THP, APY formation requires two moieties of MGO to react with an Arg side chain.[1,14,18] Our proposed mechanism involves an intermediate that includes a tautomer of CEA

on one of the Arg Nω, allowing us to hypothesize that CEA could also be a precursor to APY. To evaluate this idea, we purified CEA and MGH-1 modified peptide **1** (peptides $\mathbf{1}^{\mathbf{CEA}}$ and $\mathbf{1}^{\mathbf{MGH\text{-}1}}$, respectively). At pH 7.3, without any additional MGO added, we observed only modest conversion from $\mathbf{1}^{\mathbf{MGH\text{-}1}}$ to $\mathbf{1}^{\mathbf{CEA}}$ with little degradation to peptide **1**, consistent with our previous results.[19] Since peptide **1** does not form MGH-3 under our standard glycation reaction conditions, we do not rule out the possibility that MGH-3 can rearrange to form APY. However, upon treatment with additional equivalents of MGO, we found that peptide $\mathbf{1}^{\mathbf{CEA}}$ produced APY (**Figure 3.9**). This suggests that another source of the [M+144] precursor to APY could be due to an additional MGO modification of CEA. This alternate pathway (**Figure 3.7**, *gray path*) shares a common intermediate with the one that formally begins with THP.

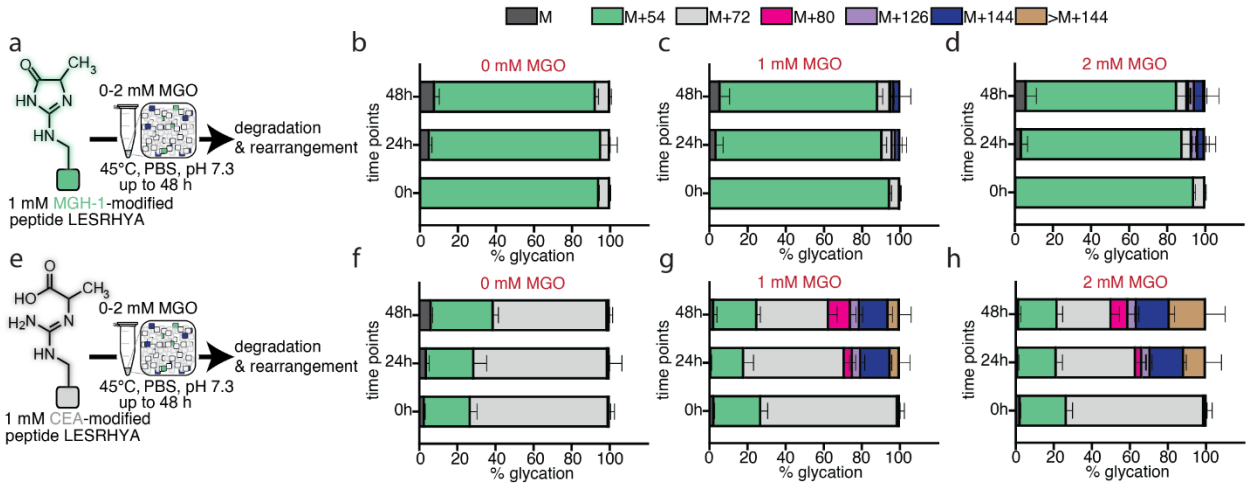

Figure 3.9. CEA is also a Precursor for APY. In order to test this hypothesis, we reacted peptide **1** to form CEA ($\mathbf{1}^{\mathbf{CEA}}$) and MGH-1 ($\mathbf{1}^{\mathbf{MGH\text{-}1}}$) and purified these AGE-modified peptides. Due to coelution, peptide $\mathbf{1}^{\mathbf{CEA}}$ contained 20% MGH-1 and 80% CEA. **(a) & (e)** General schemes describing the experimental procedure of glycation reactions on MGO-treated peptide $\mathbf{1}^{\mathbf{MGH\text{-}1}}$ (upper left) and peptide $\mathbf{1}^{\mathbf{CEA}}$ (lower left) at 0 h, 24 h, and 48 h of incubation (45 °C, pH 7.3). The reaction temperature was set at 45 °C to expedite APY formation. **(b) & (f)** Distributions of AGEs on peptide $\mathbf{1}^{\mathbf{MGH\text{-}1}}$ (upper) and peptide $\mathbf{1}^{\mathbf{CEA}}$ (lower) without MGO (0 mM) after 24 h of incubation at 45 °C (n = 3). **(c) & (g)** Distributions of AGEs on peptide $\mathbf{1}^{\mathbf{MGH\text{-}1}}$ (upper) and peptide $\mathbf{1}^{\mathbf{CEA}}$ (lower) treated with 1 mM MGO after 24 h of incubation at 45 °C (n = 3). **(d) & (h)** Distributions of AGEs on peptide $\mathbf{1}^{\mathbf{MGH\text{-}1}}$ (upper) and peptide $\mathbf{1}^{\mathbf{CEA}}$ (lower) treated with 2 mM MGO after 24 h of incubation at 45 °C (n = 3). Upon treatment with MGO, only peptide $\mathbf{1}^{\mathbf{CEA}}$ was observed with APY at 24 h and 48 h, confirming our hypothesis that CEA is another potential precursor for APY.

3.2.5. APY Formation requires a General Base

To further evaluate the feasibility of our proposed mechanism, we predicted that a general base would be necessary for the initial deprotonation step that promotes ring opening, as well as for subsequent ring closure and dehydration (**Figure 3.7**). Using a pH scan, we found that APY levels increased between pH 7.3–11 (**Figure 3.10 A, B**). There was a particularly large jump in APY levels between pH 10 (3.3 ± 1.4 %) and pH 11 (20.3 ± 1.1 %), prompting us to conduct a narrower pH scan at 0.2 increments between pH 10 and 11. In this range, we found that APY levels increased steadily, peaking at pH 11 (20.3 ± 1.1 % of total glycation) (**Figure 3.10 C & Figure 3.11**). There was a sharp transition between pH 10.2 and 10.4, suggesting a strong correlation with the protonation state of the nearby Tyr residue (pK_a 10.3).[132–134] As a control, we also synthesized a variant of peptide **1** that replaced Tyr with Phe (peptide $\mathbf{1^{Phe}}$). Compared to peptide **1**, peptide $\mathbf{1^{Phe}}$ produced substantially less glycation overall and less APY formation (**Figure 3.12**). These results suggest that, for peptide **1**, Tyr plays an active role in the APY formation mechanism.

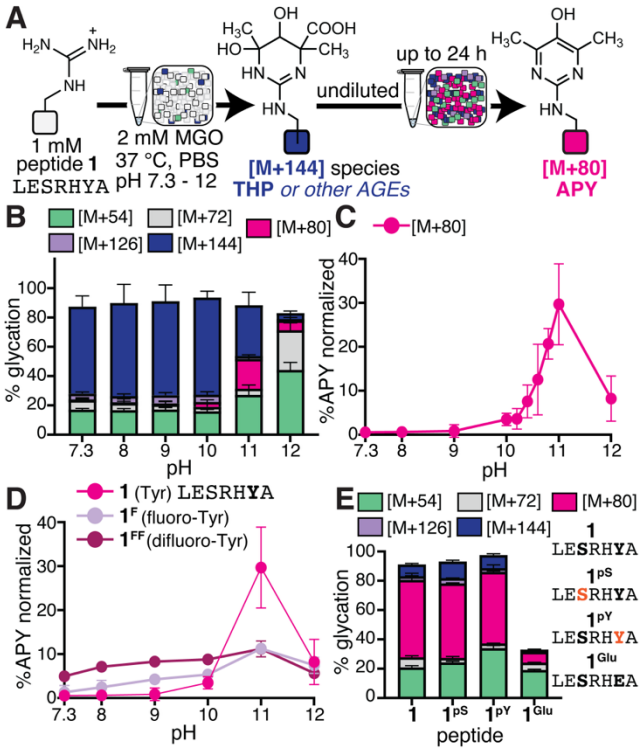

Figure 3.10. A Nearby General Base Facilitates the Rearrangement of [M+144] into APY. (A) General scheme depicting a pH scan used to evaluate the features that promote APY formation. Peptide **1** (1 mM) was treated with 2 mM MGO using pH-adjusted phosphate buffered saline (PBS) in a pH range of 7.3—12. The reaction was incubated for 24 h undiluted at 37 °C. **(B)** Stacked bar graphs showing AGE distributions, as assessed by liquid chromatography-mass spectrometry (LC-MS) analysis. **(C)** Between pH 10 and 11, we observed a marked jump in APY [M+80] (magenta) levels, as shown by proportional APY levels that were normalized to the total amount of glycation observed for MGO-treated peptide **1** across a narrower pH range between pH 10 and 11 at 0.2 increments. **(D)** To further test the hypothesis that Tyr phenoxide plays an active role in APY formation, we conducted glycation reactions on variants of peptide **1**, including peptide $\mathbf{1}^{\mathbf{F}}$ (fluoro-Tyr in lieu of Tyr) and peptide $\mathbf{1}^{\mathbf{FF}}$ (difluoro-Tyr in lieu of Tyr). Here, proportional APY levels were normalized to the total amount of glycation to account for differences in total glycation. At pH 7.3 and 37 °C, % APY was the greatest for peptide $\mathbf{1}^{\mathbf{FF}}$ (pK_a 7.2), followed by peptide $\mathbf{1}^{\mathbf{F}}$ (pK_a 8.4), and then peptide **1** (pK_a 10.3), consistent with our hypothesis. **(E)** Stacked bar graphs showing AGE distributions for glycation reactions with peptide **1**, peptide $\mathbf{1}^{\mathbf{pS}}$ (pSer in place of Ser, pK_{a2} 5.6), peptide $\mathbf{1}^{\mathbf{pY}}$ (pTyr in place of Tyr, pK_{a2} 5.9), and peptide $\mathbf{1}^{\mathbf{Glu}}$ (Glu in place of Tyr) at pH 7.3 and 60 °C (24 h incubation) (n≥3 for all reactions). Despite the introduction of up to two negative charges which has been reported to hamper glycation, absolute APY levels and total glycation levels remained virtually identical for the phosphorylated variants. Together, these results demonstrate the importance of a nearby general base to facilitate APY formation and suggest that nearby phosphorylated residues can also aid glycation.

To test the hypothesis that Tyr phenoxide facilitates APY formation, we synthesized variants of peptide **1** that incorporated noncanonical Tyr derivatives with lowered phenolic pK_a's. Specifically, 3-fluorotyrosine (peptide $\mathbf{1}^{\mathbf{F}}$) and 3,5-difluorotyrosine (peptide $\mathbf{1}^{\mathbf{FF}}$) were chosen because of their pK_a values (8.4 and 7.2, respectively) (**Figure 3.10 D**).[135] These peptides were reacted with 2 mM MGO across a range of pH between 7.3 and 12 (**Figure 3.10 D & Figure**

3.11), revealing maximal APY levels at pH 11 for all three peptides. Overall glycation was seen to decrease as more F was substituted on Tyr, which was expected as clustered negative charges impeded glycation. For reactions with peptide $\mathbf{1^{FF}}$, MGH-1 was now the predominant AGE instead of [M+144]. This observation was also consistent with previous work done in our lab on chlorinated peptide **1**.[19] The distribution of APY across the pH range between 7.3 and 12 exhibited the same trend, with the highest amount of [M+80] observed at pH 11 for all three peptides. Between pH 7.3 and 10, % APY (both absolute and normalized) in peptide $\mathbf{1^{FF}}$ was the highest, followed by peptide $\mathbf{1^{F}}$, then peptide **1**. However, when normalized to account for differences in total glycation levels, we found that proportional APY levels at pH 7.3 were greatest for peptide $\mathbf{1^{FF}}$ (5.0 ± 0.3%), followed by $\mathbf{1^{F}}$ (1.3 ± 1.5%), and then peptide **1** (0.6 ± 0.4%) (**Figure 3.11**). In order to further confirm the role of Tyr as a general base that can facilitate APY formation on peptide **1**, we also investigated two other variants of peptide **1** that incorporated a negatively charged residue Glu (peptide $\mathbf{1^{Glu}}$) and a non-polar residue Phe (peptide $\mathbf{1^{Phe}}$) in place of Tyr. Upon treatment with 2 mM MGO at 60 °C for 24 h, both peptide $\mathbf{1^{Glu}}$ and $\mathbf{1^{Phe}}$ expectedly exhibited less overall glycation and APY formation than peptide **1**, confirming the significance of Tyr on peptide **1** as a facilitator for APY formation. Together, these results demonstrate the importance of the nearby Tyr as a facilitator for [M+144] rearrangement into APY, matching our hypothesis that Tyr can act as a general base that facilitates APY formation.

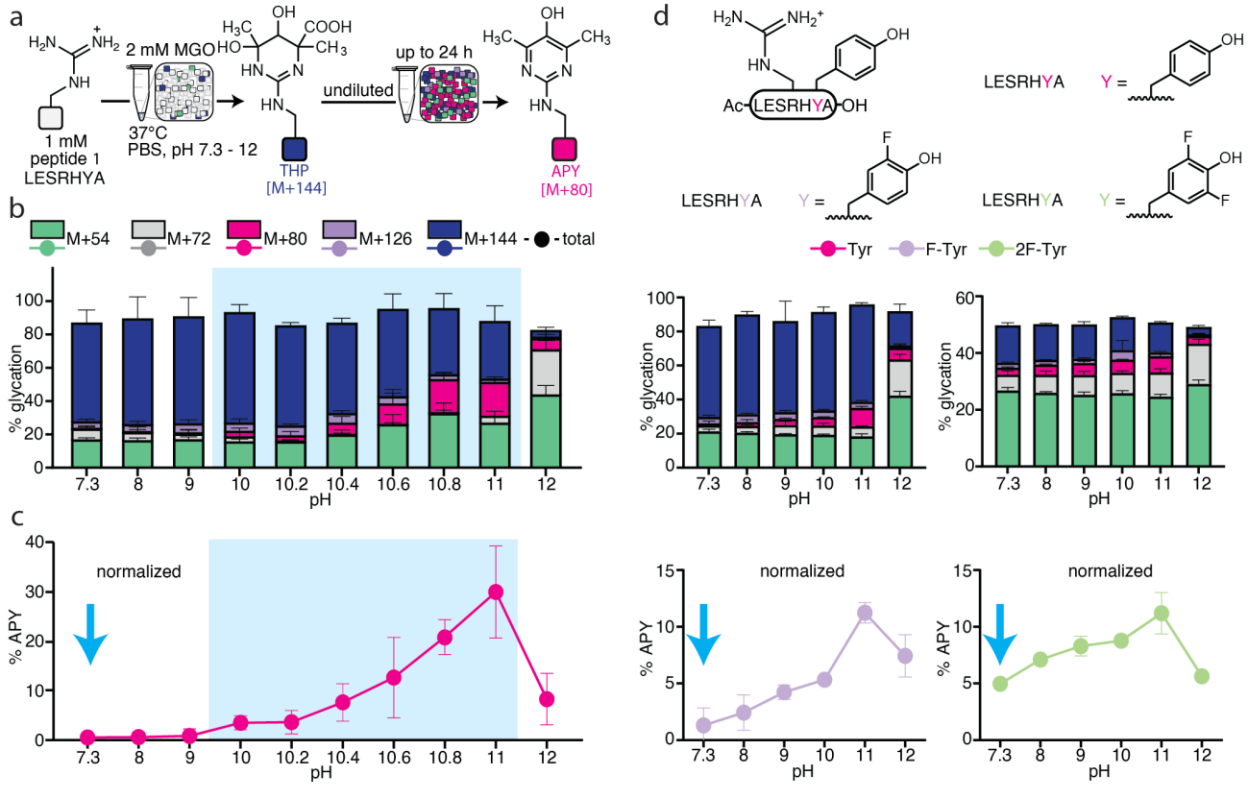

Figure 3.11. MGO Treatments of Fluorinated Variants of Peptide 1. To test the hypothesis that a nearby Tyr facilitates APY formation, we synthesized variants of peptide **1** that incorporated noncanonical Tyr derivatives with lowered pKa values. Specifically, 3-fluorotyrosine (peptide $\mathbf{1}^{\mathbf{F}}$) and 3,5-difluorotyrosine (peptide $\mathbf{1}^{\mathbf{FF}}$) were chosen because of their pKa values (8.4 and 7.2, respectively) in comparison with the pKa of Tyr (10.3).[135] **(a)** General scheme describing the experimental procedure of a pH screening of glycation reactions on MGO-treated peptide **1** using PBS buffer with pH in a range of 7.3—12 (37 °C, 24 h incubation). **(b)** Distribution of AGEs on MGO-treated peptide **1** after 24 h of incubation at 37 °C (pH 7.3—12). A short pH scan (in the blue box) was also performed for reactions between pH 10—11 in increments of 0.2 (n≥3 for all reactions). **(c)** % APY was normalized to % total glycation. We observed a sharp transition in APY levels between pH 10.2 and 10.4, suggesting Tyr plays an active role in APY formation. **(d)** Distributions of AGEs on MGO-treated peptide $\mathbf{1}^{\mathbf{F}}$ and peptide $\mathbf{1}^{\mathbf{FF}}$ after 24 h of incubation at 37 °C (pH 7.3—12) (center) and % APY for these reactions when normalized to % total glycation (lower). These results demonstrated the importance of the nearby Tyr as a facilitator for [M+144] rearrangement into APY. This matches our hypothesis that the presence of a nearby Tyr can fulfill the role of a general base according to our proposed mechanism.

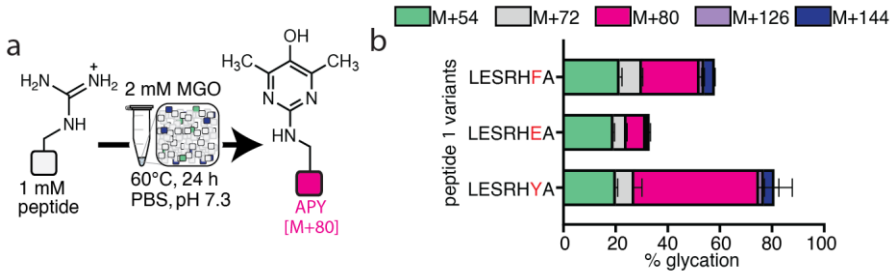

Figure 3.12. Replacing the Tyr with Glu and Phe on Peptide 1 reduced Glycation and APY Formation. (a) General scheme describing the experimental procedure of glycation reactions on MGO-treated peptide **1**, $\mathbf{1}^{\mathbf{Glu}}$, and $\mathbf{1}^{\mathbf{Phe}}$ at 60 °C (pH 7.3, 24 h incubation) (n = 3). **(b)** Distribution of AGEs on MGO-treated peptide **1**, $\mathbf{1}^{\mathbf{Glu}}$, and $\mathbf{1}^{\mathbf{Phe}}$. Upon treatment with 2 mM MGO at 60 °C for 24 h, both peptide $\mathbf{1}^{\mathbf{Glu}}$ and $\mathbf{1}^{\mathbf{Phe}}$ expectedly exhibited less overall glycation and APY formation than peptide **1**, confirming the importance of Tyr on peptide **1** as a facilitator for APY formation.

3.2.6. Phosphorylated Residues promote Equivalent APY Levels despite introducing Additional Negative Charges

Following the same logic as described above, we next considered if phosphorylated Tyr—or perhaps even Ser or Thr—might also act as a general base promoting APY formation. Phosphorylated Tyr has experimental pK_{a2} values ranging between 4.0 to 6.1.[136] Thus, we synthesized peptide $\mathbf{1^{pY}}$ that contains pTyr in place of Tyr. After glycation with 2 mM MGO at pH 7.3 at 60 °C for 24 h, there were hardly any differences in total glycation and APY levels between peptide **1** (52.8 ± 4.5 % [M+80] at 24 h) and $\mathbf{1^{pY}}$ (48.8 ± 0.6 % [M+80] at 24 h) (**Figure 3.10 E & Figure 3.13**). We performed a similar set of experiments using a peptide **1** variant with phosphorylated Ser (peptide $\mathbf{1^{pS}}$) and found that these also produced comparable levels of glycation (50.9 ± 0.3%) after 24 h, despite the addition of up to two negative charges (**Figure 3.10 E & Figure 3.13**). However, MGH-1 levels of peptide $\mathbf{1^{pS}}$ and $\mathbf{1^{pY}}$ were slightly higher than those of peptide **1**. This observation is consistent with our previous report on MGH-1 formation, which can be facilitated by a nearby Tyr residue acting as a general base. In the case of peptide $\mathbf{1^{pS}}$, both pSer and Tyr can fulfill this role. When introducing up to four negative charges on a doubly-phosphorylated peptide $\mathbf{1^{pSpY}}$, overall glycation and APY levels decreased, but MGH-1 levels remained as the predominant adduct across all time points. In contrast, the variant of peptide **1** that replaced Tyr with Glu (peptide $\mathbf{1^{Glu}}$) exhibited substantially less overall glycation and APY formation than peptide **1** and all of its other phosphorylated variants (**Figure 3.10 E & Figure 3.12**). Therefore, these results further support our proposal that a general base, such as Tyr or pSer, can be critical for APY formation, despite the inhibitive effects of negative charges on glycation.

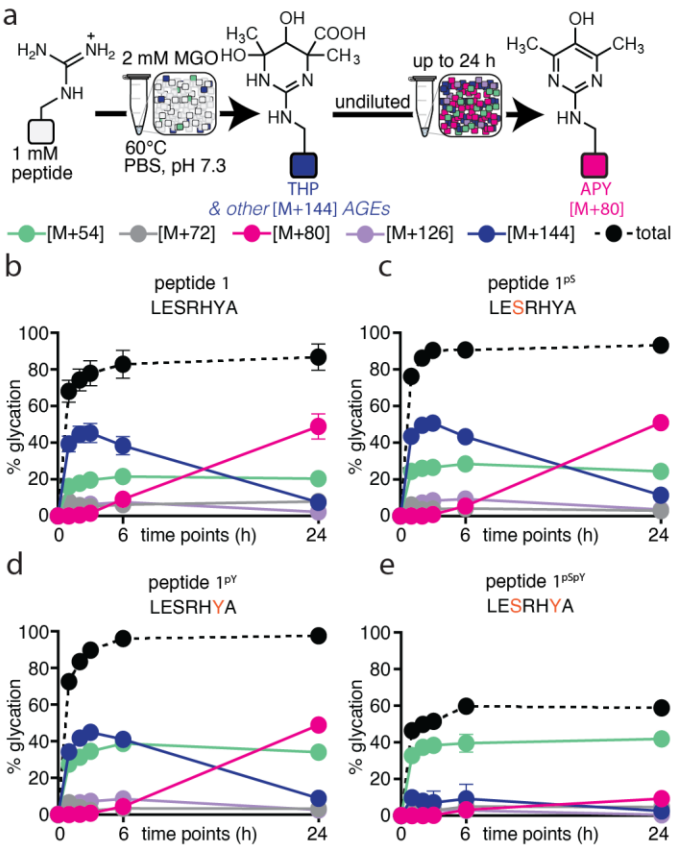

Figure 3.13. Phosphorylated Amino Acids bias Certain AGE Formation at Elevated Temperatures. To investigate the effect of phosphorylation on APY formation, we synthesized peptide **1**$^{\mathbf{pS}}$ (a variant of peptide **1** containing pSer in lieu of Ser), peptide **1**$^{\mathbf{pY}}$ (pTyr in lieu of Tyr), and peptide **1**$^{\mathbf{pSpY}}$ (containing both pSer and pTyr). **(a)** General scheme describing the experimental procedure of glycation reactions on MGO-treated peptide **1**, **1**$^{\mathbf{pS}}$, **1**$^{\mathbf{pY}}$, and **1**$^{\mathbf{pSpY}}$ at 60 °C (pH 7.3, 24 h incubation). Time points were taken at 0 h, 1 h, 2 h, 3 h, 6 h, and 24 h to monitor changes in AGE distributions. **(b)** Distribution of AGEs on MGO-treated peptide **1**. **(c)** Distribution of AGEs on MGO-treated peptide **1**$^{\mathbf{pS}}$. **(d)** Distribution of AGEs on MGO-treated peptide **1**$^{\mathbf{pY}}$. **(e)** Distribution of AGEs on MGO-treated peptide **1**$^{\mathbf{pSpY}}$. (n = 3 for all reactions). There was no difference in AGE distributions and no noticeable difference in APY levels between peptide **1**, **1**$^{\mathbf{pS}}$, and **1**$^{\mathbf{pY}}$, despite the introduction of up to two negative charges. These observations also support our proposal that a general base, such as Tyr or pSer, can be critical for APY formation, counteracting the hampering effects of negative charges on glycation.

To further examine this behavior, we evaluated the glycation of peptides **1**, **1**$^{\mathbf{pY}}$, **1**$^{\mathbf{pS}}$, and **1**$^{\mathbf{pSpY}}$ at 37 °C, over time (**Figure 3.14**). Supporting our findings at 60 °C, these studies showed APY levels to be similar across all times for peptides **1**, **1**$^{\mathbf{pY}}$, and **1**$^{\mathbf{pS}}$. However, MGH-1 levels were noticeably increased—especially at earlier times—for the phosphorylated substrates. Additionally, introduction of up to two negative charges on peptide **1**$^{\mathbf{pY}}$ and **1**$^{\mathbf{pS}}$ did not affect overall glycation but led to increased MGH-1 formation. However, at both lower and elevated

temperatures, the introduction of four negative charges on peptide **1**$^{\mathbf{pSpY}}$ decreased overall glycation (**Figures 3.13 & 3.14**).

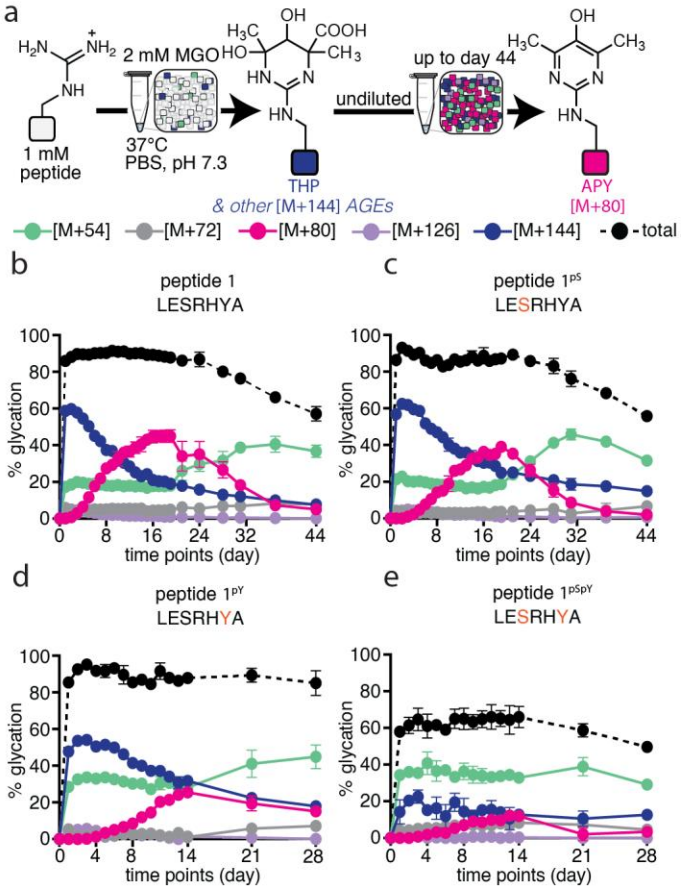

Figure 3.14. Phosphorylated Amino Acids bias Certain AGE Formation at Physiological Temperature. We extended our glycation experiments with peptide **1**, **1**$^{\mathbf{pS}}$, **1**$^{\mathbf{pY}}$, and **1**$^{\mathbf{pSpY}}$ described in **Figure 3.10.** and **Figure 3.13.** up to 44 days of incubation for peptide **1** and **1**$^{\mathbf{pS}}$, 28 days for peptide **1**$^{\mathbf{pY}}$ and peptide **1**$^{\mathbf{pSpY}}$ at 37 °C. **(a)** General scheme describing the experimental procedure of glycation reactions on MGO-treated peptides at 37 °C (pH 7.3). Time points were taken every 24 h for the first 14 days (19 days for peptide **1** and **1**$^{\mathbf{pS}}$), then on day 21, 24, and 28 (and on day 31, 37, and 44 for peptide **1** and **1**$^{\mathbf{pS}}$). **(b)** Distribution of AGEs on MGO-treated peptide **1**. **(c)** Distribution of AGEs on MGO-treated peptide **1**$^{\mathbf{pS}}$. **(d)** Distribution of AGEs on MGO-treated peptide **1**$^{\mathbf{pY}}$. **(e)** Distribution of AGEs on MGO-treated peptide **1**$^{\mathbf{pSpY}}$ (n = 2 for peptide **1**$^{\mathbf{pS}}$ reactions collected on day 9 & 31; n = 2 for peptide **1** reactions collected on day 37; n = 2 for peptide **1**$^{\mathbf{pSpY}}$ reactions collected on day 6; n = 3 for all other reactions). There was no difference in AGE distributions and no noticeable difference in APY levels between peptide **1** and **1**$^{\mathbf{pS}}$, despite the introduction of up to two negative charges. However, the introduction of four negative charges on peptide **1**$^{\mathbf{pSpY}}$ decreased overall glycation.

Specifically, we found that APY levels for both peptide **1** and **1**$^{\mathbf{pS}}$ peaked on day 19 and gradually decreased for the remaining time in this study (**Figure 3.14 B, C**). Interestingly, MGH-

1 levels remained mostly unchanged in the first 15 days, then gradually increased and peaked on day 31, and decayed steadily for the remaining time in this study. These observations are consistent with previous reports, citing that MGH-1 is a stable AGE.[34,37] As MGH-1 levels started to increase on day 16, we noticed that APY levels also began to decrease and [M+144] continued to decrease, suggesting a mechanistic correlation between these three AGEs. While MGH-1 levels significantly increased for peptide $\mathbf{1^{pY}}$ and peptide $\mathbf{1^{pSpY}}$ at earlier time points and remained fairly constant throughout the incubation period, MGH-1 was the predominant AGE at all time points for only peptide $\mathbf{1^{pSpY}}$ despite the lowered overall glycation due to four negative charges (**Figure 3.14 D, E**). These results suggest that for peptide $\mathbf{1^{pSpY}}$, phosphorylated residues bias MGH-1 formation over APY formation (**Figure 3.14 E**). Interestingly, we also noticed a continuous decay of an unknown adduct [M+126], though this adduct was observed consistently in low quantities (< 5%). In our proposed mechanism, this mass change potentially corresponds to an intermediate undergoing the final retro-aldol step to release formic acid and generate APY.

Our previous work has unambiguously shown that multiple negative charges surrounding glycation sites greatly impair AGE formation (**Figure 3.10 E**).[19,31,137] Therefore, these observations suggested to us that nearby phosphates may exert a positive influence on AGE formation, thereby counteracting any attenuation from their negative charges. Accordingly, these results imply that nearby phosphorylation may be helpful for glycation, and based on our proposed mechanism, could be particularly important for APY formation in a cellular context.

3.3. Discussion

In this chapter, we have ruled out past proposed mechanisms of APY formation by testing several key hypotheses that these mechanisms rely on. In addition, we proposed a new chemical

mechanism through which APY arises under physiological conditions that releases formic acid as a byproduct and experimentally validated this mechanism. We are the first to show that THP might not be the only [M+144] precursor to APY, observing that CEA can also participate in the same rearrangement pathway to generate another [M+144] species. We have also shown that primary sequence plays an important role in APY formation by demonstrating that the presence or absence of nearby polar and/or ionizable residues, including phosphorylated residues, significantly impact APY levels. Taken together, our studies not only reveal and validate, for the first time, a chemical mechanism for APY formation that occurs under physiological condition, but also confirm features in the surrounding microenvironment that enable this reaction. We further uncover a previously unknown potential of phosphorylated residues for glycation that can be particularly important in a cellular context.

In particular, our proposed mechanism relies on fundamental concepts of organic chemistry and provides concrete experimental evidence that reconciles several previous, conflicting mechanisms proposed for APY. While others have suggested that THP is a precursor to APY, our newly proposed mechanism circumvents the need for an unexplained, mysterious oxidation step by recognizing that THP possesses a β-hydroxycarbonyl, a common feature in retro-aldol substrates. Indeed, the retro-aldol reaction is one of the most important organic reactions in sugar fragmentations, including those in physiological systems.[138–140] Several known retro-aldol enzymes use Tyr as a general base,[141–143] which aligns with our results showing noncanonical Tyr variants with decreased phenolic pK_a to promote APY formation. However, we also identify a potential alternative pathway involving highly plausible [M+144] intermediates other than THP. While we cannot definitively confirm all steps in our proposed mechanism, it is fully consistent with our experimental results ruling out other previously proposed alternatives.

Additionally, we note that most steps are precedented in biological systems, including the retro-aldol reaction[138–140] and tautomerization of hydrated aldehyde consistent with glyoxalase activity.[77,144–146]

Our mechanism also connects APY formation to the emancipation of formate, a major reactive species in one-carbon metabolism that is involved in numerous biological processes.[147–149] While there has been some prior work connecting the metabolic processing of MGO to formate generation,[150–154] our results suggest that cellular glycation events themselves, including but not limited to APY formation, may also contribute to the cellular formate pool.

Finally, our experiments examine the ability of phosphorylated residues, including pSer and pTyr, on peptide **1** to promote formation of certain AGEs, particularly that of MGH-1 and APY, on nearby Arg despite introducing additional negative charges previously shown to hamper glycation.[19,31] Our time course data comparing AGE levels of different phosphorylated versions of peptide **1** not only confirm MGH-1 to be a stable AGE, but also reveal a potential connection between [M+144], APY, and MGH-1 over time. These results imply that previous studies using prolonged incubation periods might have overlooked certain AGEs including APY and some [M+144] species, which likely explains why MGH-1 has frequently been reported as "the most abundant". Although a decrease in overall glycation was observed for the doubly-phosphorylated variant of peptide **1**, MGH-1 remains the predominant AGE across all time points, suggesting that phosphorylated residues bias the formation of MGH-1 over APY for this variant. While inorganic phosphate has long been known to enhance glycation,[155] and MGO has been shown to stimulate phosphorylation,[156–159] we have not been able to find any reports suggesting that nearby phosphorylated sites influence glycation. Future studies looking to elucidate this particular phenomenon can begin by probing potential crosstalk between glycation and phosphorylation

events on proteins *in vitro* and/or in a cellular context. On the other hand, molecular dynamics simulation could be particularly useful in investigating the orientation and proximity of phosphorylated residues in coordination with the guanidino group on Arg to identify any distance-dependent effects.

3.4. Materials and Methods

3.4.1. General Materials

N-Fmoc-3-Fluoro-L-tyrosine (1270290) was purchased from Acrotein Chem Bio Inc. N-Fmoc-3,5-Difluoro-L-tyrosine (AS01393) was purchased from Acrotein Chem Bio Inc. Fmoc-Tyr(PO(OBzl)OH)-OH (FY2580) was purchased from Advanced ChemTech Inc. Fmoc-Ser(HPO3Bzl)-OH (101604) was purchased from ChemPep Inc. Aminoguanidine hydrochloride (396494), NAD (10127981001) and NADH (10128023001) standards were purchased from Sigma Aldrich. Formic acid assay kit was purchased from Neogen Corporation (K-FORM).

3.4.2. Peptide Synthesis

Peptides were synthesized using standard Fmoc-based solid phase peptide synthesis on Trityl chloride resin (200 mesh, 1.6 mmol/g loading, Novabiochem®) or Fmoc-Ala-Wang resin (100-200 mesh, 0.64 mmol/g loading, Creosalus Inc.), typically on a 100 µmol scale in a 3 mL polypropylene fritted syringe. For Trityl chloride resin only, C-terminal amino acids (5 equiv., 500 µmol) were coupled overnight in a solution of 10 equiv. (1 mmol) N,N-diisopropylethylamine (DIEA) in 3 mL dimethylformamide (DMF). The next day, the resin was washed and capped with a solution (3 mL) of DMF:MeOH:DIEA (17:2:1 by volume) for 1 hour before further deprotection and coupling steps. C-terminal coupling and resin capping was not required when using Fmoc-Ala-Wang resin. Fmoc deprotection was accomplished using 20%

piperidine in DMF (3 mL, 3 x 5 min), followed by washing steps with DMF (3 mL, 4 x 1 min). Amino acid couplings were completed by incubation of amino acid (5 equiv. relative to resin loading) with O-(benzotriazole-1-yl)-N,N,N',N'-tetramethyluronium hexafluorophosphate (HBTU, 5 equiv.) and DIEA (10 equiv.) in 1-2 mL of DMF for 45-90 min. To prepare for pTyr and pSer couplings, deprotection steps right before and after each coupling step were extended to 3 x 10 min, and the couplings were extended to 2-3 hours. All peptides were N-terminally acetylated following deprotection of the last amino acid coupling via incubation with acetic anhydride (4 equiv.) and DIEA (3 equiv.) in 1-2 mL DMF for 2 hours. Following the final acetylation step, peptides were washed with DMF (3 mL, 4 x 1 min), followed by dichloromethane (DCM) (3 mL, 2 x 1 min, then 2 x 15 min), and stored under vacuum desiccation until ready for side-chain deprotection and cleavage. The side chain protecting groups used were as follows: Glu (tBu), His (Trt), Lys (Boc), pSer (Bzl), pTyr (Bzl), Trp (Boc), and Tyr (tBu). Side-chain deprotection and peptide cleavage was completed by incubation with trifluoroacetic acid (TFA), triisopropylsilane (TIPS), and water (95:2.5:2.5 by volume) in 4 mL of acid solution per resin for 2 hours. The resulting crude peptide was dried under constant air flow and then dissolved in 1-3 mL of a water/acetonitrile mixture based on solubility, prior to purification.

3.4.3. Peptide Purification

All peptides were purified using a semi-preparative Agilent 1260 Infinity LC system equipped with an Agilent ZORBAX SB-C18 column (9.4 × 250 mm, 5 μm particle size). The mobile phase contained water (A) and acetonitrile (B) with 0.1% TFA. Crude peptide solutions were eluted with a gradient of 5% B to 40% B over 20 min and a flow rate of 3.0 mL/min. Crude peptide solutions of pTyr- and pSer-containing peptides were eluted with a gradient of 5% B to

35% B over 23 min and a flow rate of 2.0 mL/min. Absorbance at 215 and 280 nm was used to observe desired peptide peaks, which were then eluted and collected using an automated fraction collector. APY-specific absorbance could be detected using its characteristic absorbance at 320 nm.[18,37,126] Collected fractions were assessed for purity using matrix-assisted laser desorption/ionization time-of-flight (MALDI-TOF) mass spectrometry (Bruker) and/or an Agilent 6530 quadrupole time-of-fight (Q-TOF) mass spectrometer (Agilent). Pure fractions were combined and lyophilized. Peptide stock solutions were prepared at 20 mM concentrations in DMF. Peptide stock solutions of peptides containing multiple phosphorylated amino acid on the same sequence were prepared at 10 mM concentrations in 10 mM phosphate buffer (pH 10.0).

3.4.4. Preparation of Oxygen-free Glycation Reactions

To perform glycation reactions in inert atmosphere, each reaction component (water, 10 mM MGO stock, 100 mM PBS stock, 20 mM peptide stock) was carefully degassed using N_2 for 30 minutes and sealed inside a 20 mL glass screw-neck scintillation vial with vinyl electrical tape prior to transferring inside a VAC-ATM Genesis glovebox filled with N_2 gas (O_2<4ppm). Glycation reactions were then assembled in Eppendorf tubes inside the glovebox, according to our standard peptide glycation protocols as described above. The tape-sealed tubes were then sealed inside glass scintillation vials, which were sealed with high adhesion, moisture tight vinyl tape to limit air exposure when transferring reactions out of the glovebox and during incubation. Reactions performed at 37 °C reactions were then incubated in a VWR incubator, while those at 60 °C were incubated in a water bath for 24 h. Reactions were prepared for LC-MS analysis by diluting 100X in degassed water inside the glovebox, and sample vials were sealed with tape until ready for injection.

3.4.5. Methylglyoxal (MGO) Synthesis Protocol

MGO was synthesized as described by Riley Oxidation.[130] To start, equal parts (10 mmol) acetone and selenium dioxide powder were added to water to a total volume of 5 mL in a round bottom flask with a magnetic stir bar. The reaction was heated in an oil bath at 100 °C under reflux for 4 hours. After reflux, distillation was performed by attaching the flask to a short path distillation head, and the mixture was distilled into one fraction at an internal temperature of 100 °C. The pale-yellow distillate was lyophilized overnight, revealing a viscous yellow MGO product (134 mg, 19%). Synthetic MGO was characterized by NMR, and a synthetic MGO stock was prepared by adding ultrapure water and checked for concentration using an aminoguanidine assay.[160,161] After a 5-hour incubation of aminoguanidine and MGO at 37 °C, absorbance was measured at 320 nm to generate a standard curve, the slope of which was compared to that of a calibration curve generated by serial dilutions of commercial MGO stock to equalize MGO concentrations between synthetic and commercial stocks.

3.4.6. NMR Acquisition

^{1}H and ^{13}C spectra were acquired with a Bruker Advance III (500 MHz, 125 MHz) spectrometer. The following convention was used in data reporting: chemical shift, multiplicity (s = singlet, d = doublet, t = triplet, q = quartet, m = multiplet), coupling constants (Hz), and integration, if applicable. ^{1}H D_2O δ 5.25 (s, 1H), 4.79 (s, 1H), 2.28 (s, 3H), 1.35 (s, 3H). ^{13}C (126 MHz, D_2O) δ 209.13, 95.13, 91.89, 89.72, 24.53, 21.40.

3.4.7. Formic Acid Assay

Formic acid was detected using a formic acid assay kit purchased from Megazyme (K-FORM). This assay utilized the enzyme formate dehydrogenase (FDH) to detect formic acid in

samples by converting NAD^+ to NADH. The absorbance of NAD^+ and NADH was measured using an analytical HPLC system described above (absorbance 340 nm). While NAD^+ is not fluorescent, NADH fluorescence was measured using its fluorescence wavelengths (ex = 340 nm, em = 460 nm).[131] The identity of NAD^+ and NADH was confirmed by comparing the retention time of samples to that of NAD^+ and NADH standards (Sigma Aldrich, 10127981001 and 10128023001, respectively). A calibration curve was performed using a formic acid standard (LC-MS grade, Fisher Chemical™, A117). Samples were prepared according to the kit's instructions and injected onto the analytical HPLC system equipped with a Poroshell column (4.6 × 150 mm, 2.7 μm particle size). The mobile phase contained 10 mM ammonium acetate (A) and acetonitrile (B). NADH signal was observed using a gradient of 5% to 30% acetonitrile (B) in ammonium acetate (A) over 50 min at 2.0 mL/min.

4. Chapter 4:

Proteomics Studies of Glycation

4.1. Introduction

AGEs are hallmarks of aging and diseases, and accumulation of intracellular AGEs has been associated with numerous deleterious effects, including the induction of cell death and disruption of cellular homeostasis.[1,162–165] Recent reports have revealed the biological relevance of some MGO-derived AGEs that plays potentially important roles in cellular processes, such as regulating chromatin architecture and triggering an antioxidant response.[20,39,67] For instance, MGH-1 and CEA have been observed on several histones and their formation has been linked to global disruption of canonical histone PTMs.[39] MGH-1 and CEA form relatively quickly and are reportedly abundant AGEs that have been the focus of most glycation studies investigating the functional role of AGEs in biology. In contrast, APY is a late-stage AGE whose obscure formation mechanism renders its detection underappreciated and often overlooked. Although several reports have correlated APY with cellular processes like apoptosis, autophagy, or chaperone activity, there are still virtually no causal connections that link APY to specific biological consequences.[45,47,50,51,86,87] Moreover, while there is abundant evidence that APY is correlated with diseases like brunescent cataractous lens, filial amyloidotic polyneuropathy, and cancer, it is not known where on proteins and in cells it accumulates.[48,88,116,124,124] Indeed, the landscape of MGO modification on protein targets and their specific sites remains incompletely mapped.

Although detection of AGEs in the proteome can face challenges in low abundance and heterogeneity, several proteomics studies have begun to identify cellular targets of glycation.[39,62,122,166,167] Particularly, MGO-derived AGEs, including MGH-1, CEA, and APY, have been identified previously. Guided by our newly gained insights into the chemical formation mechanism of APY from *in vitro* experiments in **Chapter 2** and **3**, we set out to survey

its formation in HEK293T cells. Aware that intracellular concentrations of MGO is unlikely to afford detectable AGE levels and that there is a lack of suitable enrichment protocols, we chose to treat cells with additional MGO and perform our proteomics studies on unenriched cell lysates. We then validated our proteomics results with follow-up *in vitro* experiments using peptide hits identified from our proteomics analysis.

These quantitative proteomics experiments investigating APY formation in live cells treated with MGO enable us to draw a previously unknown connection between AGE formation and phosphorylation in a cellular context. Follow-up *in vitro* studies also suggest that phosphorylated residues can bias the formation of certain AGEs. Importantly, these findings provide essential mechanistic insights that are greatly needed for future studies that seek to develop chemical or fluorescent tools that can be used to predict, sense, and study glycation events in living cells.

4.2. Results

4.2.1. Control Experiments and Our Proteomics Data showed Consistent Results according to Previous MGO-treated Datasets

Guided by the chemical mechanistic insights previously defined in **Chapter 3**, we performed a quantitative proteomics experiment using HEK-293T cells treated with or without MGO. Our mechanistic studies have shown that APY can accumulate at longer times or using higher MGO concentrations. Therefore, we opted to treat cells with 2 mM MGO for 24 h to ensure that we could induce APY formation. We confirmed that these treatment conditions did not significantly decrease cell viability, as more than 95% of cells remained viable after treatment (**Figure 4.1**). Several reagents, such as dithiothreitol (DTT) and iodoacetamide, used in

proteomic experiments were also tested for their effects on AGE distribution and APY formation and found to have no interference (**Figure 4.1**).

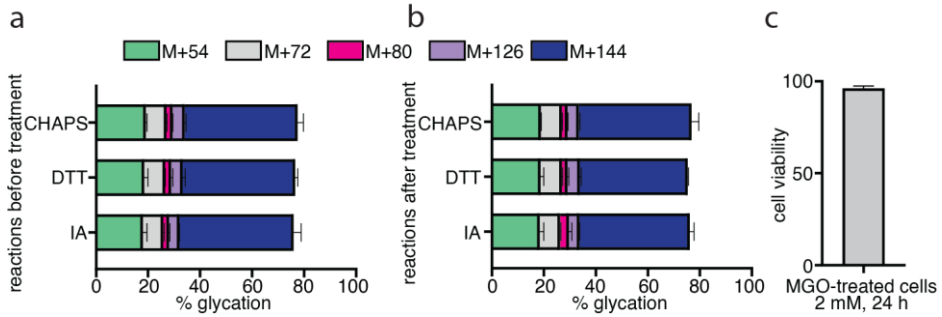

Figure 4.1. Cell Viability and Controls showing that Proteomic Reagents do not impact the AGE Distribution. Sample preparation for proteomics regularly involves reagents such as (3-((3-cholamidopropyl) dimethylammonio)-1-propanesulfonate) (CHAPS), dithiothreitol (DTT), and iodoacetamide (IA). To ensure that these reagents do not affect APY formation, we followed standard glycation reaction protocols on MGO-treated peptide **1** (2 mM MGO, pH 7.3, 37 °C, 24 h incubation), then treated AGE-modified peptide **1** with each reagent in a similar manner to how the reagent would be used as described in our proteomic protocols. Distributions of AGEs were compared before and after treatment of each reagent. **(a)** Distribution of AGEs on MGO-treated peptide **1** before treatment with proteomic reagents. **(b)** Distribution of AGEs on MGO-treated peptide **1** after treatment with proteomic reagents (n = 3 for all reactions). These results confirmed that proteomic reagents used in our studies would neither interfere with AGE distributions nor APY formation. **(c)** Cell viability of MGO-treated HEK-293T cells was measured post 24 h treatment using a Trypan blue viability assay on a plate reader (n = 3). More than 95% of treated cells remained viable, confirming that MGO treatment did not significantly decrease cell viability.

Additionally, as there are no highly specific antibodies available to enrich APY (**Figure 4.2**), we chose to label an unenriched cell lysate with isobaric tandem mass tags, allowing us to evaluate the distribution of multiple AGEs using quantitative bottom-up proteomics, including the MGH isomers ([M+54]), APY ([M+80]), THP or other [M+144] AGEs, and an [M+72] adduct that could correspond to MGH-DH, CEA, or CEL. Using this approach, we identified 7210 total proteins and 56490 peptides across all conditions tested, and found 478 unique peptides that were AGE-modified upon treatment with 2 mM MGO. This dataset shows significant similarity to other MGO-treated proteomics datasets, with AGE modifications enriched on proteins involved in processes such as protein folding and spliceosome function, along with several modified histone and heat shock proteins.[39,122,166,167]

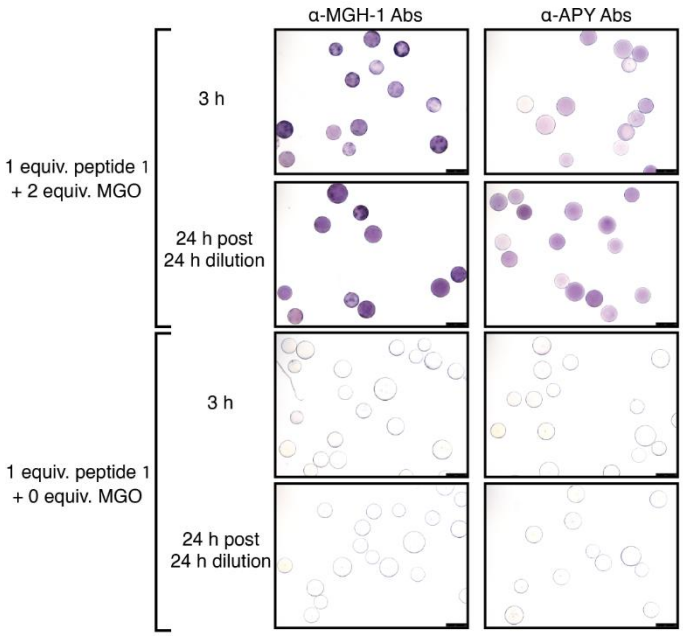

Figure 4.2. α-MGH-1 and α-APY Antibody Screening for On-bead Peptide Glycation. Upon treating on-bead peptide **1** with 2 equiv. of MGO, we observed dark colored purple beads when beads were exposed to α-MGH-1 antibody in both the 3 h and 24 h post 24 h dilution conditions, which was expected according to our peptide **1** data when peptides were free in solution. However, we have identified that APY took much longer to form and has not been observed after 3 h of incubation, only in the 24 h post 24 h dilution condition. Despite this, dark colored purple beads were still observed when beads were exposed to α-APY antibody, suggesting that the commercialized α-APY antibody is not specific to APY.

Upon meticulous inspection of our dataset, we manually removed any hits from the glycated set that had a **Δ** mass (theoretical – observed mass) > 20 ppm and/or were assigned with a modified Arg at their C-terminus, as we and others have previously shown that glycated Arg cannot be cleaved by trypsin.[31,168] After data processing, this decreased the total list of AGE-modified peptides to 204 plausible AGE-modified hits (**Table 6.2—6.5**). Without any enrichment steps during sample preparation that could bias the AGE distribution, we found that APY and [M+144] species were the predominant AGEs in the MGO-treated condition (57 unique peptides, 28%, and 53 unique peptides, 26%, respectively), followed by the MGH isomers and CEA/MGH-DH (47 unique peptides, 23% for each) (**Figure 4.3 B**). Although our dynamic modification for [M+72] (mass change 72.021) was set for both Arg and Lys, we only observed modification on Arg (MGH-DH and/or CEA, not CEL), likely due to the static TMT

modification that was set for Lys in our processing workflow. Though glycation is largely driven by chemical microenvironments that include 3D protein structure and is therefore unlikely to have a strong consensus sequence,[137] we were also able to obtain consensus features for each AGE (**Figure 4.4**). Overall, comparison with other proteomics datasets and inspection of our own data show consistency between reported proteins and those observed in our own dataset. Although we have taken a stringent approach to analyzing our own data that are not common in proteomics, we believe that these steps are necessary to reduce any artifactual hits that may arise.

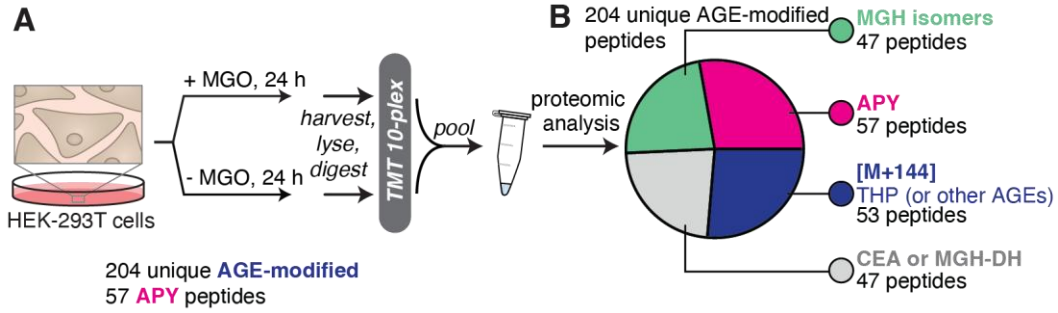

Figure 4.3. Proteomic Analysis on MGO-treated Cells shows different Sets of AGE-modified Peptides. Given that our proposed mechanism for APY formation was supported by *in vitro* peptide data, we set out to investigate APY formation in a cellular context, along with other common MGO-modified AGEs. **(A)** General scheme describing our proteomic workflow on HEK-293T cells treated with or without 2 mM MGO for 24 h. Whole cell lysates were trypsin-digested, labeled with TMT isobaric tags, and analyzed in a quantitative bottom-up workflow. The untreated sample was used as a frame of reference to identify any AGE increase in the treated condition. **(B)** Pie chart showing a set of 204 unique peptides with AGE-modified Arg in the MGO-treated condition, consisting of 57 APY-, 53 THP- (or other [M+144] AGEs), 47 MGH-, and 47 CEA/MGH-DH-containing peptides.

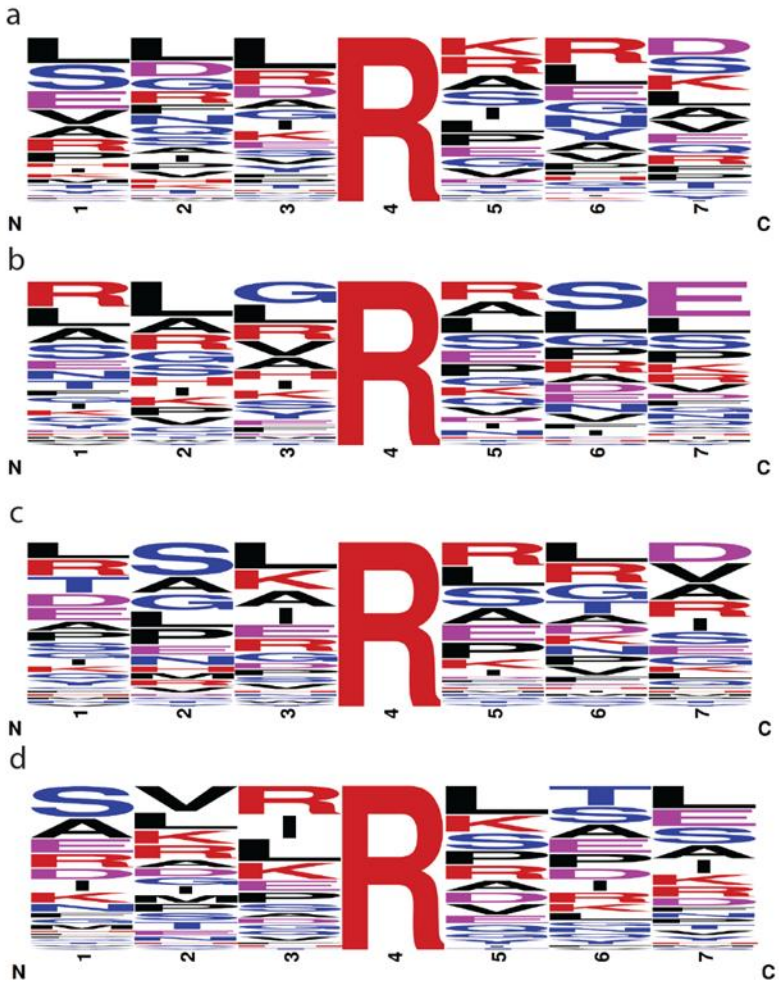

Figure 4.4. Frequency Logos for All AGE-modified Peptides Observed in Proteomic Analysis. Our prior work has shown that glycation is unlikely to have a strong consensus sequence, as it is largely driven by chemical microenvironments that include 3D protein structure. Nonetheless, it was also possible to evaluate sequence features of AGE-modified peptides. **(a)** Frequency consensus features for APY-modified peptides. **(b)** Frequency consensus features for MGH-modified peptides. **(c)** Frequency consensus features for CEA/MGH-DH-modified peptides. **(d)** Frequency consensus features for THP/other [M+144] AGE-modified peptides.

4.2.2. Uncovering a Potential Crosstalk between Cellular APY Formation and Phosphorylation

Next, we performed gene ontology (GO) analysis for the APY-modified set of proteins using DAVID. In both the biological process (BP) and molecular function (MF) annotations, APY-containing proteins showed multiple terms related to phosphorylation, including protein phosphorylation (BP) and multiple kinase activities (MF) (**Figure 4.5 B, C**). We also found that

none of the other AGE sets showed terms related to protein phosphorylation (BP) or kinase activity (MF) (**Figure 4.6—4.8**). However, due to the relatively small number of hits, the depth of our proteomic analysis was not sufficient to gain meaningful statistical information. Despite the small size of our list of hits, we performed functional annotation clustering analysis, which groups similar and/or related annotations into a focused snapshot of biologically relevant clusters.[169] From this analysis, the APY set was the only one to show clustering, producing six clusters with enrichment scores ≥ 1.3. Out of these six clusters, three were phosphorylation-related including ATP-binding (enrichment score 2.43), protein serine/threonine kinase activity (enrichment score 2.02), and histone kinase activity (enrichment score 1.48) (**Table 6.6**). Indeed, the top term for ATP-binding from this analysis showed a statistically significant -log(p. adjust) value of 1.70 (**Figure 4.5 A**). We also used an alternative database (ToppGene) and manual annotation and ID mapping (UniProtKB). Similarly, only the APY set showed multiple phosphorylation-related clusters and terms, whereas other AGEs did not.

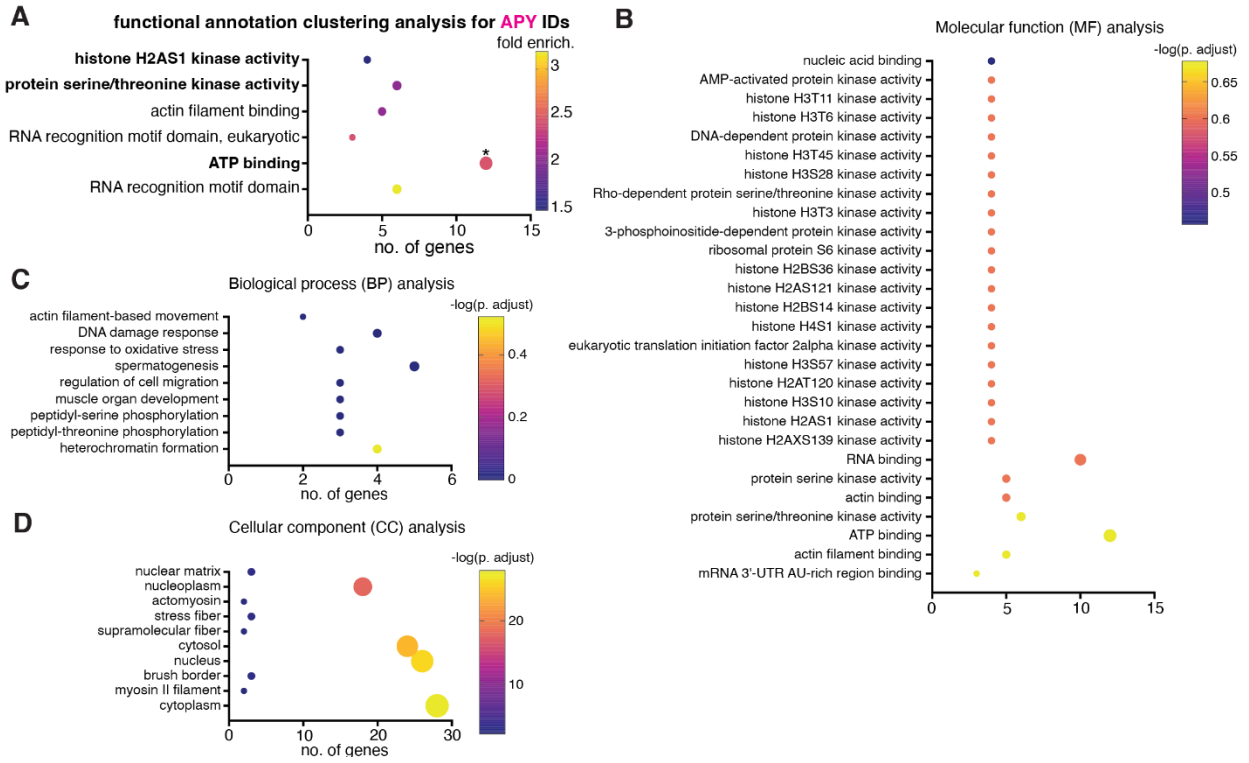

Figure 4.5. DAVID Functional Annotation Clustering and GO Analysis Annotation Charts for APY Hits. Each APY-modified peptide identified from our proteomic analysis was associated with one or more protein accession numbers (Uniprot). A list of all APY-containing accession numbers was input into DAVID for **(A)** Functional Annotation Clustering and **(B), (C), & (D)** Gene Ontology (GO) analyses, and false discovery rate (FDR) was set to 5%. All GO terms were included in this figure. Multiple protein kinase activity terms in molecular function (MF) annotation and phosphorylation terms in biological process (BP) annotation appeared to be unique for APY hits. This observation is consistent with our *in vitro* peptide data, suggesting a connection between phosphorylation and APY formation in a cellular context.

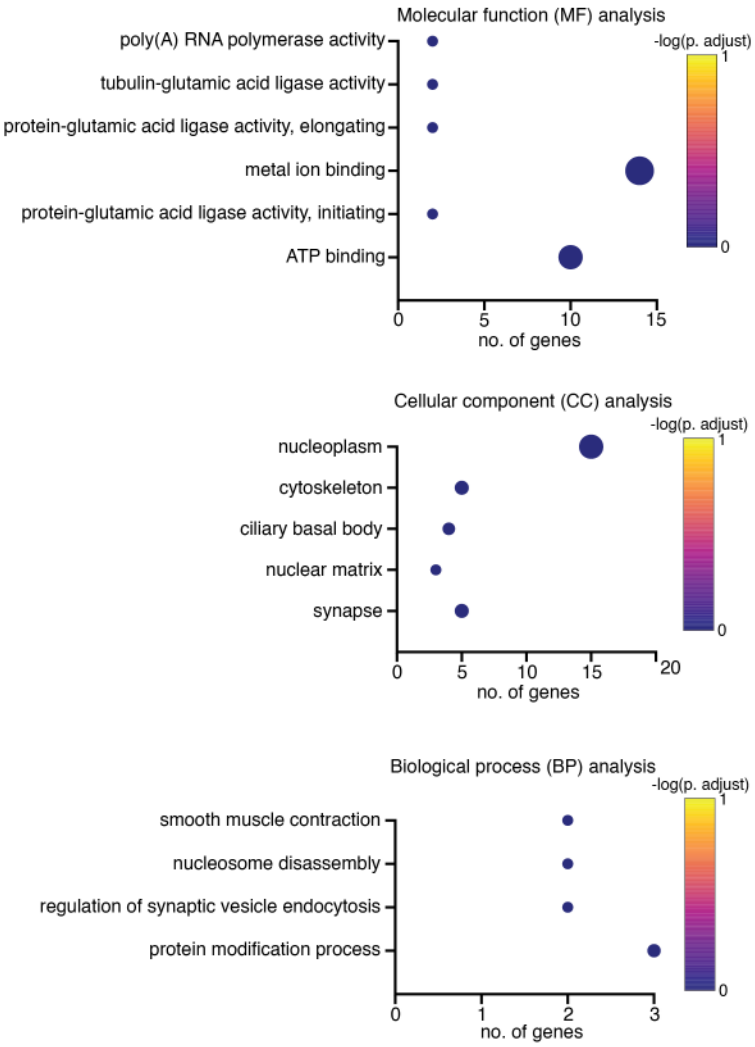

Figure 4.6. DAVID GO Analysis Annotation Charts for MGH Isomers Hits. Each MGH-modified peptide identified from our proteomic analysis was associated with one or more protein accession numbers (Uniprot). A list of all MGH-containing accession numbers was input into DAVID for Gene Ontology (GO) analysis, and false discovery rate (FDR) was set to 5%. All GO terms were included in this figure.

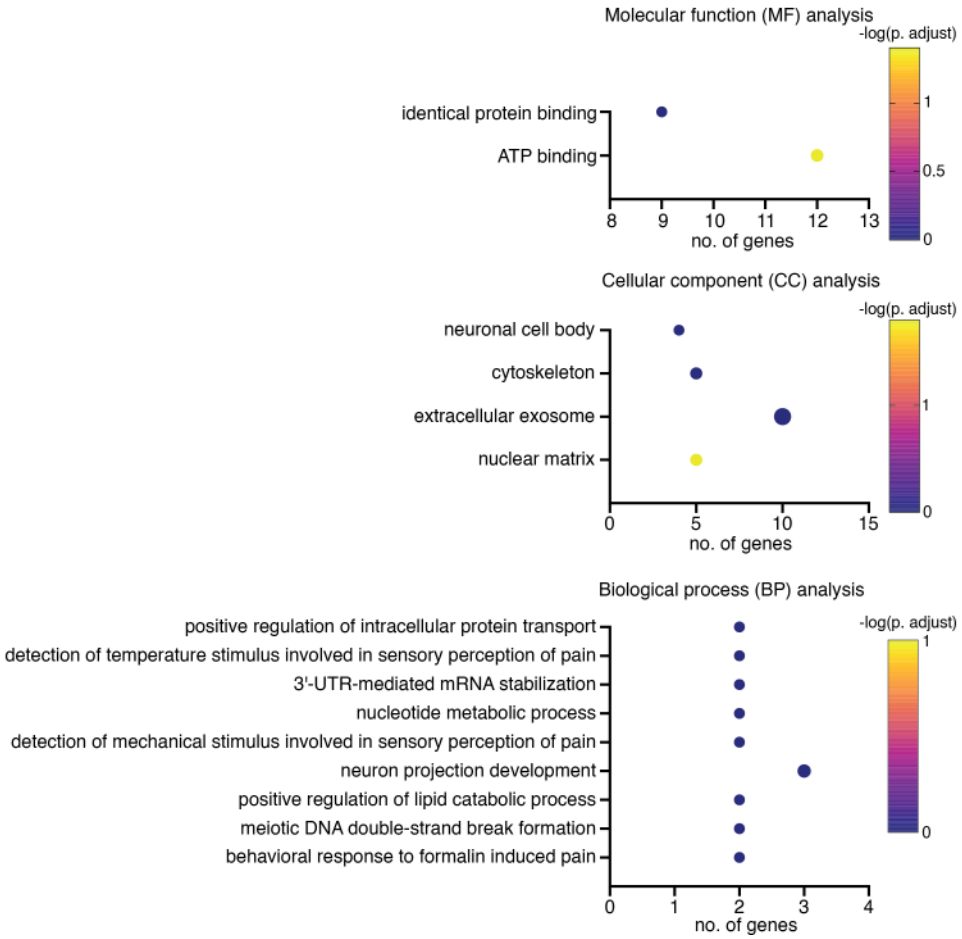

Figure 4.7. DAVID GO Analysis Annotation Charts for CEA/MGH-DH Hits. Although the dynamic modification for [M+72] adducts was set to include both Arg and Lys modifications, we only observed [M+72] adducts on Arg, corresponding to CEA and/or MGH-DH. Each CEA/MGH-DH-modified peptide identified from our proteomic analysis was associated with one or more protein accession numbers (Uniprot). A list of all CEA/MGH-DH-containing accession numbers was input into DAVID for Gene Ontology (GO) analysis, and false discovery rate (FDR) was set to 5%. All GO terms were included in this figure.

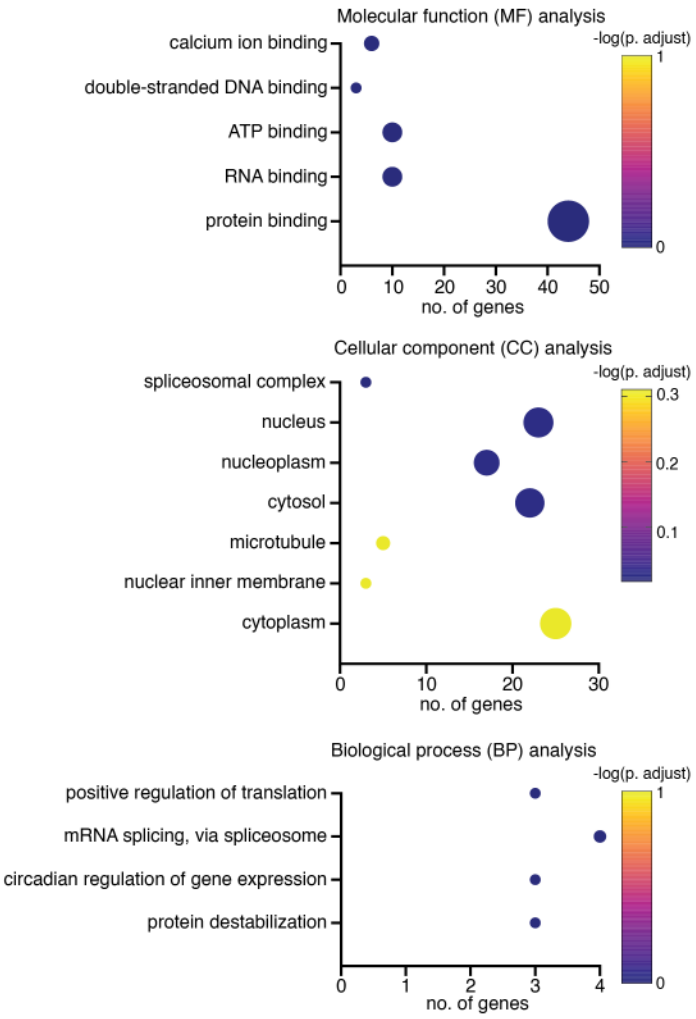

Figure 4.8. DAVID GO Analysis Annotation Charts for [M+144] Hits. Each THP/other [M+144] AGE-modified peptide identified from our proteomic analysis was associated with one or more protein accession numbers (Uniprot). A list of all [M+144]-containing accession numbers was input into DAVID for Gene Ontology (GO) analysis, and false discovery rate (FDR) was set to 5%. All GO terms were included in this figure.

Next, we further investigated the set of 57 modified APY-containing peptides, which were observed across the entire range of AGEs when ranked by abundance (**Figure 4.9 A**). Among this list of genes, eight (14.04%) were annotated with phosphorylation-related GO terms, such as ATP binding or kinase activity (**Figure 4.9 B**). Compared to other AGEs such as the MGH isomers, CEA or CEL, and [M+144] species, the APY set exhibited the greatest proportion of hits that were annotated with phosphorylation-terms. Taken together, to us these analyses

suggested a possible connection between APY formation and phosphorylation in a cellular context.

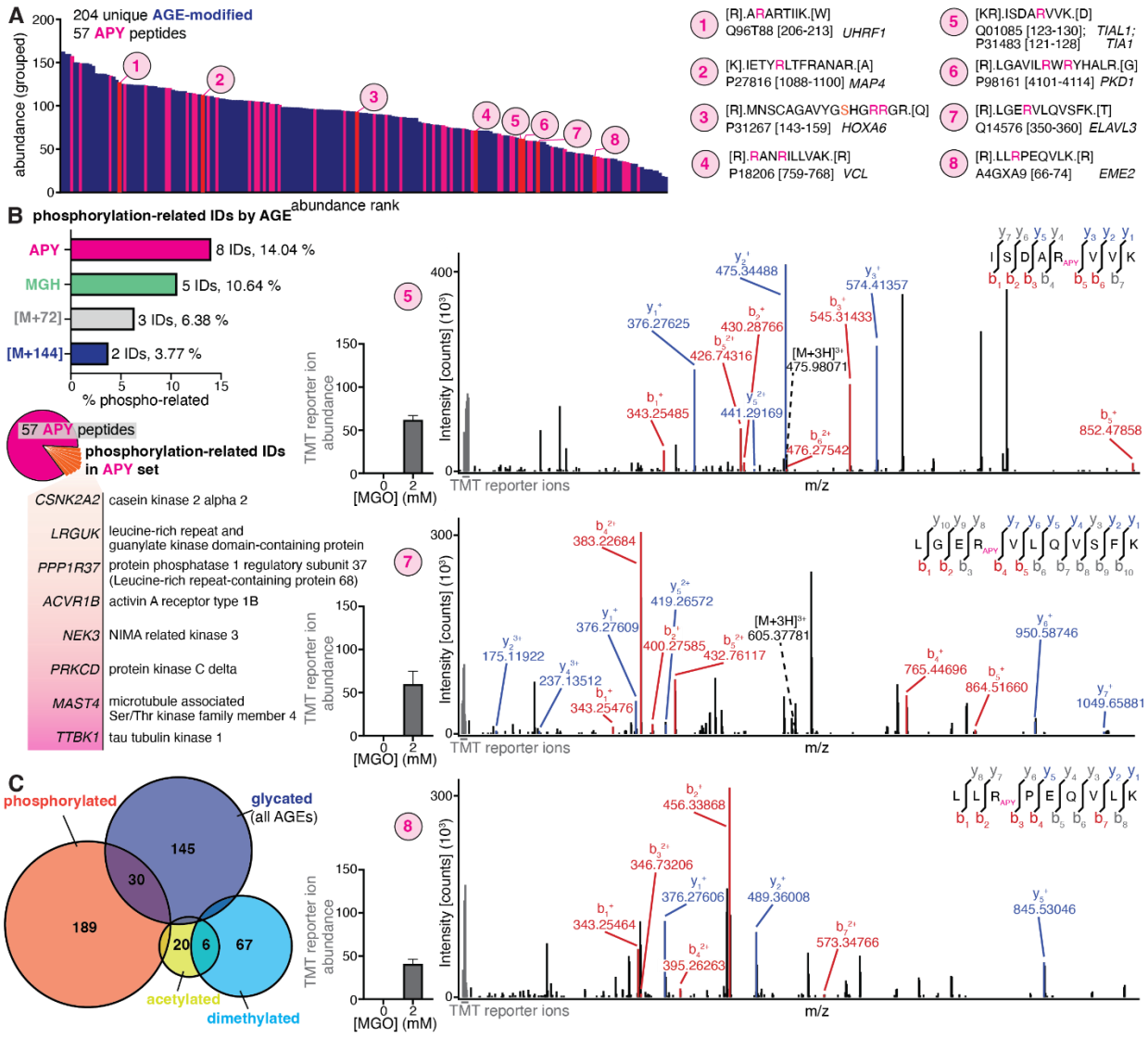

Figure 4.9. Proteomic Analysis on MGO-treated Cells Reveal a Connection between Glycation and Cellular Phosphorylation Events. (A) The abundance (grouped) for APY-containing peptides (magenta) was ranked and displayed atop the abundance of other AGE-containing peptides (blue). Eight statistically significant increased APY-containing peptides (red) are numbered 1-8. Representative b/y ion spectra and TMT reporter ion abundance quantitation for three of the high confidence APY hits are shown. **(B)** Comparison of the percent of phosphorylation-related IDs by AGE type (top) and a list of the eight phosphorylation-related IDs observed in the APY set. **(C)** Venn diagram showing overlapping IDs between AGEs or other common Arg modifications (dimethylation and acetylation) and phosphorylation. Compared to dimethylated and acetylated IDs, glycated IDs exhibited substantial overlap (30 IDs) with phosphorylated IDs, further suggesting a connection between AGE formation and phosphorylation events.

To further evaluate the possibility of a connection between protein phosphorylation and APY formation, we focused in particular on the eight highest confidence APY-modified peptides that exhibited statistically significant increases in abundance upon MGO treatment across all three biological replicates (**Figure 4.9 A**). Data imputation and statistical analysis were performed according to published protocols.[170] Among these peptides, one was also identified with a phosphorylated residue nearby the APY-modified site, corresponding to HOXA6 (hit 3) (R156, R157 with nearby pS153).

Furthermore, by cross-referencing the protein sequences, reported phosphorylated sites, and the influence of phosphorylation on protein functions, we were able to draw several correlations between reported studies and our dataset. Of the remaining seven high confidence APY hits, six were previously reported to be phosphorylated, and some are known to have their functions regulated by phosphorylation.[171] For example, phosphorylation of MAP4 (hit 2) has been reported to affect microtubule properties and cell cycle progression, while TIAL1 (hit 5) has also been found to be phosphorylated following DNA damage, and phosphorylation of PKD1 (hit 6) triggers its membrane dissociation and subsequent entry into the nucleus.[172–174] Additionally, phosphorylation of UHRF1 maintains protein stability, subcellular localization, and epigenetic regulation (hit 1).[175] Careful inspection of our data revealed that UHRF1 was APY-modified at R207, which is close to T210, a known phosphorylated site previously reported to be essential in maintaining UHRF1 stability, though phosphorylated T210 was not observed in our dataset.[176]

Similarly, S358, close in sequence to APY-modified R353, on ELAVL3 (hit 7) has also been shown to be phosphorylated.[171] We also found two APY modifications on the C-terminal domain of PKD-1 (R4107, R4109), which contains 4 Tyr residues (Y4110, Y4118, Y4127,

Y4237) and 2 putative Ser sites (S4169, S4252) that are susceptible to phosphorylation. Multiple *in vitro* studies have revealed Y4237 and S4252 to be targets of phosphorylation by pp60c-src and PKA, respectively, and shown endogenous PKD-1 to be phosphorylated at tyrosine.[177–179] Together, our data show several APY modifications on Arg residues close to known phosphorylation sites, consistent with the potential for crosstalk between cellular APY and phosphorylation events.

However, as APY (mass change 80.026) is quite close in mass to phosphorylation (mass change 79.966), we also queried our dataset for phosphorylation and found that the list of proteins generated had some overlap with the set of APY-modified targets, but the overall list of IDs was quite different, confirming that the relatively similar mass changes did not produce artifactual hits. We also found that the phosphorylated set (220 proteins) showed substantial overlap (30 proteins) with the AGE-modified set of proteins (180 proteins). To evaluate the possibility that crosstalk between nearby phosphorylation could promote AGE formation (especially for APY and MGHs), we performed a parallel analysis for other common Arg PTMs, including dimethylation and acetylation (**Figure 4.9 C** and **Figures 4.10 & 4.11**). We found 99 unique peptides with dimethylated Arg and 30 unique peptides with acetylated Arg. Importantly, the phosphorylated set of proteins did not substantially overlap with those that were observed to be dimethylated (9 IDs) or acetylated (2 IDs) (**Figure 4.9 C**). Taken together, these analyses show a unique connection between APY formation and phosphorylation that does not appear in other common PTMs.

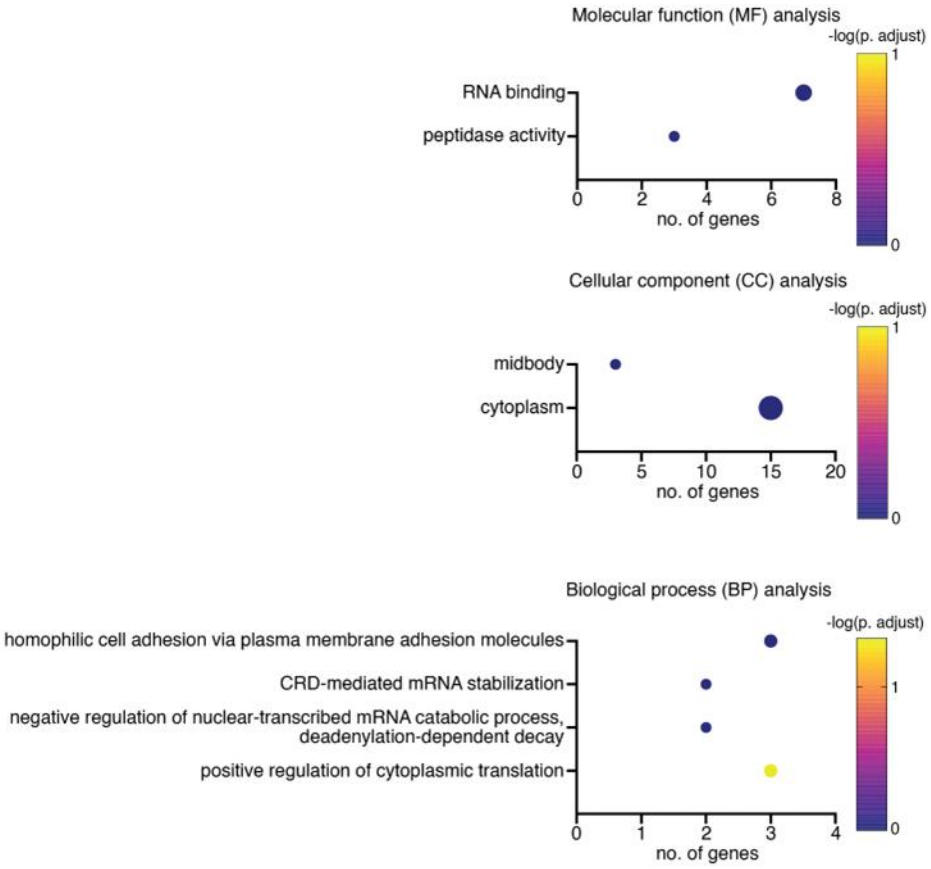

Figure 4.10. DAVID GO Analysis Annotation Charts for Acetylation Hits. Each Arg-acetylated peptide identified from our proteomic analysis was associated with one or more protein accession numbers (Uniprot). A list of all acetylation-containing accession numbers was input into DAVID for Gene Ontology (GO) analysis, and false discovery rate (FDR) was set to 5%. All GO terms were included in this figure.

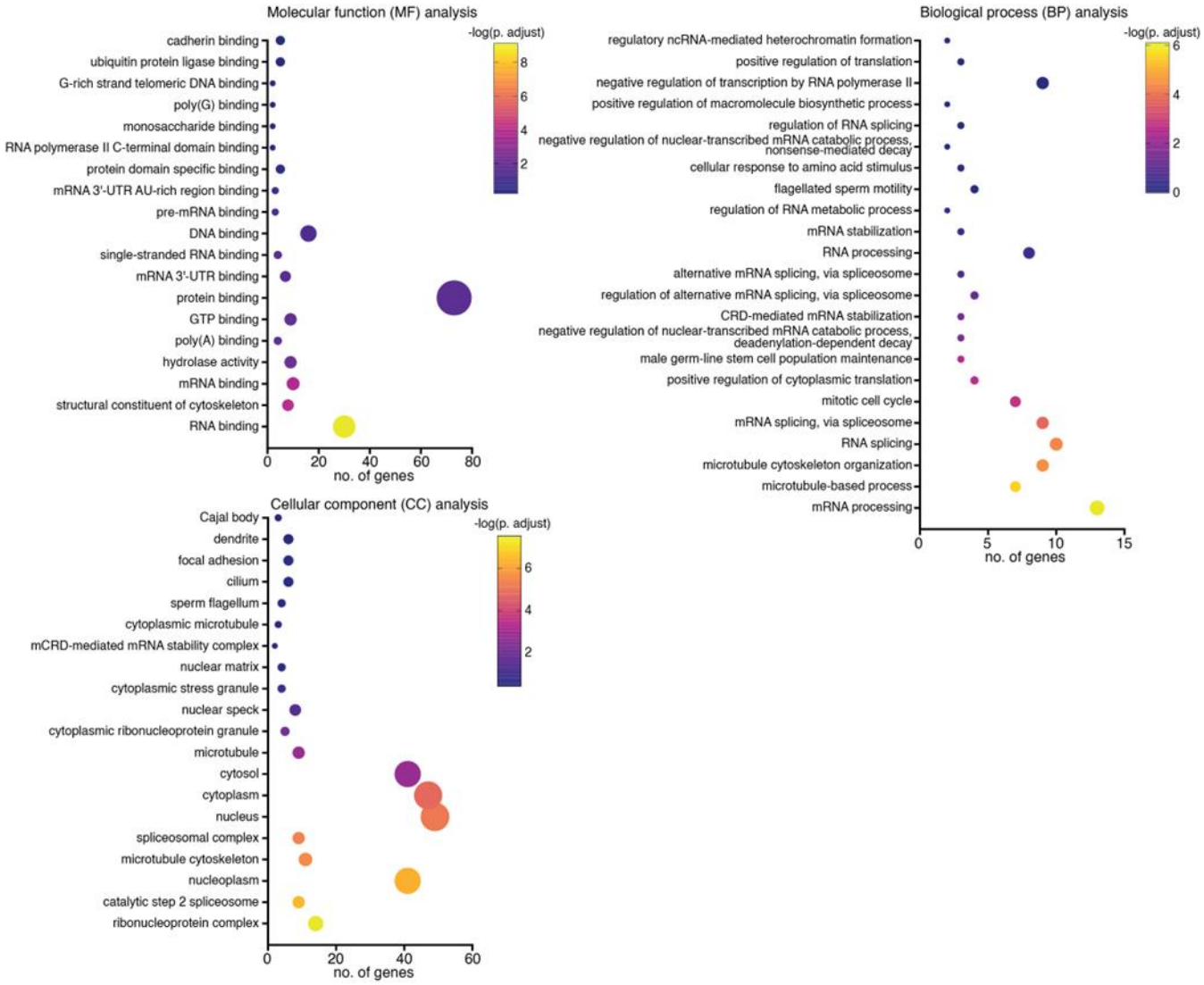

Figure 4.11. DAVID GO Analysis Annotation Charts for Dimethylation Hits. Each Arg-dimethylated peptide identified from our proteomic analysis was associated with one or more protein accession numbers (Uniprot). A list of all dimethylation-containing accession numbers was input into DAVID for Gene Ontology (GO) analysis, and false discovery rate (FDR) was set to 5%. All GO terms were included in this figure.

4.2.3. Follow-up *in vitro* Peptide Glycation Experiments confirm that Phosphorylation can potentiate Glycation

Overall, our proteomics dataset supported our *in vitro* experiments, suggesting that APY formation might be promoted by phosphorylated residues that act as general bases to facilitate rearrangement into APY (see **Figure 3.7**). To validate our findings, we synthesized three peptides matching APY-modified sequences in our dataset. These include a sequence from MAP4 (hit 2;

peptide **V1**: Ac-ETYRLTF), and one from ELAVL3 (hit 7, peptide **V2**: Ac-LGERVLQ). We also synthesized a peptide from HNRNPA3, which was found in higher abundance than either hit sequence, though it did not meet our threshold for being considered "high confidence" (peptide **V3**: Ac-YNLRDYF). Upon treatment with 2 mM MGO at 60 °C for 24 h, we confirmed that all three peptides formed APY (**Figure 4.12 A,B**). Expectedly, peptide **V2**, without a nearby Tyr, exhibited the least APY formation out of the three peptides, though we note that it produced more APY than control sequences such as peptide $\mathbf{1}^{\mathbf{Glu}}$ and peptide $\mathbf{1}^{\mathbf{Phe}}$. Matching our expectations, we found that the peptide with two Tyr residues (peptide **V3**) exhibited the most APY formation. We also found that the overall extent of glycation and the amount of APY formed for peptide **V1** and **V3** were quite similar to that observed for peptide **1**. However, as our treatment condition at 60 °C for 24 h does not reflect the initial rate of APY formation, we also monitored the AGE distributions at 37 °C at 24 and 48 h (**Figure 4.12 C & Figure 4.13)**. Under these conditions, peptide **V1** exhibited the most APY formation. This behavior was visible at earlier time points, and was particularly apparent after 48 h of treatment. Importantly, these data validate that peptides matching the APY-modified sequences identified in our proteomic analysis are indeed capable of forming APY *in vitro*.

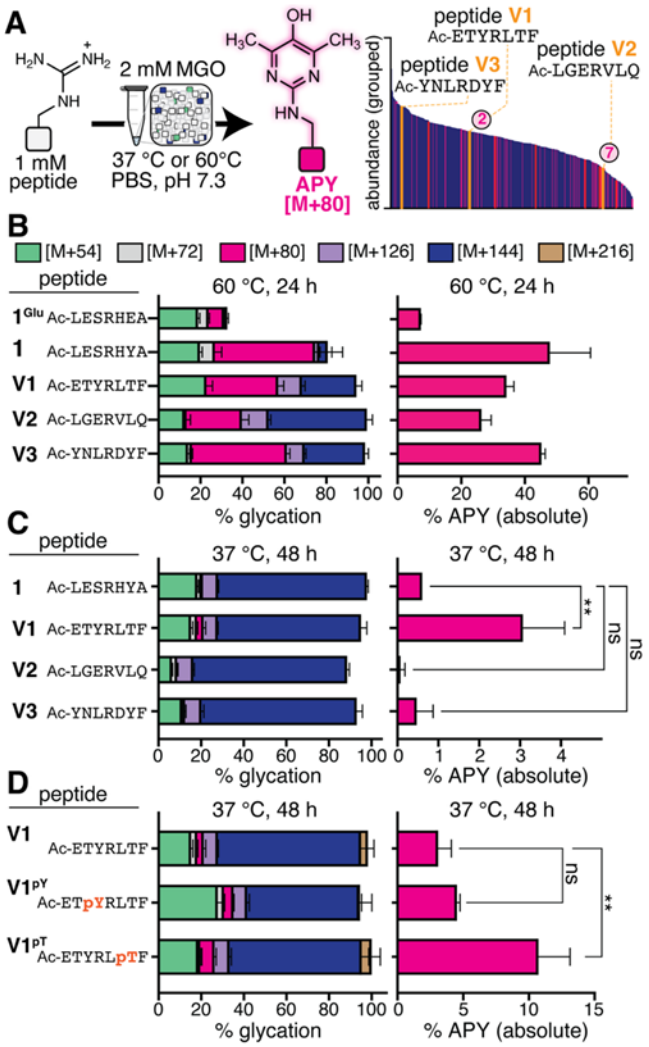

Figure 4.12. Confirming that Phosphorylation can potentiate APY Formation using Validated Hit Sequences *in vitro*. (A) To validate our proteomics analysis, we synthesized peptides matching APY-modified hit sequences in our dataset: Ac-ETYRLTF (hit 2; peptide **V1**), Ac-LGERVLQ (hit 7; peptide **V2**), and Ac-YNLRDYF (peptide **V3**), a high-abundance sequence. These peptides were evaluated after treatment with MGO **(B)** Distributions of AGEs at 60 °C after 24 h of MGO treatment (*left*) for peptides **1**, **V1**, **V2**, **V3,** and $\mathbf{1^{Glu}}$. Absolute APY levels (%) observed under the same conditions (*right*) (n = 3). All three peptides identified from proteomic analysis were confirmed to form APY. **(C)** Distributions of AGEs at 37 °C after 48 h of MGO treatment (*left*) for peptides **1**, **V1**, **V2**, and **V3**. Absolute APY levels (%) observed under the same conditions (*right*) (n = 3) show that peptide **V1** exhibits the most APY formation. Ordinary one-way ANOVA was used to determine if each variant yielded statistically significant differences in % absolute APY compared to peptide **1**. $p<0.01$(**). **(D)** Distributions of AGEs at 37 °C after 48 h of MGO treatment (*left*) for peptides **V1**, $\mathbf{V1^{pY}}$, and $\mathbf{V1^{pT}}$. Absolute APY levels (%) observed under the same conditions (*right*) (n = 3). All three peptides exhibited similar levels of overall glycation. Peptide $\mathbf{V1^{pT}}$ was the fastest to form APY, followed by peptide $\mathbf{V1^{pY}}$, and then peptide **V1**. Ordinary one-way ANOVA was used to determine if each variant yielded statistically significant differences in APY levels compared to peptide **V1** (n = 3). $p<0.01$(**). Absolute APY levels in peptide $\mathbf{V1^{pT}}$ were three-fold higher than those in peptide **V1**, and both phosphorylated variants exhibited an increase in MGH-1 formation, indicating that phosphorylation has a direct influence on glycation outcomes.

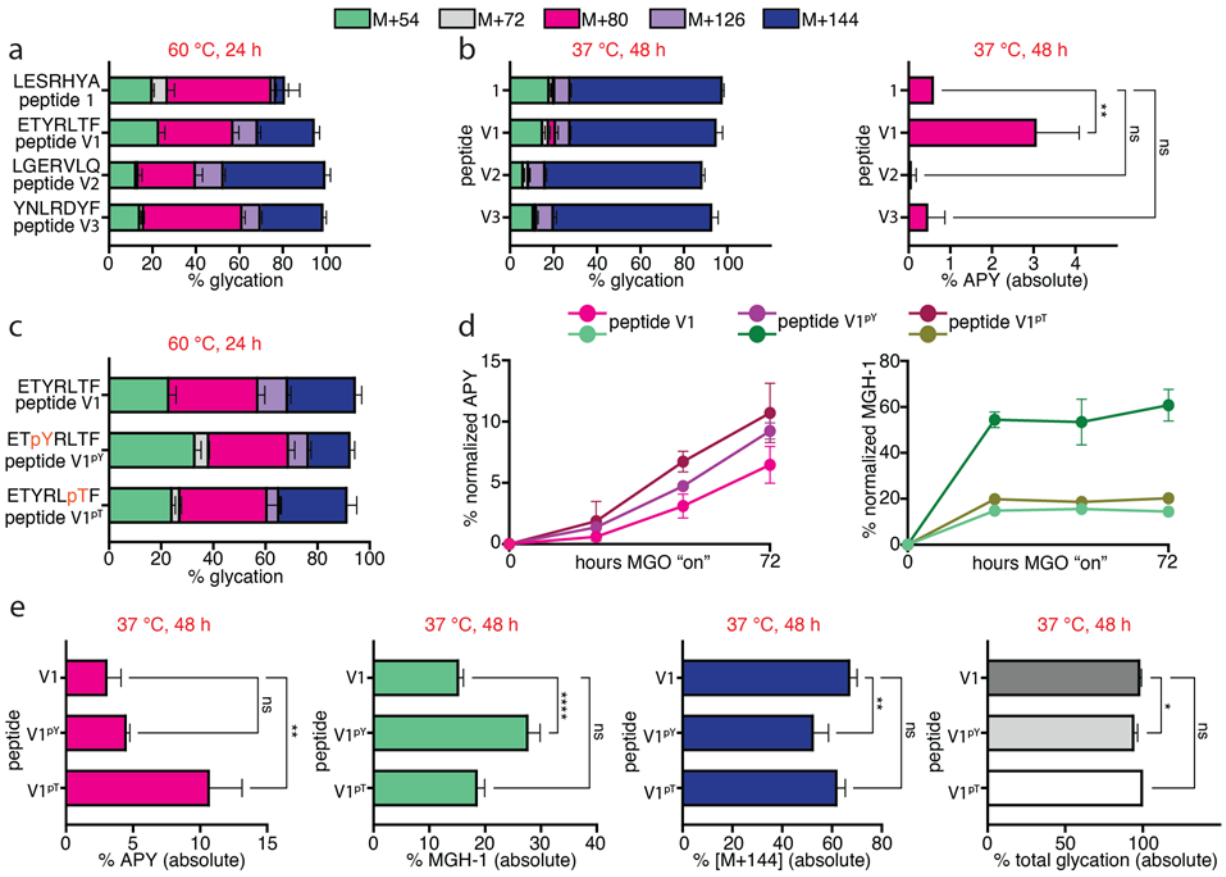

Figure 4.13. Proteomic Analysis Validation with *in vitro* Peptide Data. In order to validate our proteomic analysis, we synthesized three peptides found to be APY-modified in our dataset: Ac-ETYRLTF from MAP4 (hit 2; peptide **V1**), Ac-LGERVLQ from ELAVL3 (hit 7; peptide **V2**), and Ac-YNLRDYF from HNRNPA3, a non-hit yet high-abundant sequence (peptide **V3**). **(a)** Distributions of AGEs at 60 °C at 24 h for peptides **1**, **V1**, **V2**, and **V3** (n = 3). All three peptides were confirmed to form APY. Expectedly, peptide **V2**, without a nearby Tyr, exhibited the least APY formation out of the three peptides, while peptide **V3**, with two Tyr residues, exhibited the most APY formation. **(b)** Distributions of AGEs at 37 °C at 48 h (right stacked bar graph) for peptides **1**, **V1**, **V2**, and **V3**, and absolute APY levels (%) observed under the same conditions (left bar graph) (n = 3 for all reactions). Under these conditions, peptide **V1**, our high-confidence hit, showed the most APY formation, followed by peptides **1** and **V3**, and expectedly, peptide **V2** formed the least APY. Ordinary one-way ANOVA was used to determine if each variant yielded statistically significant differences in % absolute APY compared to peptide **1**. p<0.01(**). **(c)** Distributions of AGEs at 60 °C at 24 h for peptides **V1**, **V1^{pY}**, and **V1^{pT}** (n = 3). In order to further investigate the crosstalk between glycation and phosphorylation, we synthesized two variants of peptide **V1** that incorporated either pTyr or pThr (Ac-ETpYRLTF, peptide **V1^{pY}**, and ETYRLpTF, peptide **V1^{pT}**). All three peptides exhibited similar levels of overall glycation and APY formation, despite the introduction of extra negative charges. **(d)** Time course data (% normalized APY, left; % normalized MGH-1, right) at 37 °C for peptides **V1**, **V1^{pY}**, and **V1^{pT}** taken over 24 h, 48 h, and 72 h (n = 3). Peptide **V1^{pT}** was the fastest to form APY, followed by peptide **V1^{pY}**, and then peptide **V1**. **(e)** Ordinary one-way ANOVA was used to determine if each variant yielded statistically significant differences in % absolute APY (left), % absolute MGH-1 (middle left), % absolute [M+144] (middle right), and % absolute total glycation (right) of **V1^{pY}** and **V1^{pT}** compared to peptide **V1** (n = 3). p<0.05(*), p<0.01(**), p<0.0001(****). Absolute APY levels in peptide **V1^{pT}** were three-fold higher than those in peptide **V1**, and both phosphorylated variants exhibited an increase in MGH-1 formation, indicating that phosphorylation can also bias the formation of certain AGEs.

As peptide **1** was identified from a prior study focused on MGH-1, we found that introduction of nearby phosphates appeared to have an impact on MGH-1, rather than APY, formation. To determine if this was also the case for hit peptides, we synthesized two variants of peptide **V1** that incorporated either pTyr or pThr (Ac-ETpYRLTF, peptide **V1^{pY}**, and ETYRLpTF, peptide **V1^{pT}**) (**Figure 4.12 D & Figure 4.13**). At 60 °C for 24 h, all three peptides exhibited similar levels of overall glycation and APY formation, despite the introduction of extra negative charges. Compared to peptide **V1^{pY}** and non-phosphorylated peptide **V1**, peptide **V1^{pT}** showed a significant increase in MGH-1 formation. However, at 37 °C, peptide **V1^{pT}** was the fastest to form APY, followed by peptide **V1^{pY}**, and then peptide **V1** (**Figure 4.12 D**). Absolute APY levels in peptide **V1^{pT}** were three-fold higher than those in peptide **V1**. Interestingly, similar to the trends observed for peptide **1** and its phosphorylated variants, peptide **V1^{pT}** and **V1^{pY}** also exhibited an increase in MGH-1 formation, with absolute MGH-1 levels in peptide **V1^{pY}** observed to be approximately two-fold higher than those in peptide **V1** (**Figure 4.12 D & Figure 4.13**), indicating that phosphorylation can also bias the formation of certain AGEs. Taken together, these data support a model in which crosstalk with protein phosphorylation could have an important, but previously underappreciated role in regulating cellular glycation events.

For peptide **V1** and other peptides we have tested, including phosphorylated versions of peptide **1**, we consistently observe up to four [M+144] species. However, our experiments using phosphorylated variants of peptide **V1** revealed that, for these **V1^{pY}** and **V1^{pT}** variants, we detected only one [M+144] species across all replicates. These findings allowed us to isolate and purify this [M+144] species using HPLC, obtaining purified [M+144]-modified peptide: peptide **V1$^{pT\ [M+144]}$** (**Figure 4.14**). Upon incubating this peptide in PBS without any additional MGO, we observed a conversion from [M+144] to APY over time, further confirming our hypothesis

that [M+144] is a precursor to APY (**Figure 4.14 A**). When incubated at 60 °C, this peptide produced significant APY levels (45.7 ± 1.6 %), consistent with previous results from incubating peptide **V1^{pT}** in the same condition. Therefore, these data not only validate our hypothesis but also suggest that phosphorylated residues can stabilize a specific [M+144] species, showing that phosphorylation has a direct influence on glycation outcomes.

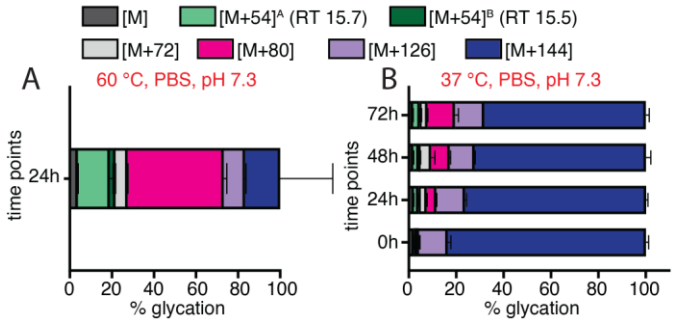

Figure 4.14. [M+144] is a Precursor to APY. Noticing a consistently observed [M+144] species in our dataset on peptide **V1^{pT}**, we purified [M+144]-modified peptide **V1^{pT}**, obtaining peptide **V1$^{pT\ [M+144]}$**. Due to coelution, we also observed an [M+126] adduct in our samples. **(A)** Distributions of AGEs at 60 °C at 24 h for peptide **V1$^{pT\ [M+144]}$** (n = 3). This peptide was confirmed to form APY. **(B)** Distributions of AGEs at 37 °C at 0 h, 24 h, 48 h, and 72 h (right stacked bar graph) for peptide **V1$^{pT\ [M+144]}$** (n = 3 for all reactions). Under these conditions, peptide **V1$^{pT\ [M+144]}$** also showed APY formation over time.

4.3. Discussion

Despite identifying all four sets of common AGEs (MGH-isomers, CEA/MGH-DH, APY, and [M+144]) on a complete proteomics dataset, the limited number of peptides in each set after data processing significantly hindered the statistical power in our gene ontology analyses. Indeed, this is a problem many PTM proteomics studies looking to identify peptide modifications currently face. Specifically, for glycation proteomics, this challenge is exacerbated by the lack of enrichment protocols that can be used to enrich for all AGEs, so we envision that an antibody specific to all MGO-modified AGEs can also be helpful in increasing the number and abundance quality of all AGEs identified in proteomic datasets. Future glycation proteomics studies may also consider using a specific antibody to enrich for a particular AGE of interest (i.e. using a

specific MGH-1 antibody to enrich for MGH-1). Unfortunately, there is no current antibody specific only to APY. Another challenge in proteomics is the lack of clarification on AGEs with the same mass change. This is also seen as we could not separate MGH-DH from CEA, MGH isomers, and [M+144] species from one another. In metabolomics, isotopically labeled standards can be used to address this problem. Similarly, we envision that deuterated MGO can be use in future studies to distinguish confounding AGE isomers from one another. Despite the lack of enrichment tools, we were able to obtain statistically significant data *via* functional clustering analyses that suggest a connection between APY formation and phosphorylation in the cellular context.

Encouragingly, our proteomics data show that APY is likely to be a major AGE in cells. We suspect the prevalence of APY has seemingly been underestimated in previous studies, either due to the use of enrichment protocols that are poorly suited to capture APY,[52,54] or due to a focus on AGEs that were previously established to be abundant in prior work.[62,180] In **Chapter 3**, our *in vitro* studies revealed the potential for crosstalk between glycation and phosphorylation, showing the presence of nearby phosphorylated side chains to enhance, and potentially bias, particular AGEs to form. In this chapter, these peptide data are now supplemented with quantitative proteomics analysis on MGO-treated cells, revealing a possible correlation between phosphorylation and APY formation that was notably missing for other AGEs and Arg PTMs like acetylation and dimethylation. This correlation was further confirmed using *in vitro* glycation experiments on phosphorylated peptide substrates. As mentioned, we have not been able to find any reports suggesting that nearby phosphorylated sites influence glycation. Therefore, our study is the first to show that glycation may be coincident with phosphorylation on the same substrates, and that the presence of these nearby phosphates may bias the resulting AGE distribution. Our

future work will seek to fully elucidate both the chemical and biological significance of this phenomenon.

Finally, our mechanistic studies on APY formation on a short peptide model allowed us to draw a potential correlation between two distinct PTMs that was further supported via proteomics experiments, bridging the chemical mechanism of APY and its cellular formation. These studies therefore not only provide much needed insights into APY formation under physiologically relevant conditions, but also reveal critical aspects of the glycation landscape. In future studies, we plan to leverage this information to generate novel chemical tools that can be used to track and/or control APY formation in living cells, including the development of tools that harness APY's unique autofluorescent properties for bioconjugation and to assist in the study of APY biology.

4.4. Materials and Methods

4.4.1. General Materials

HEK-293T cells were purchased from ATCC. Water used in glycation experiments was distilled and deionized using an Arium Pro purification system (Sartorius). All statistical analysis was conducted using Prism GraphPad.

4.4.2. α-MGH-1 and α-APY Antibody Screening for On-bead Peptide Glycation

To test the specificity of the α-APY antibody, peptide 1 was synthesized using Fmoc-based solid phase peptide synthesis on ChemMatrix® resin (100-200 mesh, 0.51 mmol/g loading, PCAS BioMatrix, Inc., 1040378). On-bead peptide synthesis was adapted from protocols reported by McEwen et al.[19] After side chain deprotection, beads were washed with DMF (3 x 1 min), DCM (3 x 1 min), followed by ultrapure water (3 x 1 min), and allowed to

equilibrate in ultrapure water overnight. The following day, on-bead peptides (2.55 µmol) were treated with 2 equiv. of MGO (5.1 µmol) in water and PBS (20 mM final concentration) and allowed to incubate at 37°C for 3 hours (or 24 hours followed by 24 hours of dilution for a total of 48 hours according to dilution protocols). Following incubation, beads were washed (3 x 1 min) with 20 mM Tris buffered with 150 mM NaCl containing 0.1% Tween (TBST) to remove excess MGO. Subsequently, beads were blocked using a 1% solution of bovine serum albumin (BSA) in TBST for 2 hours at room temperature. The blocked beads were then incubated with a 1:1000 dilution of either α-MGH-1 antibody (Cell BioLabs, Inc. STA-011) or α-APY antibody (Cosmo Bio Co., LTD., NOF-N213430-EX) for 18 to 20 hours at room temperature. After incubation with primary antibody, beads were washed with TBST (5 x 1 min) and exposed to a 1:1000 dilution of α-mouse secondary antibody (Abcam, AB7069) conjugated to alkaline phosphatase for 2 hours at room temperature. After incubation with secondary antibody, beads were washed with TBST (3 x 1 min) and alkaline phosphatase buffer (100 mM Tris-HCl, 150 mM NaCl, 1 mM $MgCl_2$ at pH 9.0) (3 x 1 min) and allowed to equilibrate in the buffer for 15 min. Afterwards, beads were exposed to color-developing reagents 5-bromo-4-chloro-3-indolyl phosphate and nitro blue tetrazolium (BCIP/NBT, Promega, S3771), washed with TBST (3 x 1 min), and transferred to a petri dish for microscopic imaging (Leica DMi8).

4.4.3. Mammalian Cell Culture and Sample Preparation of TMT-labeled Peptides

150 mm culture dishes were seeded with 10 x 10^6 HEK-293T cells in triplicates and grown to confluency in DMEM with 10% FBS supplementation. Cells were treated with 2 mM MGO in serum free DMEM for 24 hours and harvested using TrypLE Express (Gibco). Following MGO treatment, cell viability was accessed using a Trypan blue viability assay on a plate reader. Cell pellets were lysed in 200 µl ice cold 8 M Urea/50 mM triethylammonium

bicarbonate (TEAB) with phosphatase/protease inhibitors (Pierce) and sonicated at 10% amplitude with 3 x 10 s pulses, followed by centrifugation at 15000 rpm for 15 min. Supernatant was collected, reduced with 8 mM dithiothreitol for 1 h, alkylated with 20 mM iodoacetamide for 30 min at room temperature in the dark. Subsequently, samples were digested overnight with trypsin at 37 °C. The digestion reaction was quenched using 0.1% trifluoroacetic acid, and samples were desalted using Pierce™ Peptide Desalting C_{18} Spin Columns (#89852). Peptides were collected and dried using a speedvac prior to TMT labeling.

4.4.4. TMT Labeling Protocol

100 µg of the dried peptide samples were reconstituted in 100 µL of 100 mM TEAB buffer. Each sample was then labeled using TMT 10-plex as per the manufacturer's instructions (TMT10plex™ Isobaric Label Reagents and Kits, #90111). The labeling reaction mixture was incubated at room temperature for 1 h and quenched using 5 µL of 5% hydroxylamine solution with incubation for 15 min at room temperature prior to pooling. The pooled sample was then dried, desalted and reconstituted in 0.1% formic acid for LC-MS/MS analysis. The 10 TMT channels are composed of three biological replicates (each with three technical replicates) and one pool sample, in which the sample ratio between the pool channel (i.e., channel 126) and channels 127N, 127C, 128N, 128C, 129N, 129C, 130N, 130C and 131 is expected to be 1. The experiment was carried out in two batches where the pooled samples (i.e. channel 126) served as the bridge channel. In the first batch, 3 biological replicates of the untreated samples were labeled with 127N, 127C, 128N TMT tags, 3 biological replicates of the samples treated with 0.5 mM MGO were labeled with 128C, 129N, 129C and 3 biological replicates of the samples treated with 1 mM MGO were labeled with 130N, 130C, 131 TMT tags. In the second batch, 3 biological replicates of the samples treated with 2 mM MGO were labeled with 127N, 127C,

128N TMT tags, 3 biological replicates of the untreated mitochondrial samples were labeled with 128C, 129N, 129C and 3 biological replicates of the mitochondrial samples treated with 1mM MGO were labeled with 130N, 130C, 131 TMT tags.

4.4.5. Mass Spectrometry Data Acquisition for Proteomic Analysis

LC-MS/MS data acquisition for TMT-labeled pooled sample was carried out using Thermo Scientific Orbitrap Exploris 240 (Thermo Fisher Scientific, Bremen, Germany) connected with Vanquish Neo UHPLC system (Thermo Fisher Scientific, Germany). Reconstituted peptides were loaded onto a trap column (300µm x 5mm, Thermo Scientific PepMap Neo Trap Cartridge, 174500). Peptides were separated on an analytical column (75µM x 150mm, Thermo Scientific EASY-Spray™ PepMap™ Neo UHPLC columns, ES75150PN) at a flow rate of 300 nL/min using an optimized linear gradient of 2%-45% acetonitrile for 235 min. Mass spectrometry data were acquired in data-dependent acquisition (DDA) mode with "top speed" of 3 sec cycle time. MS1 scans were acquired at a mass resolution of 60,000. The automatic gain control (AGC) target value for precursor ion acquisition was set to 1×10^6 and maximum ion injection time was set to automatic mode. Scan range of masses was at 350-1400 m/z. RF lens was set at 70%. Isolation width of 0.4 m/z was used for precursor ion selection and fragmented using higher-energy collision dissociation (HCD) with 36% normalized collision energy. MS2 scans were acquired at a mass resolution of 45,000 with AGC target as 1×10^6 and maximum ion injection time at auto mode. A FAIMS Pro Interface was connected to the Exploris 240 mass spectrometer. The compensation voltage (CV) of the FAIMS Pro interface was set to a combination of -45, -60 and -75 CVs. Each of the three CVs used was set to run DDA mode for 1 s cycle to build a big cycle of 3 s.

4.4.6. Mass Spectrometry Proteomic Data Processing and Analysis

All RAW files were processed and analyzed using Thermo Proteome Discoverer (PD) v.3.0. All database searches were performed using MSFragger-PD node (PMID: 36475762) as the combination of MSFragger and PeptideProphet (Philosopher) processing nodes. The default settings were predominantly used in MSFragger-PD node unless otherwise stated. Homo sapiens (SwissProt TaxID 9606, 20422 proteins) was used for the protein database. For all searches, trypsin cleavage was set to full, a precursor mass tolerance of 20 ppm was used, with a fragment mass tolerance of 0.6 Da allowing tryptic peptides only with up to two missed cleavages. The raw data was searched for five dynamic PTM combinations that could be found on peptides. The static modifications included carbamidomethylation (+57.021 Da) of cysteine and TMT-modification (+229.163 Da) of lysine and peptide N-terminus, and the dynamic modifications included argpyrimidine (+80.026 Da, R), methylglyoxal-derived hydroxyimidazolone isomers (MGH-isomers) (+54.011 Da, R), carboxyethyl arginine/lysine or MGH-DH (CEA/CEL/MGH-DH) (+72.021, R, K), tetrahydropyriminidine (THP) and/or other [M+144] AGEs (+144.041 Da, R), and phosphorylation (+79.966 Da; S, T, Y). A separate, parallel analysis was performed using the same static modifications but a different combination of dynamic modifications, including dimethylation (+28.031 Da, R), acetylation (+42.011 Da, R), argpyrimidine (+80.026 Da, R), and phosphorylation (+79.966 Da; S, T, Y). A “closed” search was performed to minimize the computational requirements for database searching for each technical replicate and all FAIMS parameters included in this study. PeptideProphet was used for PSM validation on these searches allowing a 1% FDR (false discovery rate). All bioinformatic analysis of LC-MS/MS data was performed in the R statistical computing environment. Gene Ontology (GO) enrichment analysis was performed using DAVID (PMID: 19131956) and proportional venn diagrams were generated using https://www.deepvenn.com/.

4.4.7. MassIVE Submission

The mass spectrometry proteomics data have been deposited to the MassIVE repository with the dataset identifier MSV000097149.

5. Chapter 5:

Harnessing Autofluorescent Properties of a Native Arginine Modification

5.1. Introduction

While MGO-derived AGEs have been correlated with numerous diseases, the causal relationship between AGEs and disease remains unknown. Since glycation occurs non-enzymatically, traditional tools used to study PTM via enzymatic inhibition or profiling are unsuitable for studying AGEs and glycation biology. Furthermore, there is a lack of tools and methods to monitor MGO in live cells, complicating our understanding of its cellular localization and accumulation and its role in biological processes and diseases. Therefore, the development of a fluorescence tool that can be used to visualize AGE formation in live cells as a result of MGO modification is of utmost importance.

Classically, fluorescent AGE contents in biological samples such as tissues, extracts from homogenates of skin biopsies, and processed food samples are typically analyzed using fluorescence spectroscopy ($\lambda_{emission}$ = 440-460 nm, $\lambda_{excitation}$ = 360-370 nm).[181–183] However, these studies detected fluorescent AGEs as a whole, with little to no chemical or structural information. In addition, this approach does not account for crosstalk with other autofluorescent AGEs or compounds in biological samples that might result in an increased background noise. Measuring fluorescence intensity of AGEs as a sum can also skew data towards stable AGEs that accumulate on long-lived proteins rather than AGEs that forms at earlier time points or are short-lived due to degradation or conversion into other AGEs.

Many recent studies have focused on developing small molecule fluorescent probe to track MGO and AGE formation in tissue and cells.[26,184–186] For instance, a recent study has reported the development of a specific fluorescent probe to detect ribose-derived AGEs using a diversity oriented fluorescence library (DOFL) approach to screen for an increase in fluorescence intensity in AGE-modified compared to untreated BSA samples.[184] However, while this

BODIPY-based small molecule fluorescent probe, called AGO, was shown to detect AGE fluorescence on BSA over time and in a glycated collagen mimicking model, the DOFL design still lacks an inherent understanding of the target recognition mechanism as AGEs were treated as a collective in these experiments. Without knowing what AGE species were generated in the glycated condition, the mechanism through which this probe binds or covalently reacts with these AGEs remains a mystery. Therefore, while AGO is suitable to be used as an indication of increased AGE formation on proteins and can be monitored using fluorescence microscopy, it does not address the heterogeneity inherent to glycation. While other turn-on fluorescent probes for MGO have also been reported with demonstrated chemical mechanisms, these probes targeting free MGO are diffusely localized and cannot provide information about local changes in specific subcellular compartments.[26,186]

Overall, AGEs can be classified into crosslinking and non-crosslinking AGEs. Thanks to their ability to assemble conjugated ring structures from two nucleophilic residues, several crosslinking AGEs, including pentosidine, vesperlysine, and crossline, are autofluorescent. In contrast, APY is the only known characterized non-crosslinking autofluorescent AGE from MGO modification of Arg. This represents a potential for APY to be used as a naturally occurring autofluorescent biomarker that is known to occur *in vivo* with site-selectivity. However, until this work, it has been difficult to form APY in experimentally convenient amounts and to track APY formation, both *in vitro* and *in vivo*, due to an unknown chemical mechanism of formation. Therefore, our studies provide essential mechanistic insights that enable future research on developing APY as a native, autofluorescent tool that can be used to track AGE formation and MGO accumulation in cells.

Toward this goal, the preliminary work in this chapter begins by investigating the fluorescence properties of APY and confirming its wavelengths on a short peptide *in vitro*. We conduct excitation and emission scans of APY fluorescence and confirm its detection compatibility with several different instruments, including UV-Vis, plate reader, spectrophotometer, and two photon microscopy. We also report a first measurement of relative quantum yield of APY on purified peptide $\mathbf{1}^{\mathbf{APY}}$. These results will inform future studies on developing analytical methods to track MGO-derived glycation using APY fluorescence and potential chemical fluorescent probes based on APY chemistry.

5.2. Results

5.2.1. Detection of APY Fluorescence using HPLC

The characteristic fluorescence wavelengths of APY (ex = 320 nm, em = 385 nm) have been reported and can be measured using an HPLC system equipped with a fluorescence detector.[18,37,126] In **Chapter 2**, we have successfully identified a condition at which APY become the predominant AGE with >50% conversion on peptide **1**. Due to high levels of APY observed at 60 °C, we were able to confirm its identity using its characteristic fluorescence wavelengths (**Figure 5.1**).[18,88,100,187] APY absorbance and fluorescence peaks were observed in both the reaction and purified peptide $\mathbf{1}^{\mathbf{APY}}$ samples (**Figure 5.1 a, c**), yet were absent in the control sample (**Figure 5.1 b**), confirming the presence and identity of APY in our samples.

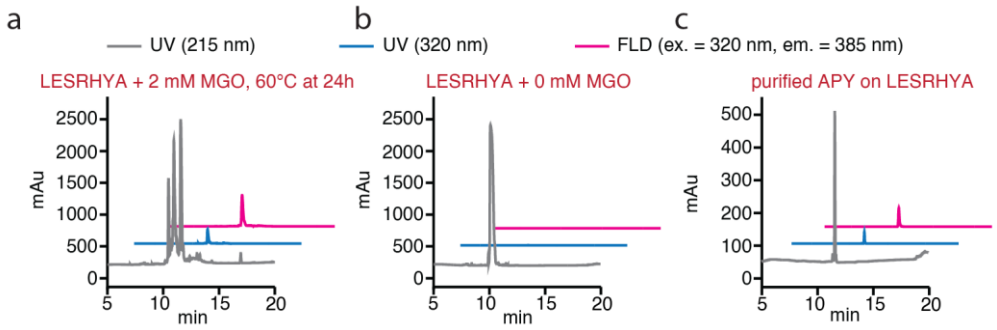

Figure 5.1. Detection of APY Fluorescence by Analytical HPLC. (a) HPLC chromatogram for the reaction of peptide **1** treated with MGO at 60 °C. **(b)** HPLC chromatogram for peptide **1** in the absence of MGO at 0 h. **(c)** HPLC chromatogram for purified APY-modified peptide **1** (peptide $\mathbf{1}^{\mathbf{APY}}$). Absorbance at 215 nm and 320 nm was collected to observe peptide bond and APY absorbance wavelengths, respectively. Fluorescence excitation at 320 nm and emission at 385 nm were collected based on reported APY characteristic fluorescence wavelengths.

5.2.2. Surveying the Excitation and Emission Wavelengths of APY on Short Peptides

Following its purification, we set out to investigate its fluorescence properties using different instruments to further explore its potential for developing into an autofluorescent sensor in our peptide platform. Since APY is typically detected using HPLC, which is unsuited for obtaining full excitation and emission spectra, we sought to obtain the full APY fluorescence spectra. In collaboration with the Thomas lab, we were able to conduct excitation and emission scans for peptide $\mathbf{1}^{\mathbf{APY}}$ and MGO-treated peptide **1** for 24 h at 60 °C, a condition which we have shown to produce APY as a major adduct (**Figure 5.2 a, b**). As controls, we also conducted scans for peptide **1** treated with/without MGO following the standard 24 h post 24 h dilution protocol at 37 °C (**Figure 5.2 c, d**) and for peptide **1** treated with MGO at 60 °C for 5 minutes (instant control), a condition at which no APY was observed but accounted for all other reaction components in the reaction mixture (**Figure 5.2 e**). Reaction components such as tris, PBS, and ultrapure water did not interfere with APY fluorescence (**Figure 5.2 f**). Comparison between modified samples with unmodified peptide **1** revealed two separate peaks with maxima at 320 nm and 385 nm that appear only for samples containing APY. We also obtained UV-Vis data for peptide **1**, showing APY absorbance at 320 nm (**Figure 5.2 e**). The absorbance at 280 nm

matches that of the Tyr residue on peptide **1**. These results are consistent with our and other's HPLC data, confirming its excitation and emission maxima.[18,36,88,187]

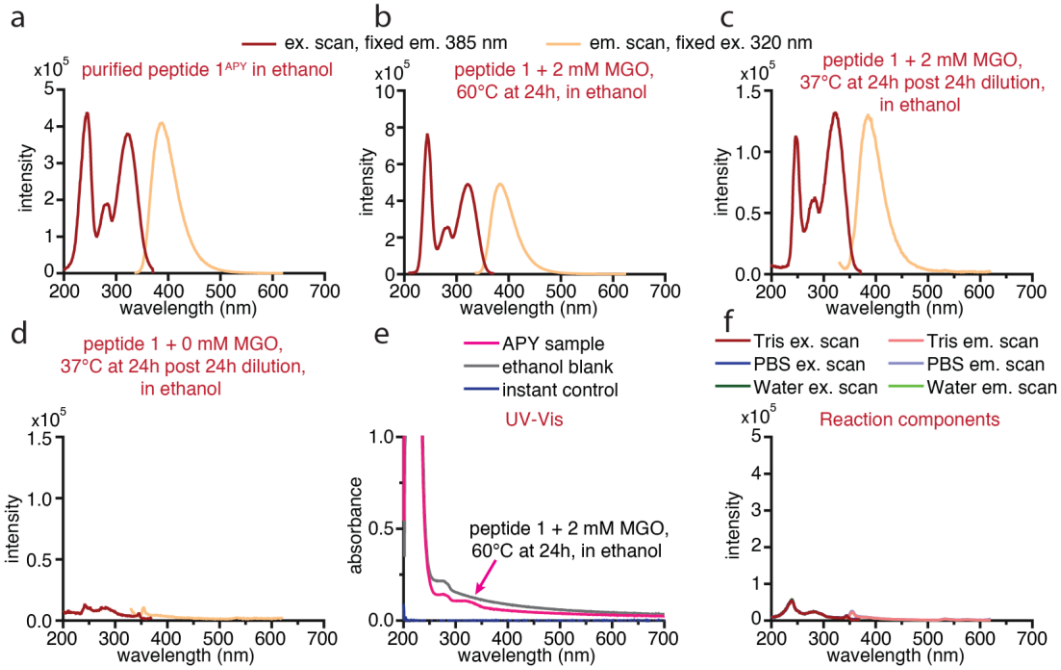

Figure 5.2. Optical Spectra obtained from spectrofluorometer confirm APY Fluorescence. Fluorescence excitation at 320 nm and emission at 385 nm were collected based on reported APY characteristic fluorescence wavelengths. Excitation scans are conducted with a fixed emission wavelength at 385 nm, and emission scans are conducted with a fixed excitation wavelength at 320 nm. Reactions were performed following standard glycation protocols and were solubilized in spectroscopy grade ethanol in a quartz cuvette for measurements. Absolute intensity is reported. **(a)** Spectra for purified peptide $\mathbf{1}^{\mathbf{APY}}$. **(b)** Spectra for the reaction of peptide **1** with MGO at 60 °C for 24 h. **(c)** Spectra for the reaction of peptide **1** with MGO at 37 °C. This reaction was incubated for 24 h, then diluted 100X in PBS for another 24 h following standard dilution protocols to observe AGE rearrangements. In Chapter 2, we showed that APY levels approximated 10% under this condition. **(d)** Spectra for the reaction of peptide **1** without MGO following the same dilution protocols as described in **(c)**, showing no APY fluorescence. **(e)** UV-Vis absorbance of APY sample (peptide 1 treated with MGO 60 °C for 24 h), instant control (peptide 1 treated with MGO 60 °C for 5 minutes), and ethanol blank, showing absorbance at 320 nm observed only in the APY sample. **(f)** Spectra of other components in our reactions, including tris (used to quench MGO), PBS, and ultrapure water.

While the spectrofluorometer provides more precise and accurate measurements of APY fluorescence, it is technically cumbersome and is inaccessible to many researchers. In contrast, the plate reader as a benchtop instrument is widely available, easy to use, and compatible with low reaction volumes (50 µL) typical in our glycation reaction protocols. Therefore, we investigated whether we could also obtain similar spectra of APY fluorescence on our short

peptides. To start, we performed excitation and emission scans for purified peptide $\mathbf{1}^{\mathbf{APY}}$ in serial dilution and found that the best spectra were observed when APY concentration was between 0.0375 mM and 0.15 mM. Excitation maxima were observed at 320 nm, while emission maxima were observed at 395 nm. These values match those of purified peptide $\mathbf{1}^{\mathbf{APY}}$ and MGO-treated peptide **1** samples containing APY obtained from the spectrofluorometer, confirming that APY can be detected on peptide $\mathbf{1}^{\mathbf{APY}}$ using a plate reader.

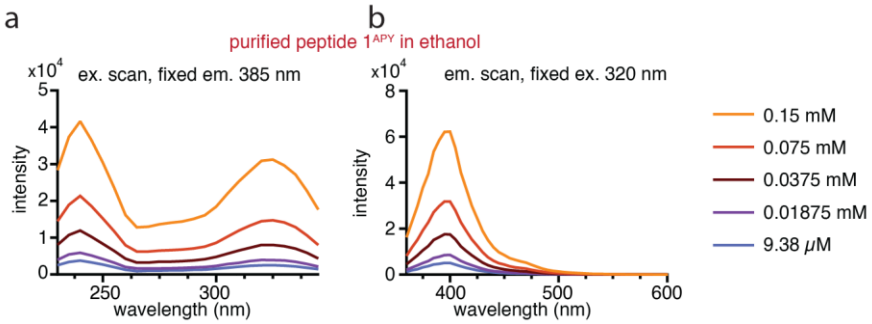

Figure 5.3. Optical Spectra obtained from Plate Reader confirm APY Fluorescence. Fluorescence excitation at 320 nm and emission at 385 nm were collected based on reported APY characteristic fluorescence wavelengths. Excitation scans are conducted with a fixed emission wavelength at 385 nm, and emission scans are conducted with a fixed excitation wavelength at 320 nm. Absolute intensity is reported. For purified peptide $\mathbf{1}^{\mathbf{APY}}$, **(a)** excitation scans and **(b)** emission scans were conducted over a range of concentrations. Serial dilution was performed by diluting the peptide $\mathbf{1}^{\mathbf{APY}}$ stock in ultrapure water to the desired concentration.

To further explore APY detection on sequences other than peptide **1** that might contain other fluorescent amino acid residues, we synthesized four different sequences following the motif YLRGPGXLA, where X is Trp (peptide **W**), Phe (peptide **F**), Tyr (peptide **Y**), or His (peptide **H**) (**Figure 5.4**). This peptide platform was previously developed in our lab for the discovery of an Arg-Arg crosslink with MGO, in which X is Arg.[11] In this study, the two Arg were found to be in proximity and face one another, allowing for the crosslink to form. Therefore, we hypothesized that we could use the same sequence motif to observe whether the fluorescence of any aromatic residue would interact with that of APY. First, we confirm that after incubation for 24 h at 60 °C, all four sequences formed APY as the predominant adduct,

consistent with previous results reported in **Chapter 2 and 3** (**Figure 5.4 a, b**). Upon conducting excitation and emission scans for these peptides, we found that while the absorbance at 280 nm increased for peptide **Y** and peptide **W** due to Tyr and Trp absorbance,[188–190] there were negligible differences in the excitation and emission maxima for APY, confirming that APY fluorescence does not overlap with that of other native aromatic residues. Importantly, comparisons between 0 h and 24 h time points show that APY characteristic excitation and emission wavelengths only appear in samples after 24 h incubation. Together, these preliminary data confirm that APY fluorescence can be reliably detected on short peptides comprising various aromatic residues using not only HPLC but also a plate reader, with similar spectra to those obtained from a spectrofluorometer. These results suggest that a plate reader compatible assay can be developed to detect APY fluorescence in future studies.

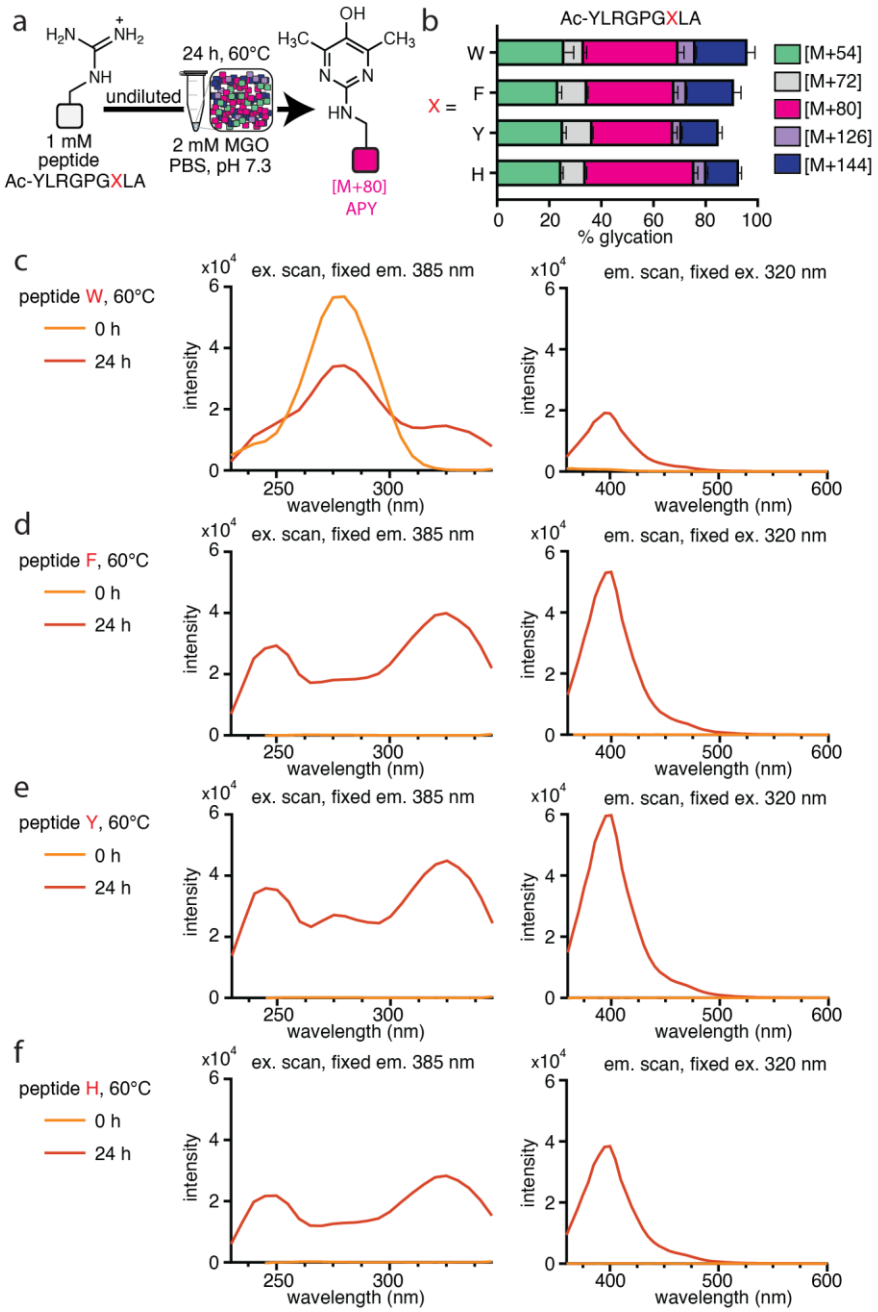

Figure 5.4. Aromatic Residues do not interfere with APY Fluorescence. Fluorescence excitation at 320 nm and emission at 385 nm were collected based on reported APY characteristic fluorescence wavelengths. Excitation scans are conducted with a fixed emission wavelength at 385 nm, and emission scans are conducted with a fixed excitation wavelength at 320 nm. Absolute intensity is reported. **(a)** General scheme depicting the glycation reactions of peptides and MGO at 60 °C. These peptides contain aromatic residues in place of the **X** position: peptides **W**, **F**, **Y**, and **H** were synthesized and tested. **(b)** Distribution of AGEs observed for peptides **W**, **F**, **Y**, and **H** (n = 3), showing APY as the predominant adduct after 24 h incubation at 60 °C. **(c)** Excitation (left) and emission (right) scans for peptide **W**. **(d)** Excitation (left) and emission (right) scans for peptide **F**. **(e)** Excitation (left) and emission (right) scans for peptide **Y**. **(f)** Excitation (left) and emission (right) scans for peptide **H**.

5.2.3. Investigating APY Fluorescence for On-bead Visualization

Because APY fluorescence cannot be observed using our confocal microscope due to its short wavelengths, we hypothesized that we would be able to observed APY fluorescence on beads using two photon microscopy. However, the multiphoton microscope that we have access to at the Tufts Imaging Center does not accommodate these wavelengths (lowest excitation at 690 nm, but for APY, 320 x 2 = 640 nm), so we were not able to accomplish this objective.

Since we could not observe any fluorescence under a microscope, we were curious to see how bright APY is as a fluorophore, which can be quantified using quantum yield (QY) calculations. With the help of the Thomas lab and Dr. Guzman, we report, for the first time, the QY value of APY on purified peptide $\mathbf{1}^{\mathbf{APY}}$. Relative QY was calculated using an anthracene standard and was determined to be **0.21**. This QY is significantly higher than that of the APY in the reaction mixture (24 h post 24 h dilution) before purification (**0.03**), which has all of the other AGEs from incubation of peptide **1** with MGO and other reaction components such as PBS and DMF. Before purification, APY makes up of approximately 10% of the sample, so this QY value of **0.21** is consistent with an expected higher value for purified peptide $\mathbf{1}^{\mathbf{APY}}$. Compare to the reported QY values for other native fluorescent residues such as Tyr (QY = 0.14), Trp (0.13), and Phe (0.024), the QY of APY suggests that it is potentially bright enough for fluorescent microscopy.[188] However, these preliminary data only represent one replicate, so future studies should confirm the relative QY of APY by performing more replicates before further testing. Since relative QY was determined because our APY samples are always in solutions, crystallization of purified peptide $\mathbf{1}^{\mathbf{APY}}$ might be necessary for future experiments looking to calculate an absolute QY value using an integrating sphere.

5.3. Discussion

Understanding the causal relationship between AGE accumulation and certain diseases is important for demystifying glycation biology. Therefore, monitoring AGE levels and MGO localization in biological samples using fluorescent tools can provide critical insights into the glycation as a functional PTM. Given the fluorescent properties of APY, several studies have suggested that APY can be an important biomarker in diseases.[47,88,191] However, detection of APY fluorescence remains limited to HPLC methods. In particular, the excitation and emission wavelengths of APY are known to be 320 nm and 385 nm, respectively. Although this range is too low for current commercial confocal microscopy systems to visualize its fluorescence under a microscope, future studies can explore methods to induce a red shift in APY wavelengths such as employing chemical modification of the conjugated APY ring or using Förster resonance energy transfer (FRET).

In this chapter, we have shown that APY fluorescence can be reliably detected using instruments other than the traditional HPLC, including spectrofluorometer, UV-Vis, and plate reader. Our studies revealed that other native aromatic residues do not interfere with APY autofluorescence. These results, obtaining excitation and emission spectra using a plate reader, will inform future research on the development of a plate reader assay that can potentially detect and quantify APY levels in cells.

Finally, despite considerable interest in APY as an autofluorescent biomarker, there is virtually no known information about its QY or fluorescence lifetime. Herein we calculated a relative QY value for APY on a short peptide, which to our knowledge has not been reported. Our relative QY calculations revealed that, for pure APY on a short peptide sample, APY is considerably brighter than other native aromatic residues as a fluorophore. Our future work will

continue to explore its other autofluorescent properties to develop fluorescent tools that can be used to predict and/or track AGE formation and MGO accumulation in live cells.

5.4. Materials and Methods

5.4.1. General Materials

All chemical reagents and solvents were of analytical grade, obtained from commercial suppliers, and used without further purification, unless otherwise noted. Methylglyoxal (MGO) (40% w/v in water) was purchased from MilliporeSigma (M0252). Water used in glycation experiments was distilled and deionized using an Arium Pro purification system (Sartorius). All statistical analysis was conducted using Prism GraphPad.

5.4.2. Preparation of APY-Modified Peptide 1

APY-modified peptide **1** (peptide $\mathbf{1}^{\mathbf{APY}}$) was prepared by incubation of 200 µL of 20 mM peptide 1 stock in DMF with 400 µL of 10 mM MGO stock in ultrapure water and 400 µL of 100 mM PBS stock in ultrapure water (pH 7.3) at 60 °C for 24 hours. Under this condition, APY was the predominant adduct (roughly 50% yield by LC-MS) and was purified by semi-preparative HPLC system as described above using a gradient of 5% to 50% acetonitrile (B) in water (A) over 14.25 min at 3.0 mL/min. Collected fractions were characterized by MALDI-TOF, pooled, lyophilized, and assessed for purity by LC-MS prior to further experiments. The identity of peptide $\mathbf{1}^{\mathbf{APY}}$ was confirmed by its characteristic absorbance at 320 nm and fluorescence excitation and emission at 320 nm and 385 nm, respectively.

5.4.3. Analytical HPLC Assay for APY-Modified Peptide 1 Fluorescence

The mobile phase contained water (A) and acetonitrile (B) with 0.1% formic acid. Peptide glycation reactions were injected onto an AdvanceBio Peptide 2.7 µm column (2.1 × 150 mm, Agilent) with the following method with a flow rate of 0.4 mL/min: isocratic at 5% B between 0.00-1.75 min, gradient change from 5% B to 40% B between 1.75-16.00 min, gradient change from 40% B to 100% B between 16.00-20.00 min, isocratic column washing at 100% B between 20.00-23.00 min, and re-equilibration at 5% B between 23.01-30.00 min. APY-specific absorbance could be detected using its characteristic absorbance at 320 nm.

5.4.4. Plate Reader Assay for APY Fluorescence

Following peptide glycation reactions, 50µL of each reaction was pipetted into separate wells in a 384 well plate (Corning 384 Flat Black, Cat. No. 3764), and excitation and emission scans were performed using top reading (no lid) on a Tecan Spark 10M plate reader. For excitation scans between 230 nm and 340 nm, emission wavelength was held constant at 385 nm. For emission scans between 360 nm and 600 nm, excitation wavelength was held constant at 320 nm. Step size was 5 nm. Z-position mode was set to manual, and Z-position was 26000 µm. Number of flashes was 30, and integration time was 40 µs.

5.4.5. Acquisition of Optical Properties for APY using Spectrofluorometer

In collaboration with Dr. Elisa Guzman and the Thomas lab, solution samples for optical data were prepared in quartz cuvettes and spectroscopy grade ethanol. Peptide samples were diluted in a solution until optical density was less than 0.1 as measured by a Varian Cary-Flexible spectrometer UV-Vis to measure absorbance. Using the solutions with an optical density less than 0.1, emission spectra were collected using a PTI Quantum Master 4 with a 90° angle detector and a 75 W Xe lamp radiation source. Starting with the maximum absorbance

wavelength as the excitation wavelength, emission spectra were optimized shifting the excitation wavelength until the full curve was recorded. Using the same solutions as above, excitation spectra were collected using the PTI Quantum Master 4 with a 90° angle detector and a 75 W Xe lamp radiation source. Starting with the maximum emission wavelength found previously, excitation spectra were optimized shifting the emission wavelength until the full curve was recorded. Data analysis used the software FelixGX. Quantum yield measurements for the peptides in solution were calculated using data obtained from the PTI Quantum Master 4 with a 90° angle detector and a 75 W Xe lamp radiation. Dilute ethanol solutions were compared to anthracene as the reference standard[192] for calculating quantum yield in accordance to the protocol outlined in *A Guide to Recording Fluorescence Quantum Yields* by Horiba Scientific.[193]

6. Appendices

	Exact Mass (Da)	Δ Mass (Da)	RT (min)
unmodified peptide 1	916.4368	0	9.33
$\mathbf{1}^{\mathbf{MGH\text{-}1}}$	970.4482	54.0114	10.0
$\mathbf{1}^{\mathbf{MGH\text{-}DH}}$	988.4621	72.0253	9.43
$\mathbf{1}^{\mathbf{CEA}}$	988.4591	72.0223	10.10
$\mathbf{1}^{\mathbf{APY}}$	996.4646	80.0278	11.04
$\mathbf{1}^{\mathbf{[M+144]}}$	1060.4814	144.0446	10.03
$\mathbf{1}^{\mathbf{[M+144]}}$	1060.4818	144.0450	10.35
$\mathbf{1}^{\mathbf{[M+144]}}$	1060.4822	144.0454	9.55
$\mathbf{1}^{\mathbf{[M+144]}}$	1060.483	144.0462	9.90

Table 6.1. AGE Adducts for Peptide 1, reported with exact mass (Da), Δ Mass (Da), and retention time (RT, min).

Annotated Sequence	Gene	Master Proteins	Modifications in Master Proteins
[K].LDVTILSPSRK.[V]	FLNB	O75369-8 [977-987]	1xAPY [R986]
[K].RILDIGK.[K]	TAF4B	Q92750-1 [663-669]	1xAPY [R663]
[K].IFVGGIKEDTEEYNLRDYFEK.[Y]	HNRNPA3	P51991-1 [128-148]	1xPhospho [Y/T]; 1xAPY [R143]
[R].ARARTIIK.[W]	UHRF1	Q96T88 [206-213]	1xAPY [R207]
[R].VHASFTRK.[Y]	SCAND3	Q6R2W3 [729-736]	1xAPY [R735]
[R].LAVYIDRVR.[S]	LMNA	P02545-2 [42-50]; P02545 [42-50]	P02545-2 1xAPY [R48]; P02545 1xAPY [R48]
[K].HRNTSAVLGCLAEK.[L]	RSPRY1	Q96DX4 [199-212]	1xAPY [R200]
[K].VLVPQRR.[L]	STAB2	Q8WWQ8 [1126-1132]	1xAPY [R1131]
[K].RGVLGMANK.[G]	PPIL6	Q8IXY8 [240-248]	1xAPY [R240]
[K].RIPPAIK.[S]	COPS8	Q99627-1 [59-65]	1xAPY [R59]
[K].EKLCYVALDFEQEMVRAAASSSPER.[S]	ACTBL2	Q562R1 [215-239]	1xAPY [R]; 1xTHP [R230]
[K].IETYRLTFRANAR.[A]	MAP4	P27816-6 [1088-1100]	1xAPY [R1092]
[K].RLNIRVISGQQLPK.[V]	PLCD1	P51178-1 [630-643]	1xAPY [R634]; 1xTHP [R630]
[K].ILENLRGGTNIIK.[L]	CSNK2A2	P19784 [85-97]	1xAPY [R90]
[R].TGARSLQFR.[A]	LRGUK	Q96M69 [25-33]	1xPhospho [S29]; 1xAPY [R28]
[K].HGDTGRR.[Y]	FGF20	Q9NP95 [158-164]	1xAPY [R163]
[R].DGSLLRSSSRR.[R]	MYOM3	Q5VTT5 [309-318]	1xMGH [R314]; 1xAPY [R317]
[K].KIIVLTGAGVSVSCGIPDFRSR.[D]	SIRT1	Q96EB6 [255-276]	1xAPY [R276]; 1xTHP [R274]
[K].GLTLLRIQIFK.[M]	SLC23A1	Q9UHI7-1 [243-253]	1xAPY [R248]
[K].GERLRLPPWLK.[T]	LIAS	O43766-1 [71-81]	1xCarboxyethyl (CEL/CEA) [R73]; 1xAPY [R75]
[R].YMLVRYEDVARGPLQK.[A]	CHST3	Q7LGC8 [366-381]	1xPhospho [Y371]; 1xAPY [R370]
[R].ADTLDPALLRPGRLDRK.[I]	PSMC4	P43686 [314-330]	1xCarboxyethyl (CEL/CEA) [R326]; 1xAPY [R323]; 1xTHP [R329]
[K].ASLPTVSSRPRDPLDILTK.[I]	DMRTA1	Q5VZB9 [317-335]	1xAPY [R325]
[R].MNSCAGAVYGSHGRRGR.[Q]	HOXA6	P31267 [143-159]	1xPhospho [S153]; 2xAPY [R156; R157]
[K].DFGLGPRTFK.[R]	GPALPP1	Q8IXQ4 [201-210]	1xAPY [R207]
[R].AQGSVAFDYRK.[R]	SPTBN2	O15020 [2281-2291]	1xPhospho [Y2289]; 1xAPY [R2290]
[R].LLRLDLRENEIK.[T]	PPP1R37	O75864-1 [391-402]	1xMGH [R393]; 1xAPY [R397]
[R].EFIREGCLHK.[L]	FARP2	O94887-1 [755-764]	1xAPY [R758]
[K].NFPFERLYDLNHNEIGELIRMPK.[M]	SNRNP200	O75643-1 [1147-1169]	1xCarboxyethyl (CEL/CEA) [R1166]; 1xAPY [R1152]
[R].AMEARGLDARGLEAR.[A]	CSTF2	P33240 [419-433]	1xAPY [R423]
[K].RIEALRR.[K]	CCDC9	Q9Y3X0 [20-26]	1xAPY [R20]
[R].INHTVILDDPFDDPPDLLIPDRSPEPTREQLDSGR.[I]	PPIL4	Q8WUA2 [156-190]	1xAPY [R177]
[R].WNITSQRR.[K]	MARVELD3	Q96A59-3 [121-128]	1xPhospho [S125]; 1xCarboxyethyl (CEL/CEA) [R127]; 1xAPY [R]
[R].TLILSSGFRLVKK.[K]	DDIT4L	Q96D03 [167-179]	2xPhospho [T167; S171]; 1xAPY [R175]
[R].RANRILLVAK.[R]	VCL	P18206 [759-768]	2xAPY [R759; R762]
[R].VPAAPPALRR.[N]	CDRT15L2	A8MXV6 [244-253]	1xAPY [R252]
[K].DIRPRSARAACK.[G]	NDUFA6	P56556 [4-15]	1xAPY [R6]; 1xTHP [R8]
[K].LRSLRLQYK.[G]	ACVR1B	P36896-4 [291-299]	2xAPY [R292; R295]
[K].KQEEEQDRK.[G]	NEK3	P51956-2 [292-300]	1xAPY [R299]
[KR].ISDARVVK.[D]	TIA1; TIAL1	Q01085 [123-130]; P31483-2 [121-128]; Q01085-2 [140-147]	Q01085 1xAPY [R127]; P31483-2 1xAPY [R125]; Q01085-2 1xAPY [R144]
[R].LGAVILRWRYHALR.[G]	PKD1	P98161 [4101-4114]	2xAPY [R4107; R4109]
[R].VIQIVLMRAAEEPVSEVTVGVSVLAER.[C]	PRKCD	Q05655 [68-94]	1xAPY [R75]
[K].FLGTALRR.[T]	ABCA11P	Q4W5N1 [141-148]	1xCarboxyethyl (CEL/CEA) [R147]; 1xAPY [R]
[R].LGERVLQVSFK.[T]	ELAVL3	Q14576 [350-360]	1xAPY [R353]
[R].SYVQRLQERR.[S]	USHBP1	Q8N6Y0-1 [427-436]	1xMGH [R431]; 1xAPY [R435]
[R].RAAVLIQKYYR.[S]	CAMTA1	Q9Y6Y1-1 [1595-1605]	1xAPY [R1595]
[R].IPRPALIYGRAVVTR.[T]	FAM87A	P0C7U9 [230-244]	2xMGH [R]; 1xAPY [R232]
[K].LDKLLQEAHDRSESGELAFIK.[Q]	MAST4	O15021 [449-469]	1xAPY [R459]
[R].LLRPEQVLK.[R]	EME2	A4GXA9-1 [66-74]	1xAPY [R68]
[K].LEVLRRFEAGEK.[L]	CENPBD1P	B2RD01 [28-39]	2xAPY [R32; R33]
[K].LEAVDRK.[N]	SCMH1	Q96GD3 [173-179]	1xAPY [R178]
[R].IREELDRER.[E]	GAS8	O95995 [38-46]	1xMGH [R44]; 1xAPY [R39]
[R].RELSLGRK.[K]	SCARF2	Q96GP6-1 [480-487]	1xAPY [R486]; 1xTHP [R480]
[R].AILTPRIKVGR.[D]	MYH10; MYH14	P35580 [395-405]; Q7Z406-1 [414-424]	P35580 1xAPY [R]; Q7Z406-1 1xAPY [R]
[M].DLLTRENVALK.[V]	TTBK1	Q5TCY1-2 [2-12]	1xAPY [R6]
[K].DKPSFVRARVK.[K]	UNC45A	Q9H3U1 [627-637]	1xAPY [R633]
[R].TSRYRSLK.[L]	ZNF318	Q5VUA4 [1932-1939]	1xPhospho [Y1935]; 1xMGH [R1934]; 1xAPY [R1936]

Table 6.2. APY-modified Peptides Observed in Proteomic Analysis. After data processing, we observed a list of 57 APY-modified peptides. Highlighted in pink are eight highest confidence hits.

Annotated Sequence	Gene	Positions in Master Proteins	Modifications in Master Proteins
[K].RHFNAPSHIRR.[K]	RPL26	P61254 [17-27]	1xMGH [R17]; 1xTHP [R26]
[K].RLLVESLFR.[D]	FSTL4	Q6MZW2 [176-184]	1xMGH [R]
[K].TIRRDIFGGLVLLK.[V]	SLC27A4	Q6P1M0 [48-61]	1xMGH [R51]; 1xPhospho [T48]; 1xCarboxyethyl (CEL/CEA) [R50]
[R].ILGPGRK.[C]	GEMIN4	P57678 [230-236]	1xMGH [R235]
[R].LNGGRNPYEGR.[V]	LOXL2	Q9Y4K0 [437-447]	1xMGH [R441]
[R].HIHRSGPIITHCSAGIGR.[S]	PTPN13	Q12923 [2397-2414]	1xMGH [R2400]; 1xPhospho [S2401]
[R].SESIRSLQSVRR.[S]	GPR87	Q9BY21 [335-346]	1xMGH [R345]; 1xCarboxyethyl (CEL/CEA) [R339]
[R].EFLHRGEKK.[N]	HTRA2	O43464 [340-348]	1xMGH [R344]
[K].LAAVDATVNQVLASRYGIR.[G]	PDIA6	Q15084-1 [217-235]	1xMGH [R]; 1xCarboxyethyl (CEL/CEA) [R231]
[R].QMTVIRK.[V]	MRPL49	Q13405 [106-112]	1xMGH [R111]
[K].LLARRSNSLLK.[Y]	CENPS	Q8N2Z9 [84-94]	2xMGH [R87; R88]; 1xPhospho [S89]
[R].DWLRVGSVLDK.[L]	HTR3A	P46098-1 [441-451]	1xMGH [R444]
[R].EQLQMLRERELER.[E]	RBSN	Q9H1K0 [520-532]	1xMGH [R528]; 1xCarboxyethyl (CEL/CEA) [R526]
[K].LYIDSCARR.[N]	SEC22B	O75396 [125-133]	1xMGH [R132]
[R].DGSLLRSSRR.[R]	MYOM3	Q5VTT5 [309-318]	1xMGH [R314]; 1xArgpyrimidine (Delta:H(4)C(5)O(1)) (APY) [R317]
[K].LVRLPGLIDVHVHLREPGGTHK.[E]	CAD	P27708 [1461-1482]	1xMGH [R1463]; 1xCarboxyethyl (CEL/CEA) [R1475]
[R].RTEQEEDEELLSESR.[K]	SMARCA1	P28370-1 [148-162]	1xMGH [R148]; 1xTHP [R]
[K].DANYRQSIDK.[L]	NRAP	Q86VF7-1 [476-485]	1xMGH [R480]; 1xPhospho [Y479]
[K].VRAGESVELFGK.[V]	MYLK	Q15746-1 [1249-1260]	1xMGH [R1250]
[-].MRLSVRR.[V]	TPST2	O60704 [1-7]	1xMGH [R2]
[R].LRSLVLPPACVRLLPGGFSK.[T]	DGKQ	P52824 [239-258]	1xMGH [R250]; 1xCarboxyethyl (CEL/CEA) [R240]
[R].DEGSSARSRMLR.[F]	CCDC80	Q76M96-1 [120-131]	1xMGH [R126]
[R].EPCNLALRRAEEYLILEK.[Y]	TXK	P42681 [97-114]	1xMGH [R104]; 1xPhospho [Y109]; 1xTHP [R105]
[R].YQIELLLRELDDQEK.[V]	PPL	O60437 [355-369]	1xMGH [R362]; 1xPhospho [Y355]
[R].SGRVSRPPK.[Y]	ZNF839	A8K0R7-1 [134-142]	2xMGH [R136; R139]; 1xPhospho [S134]
[R].LLRLDLRENEIK.[T]	PPP1R37	O75864-1 [391-402]	1xMGH [R393]; 1xAPY [R397]
[K].AAARVDQEINR.[I]	GNA15	P30679 [20-30]	1xMGH [R23]
[K].VDISFNMETGVRAAEFIK.[N]	TENT4A	Q5XG87 [331-348]	1xMGH [R342]
[K].RESELLLFTERLTSK.[N]	CCDC186	Q7Z3E2 [584-598]	1xMGH [R584]; 1xPhospho [S586]; 1xTHP [R594]
[K].RLDALLSEPIPIHGRGNFPTLSVQPR.[Q]	TENT5B	Q96A09 [59-84]	1xMGH [R73]; 2xTHP [R; R]
[M].AGAAAAVAAGAAAGAAAAAVSVAAPGRASAPPPPPPVYCVCR.[Q]	KDM7A	Q6ZMT4 [2-43]	1xMGH [R28]
[R].KRPASMAVMEGDLVK.[K]	ARHGAP17	Q68EM7 [480-494]	1xMGH [R481]; 1xPhospho [S484]
[R].RSLLTGR.[T]	TTLL5	Q6EMB2-2 [60-66]	1xMGH [R60]; 1xPhospho [S61]
[K].IRPVSQPFVNPAVK.[N]	C1orf87	Q8N0U7-1 [452-465]	1xMGH [R453]; 1xPhospho [S456]
[R].ATRKPLVQTTPRLVYK.[W]	RNF121	Q9H920 [122-137]	1xMGH [R]; 1xPhospho [T123]
[R].SYVQRLQERR.[S]	USHBP1	Q8N6Y0-1 [427-436]	1xMGH [R431]; 1xAPY [R435]
[R].VLLRPEK.[R]	HTR7	P34969-1 [439-445]	1xMGH [R442]
[R].HFNLAPLGRR.[R]	TINF2	Q9BSI4 [257-266]	1xMGH [R265]
[R].IPRPALIYGRAVVTR.[T]	FAM87A	P0C7U9 [230-244]	2xMGH [R]; 1xAPY [R232]
[R].HRRIHPGK.[K]	ZNF600	Q6ZNG1 [656-663]	2xMGH [R657; R658]
[R].IREELDRER.[E]	GAS8	O95995 [38-46]	1xMGH [R44]; 1xAPY [R39]
[R].LSRAGEKK.[V]	LEMD1	Q68G75-5 [96-103]	1xMGH [R98]
[R].DLTPSHQLEVGGGFRISESK.[C]	KMT2E	Q8IZD2-1 [1086-1105]	1xMGH [R1100]
[R].TSRYRSLK.[L]	ZNF318	Q5VUA4 [1932-1939]	1xMGH [R1934]; 1xPhospho [Y1935]; 1xAPY [R1936]
[K].RFIYRQDLYK.[H]	ZNF225	Q9UK10 [352-361]	1xMGH [R356]; 1xCarboxyethyl (CEL/CEA) [R352]
[K].QTGMKYRNLGK.[S]	KCNAB1	Q14722-2 [68-78]	1xMGH [R74]
[K].WVGESERQLR.[L]	ATAD2; ATAD2B	Q6PL18-1 [505-514]; Q9ULI0 [479-488]	Q6PL18-1 1xMGH [R511]; Q9ULI0 1xMGH [R485]

Table 6.3. MGH-modified Peptides Observed in Proteomic Analysis. After data processing, we observed a list of 47 MGH-modified peptides.

Annotated Sequence	Gene	Positions in Master Proteins	Modifications in Master Proteins
[R].RIRVDYSITK.[R]	TRA2A	Q13595-1 [189-198]	1xCarboxyethyl (CEL/CEA) [R189]; 1xTHP [R191]
[K].TIRRDIFGGLVLLK.[V]	SLC27A4	Q6P1M0 [48-61]	1xPhospho [T48]; 1xCarboxyethyl (CEL/CEA) [R50]; 1xMGH [R51]
[R].DLISDRNK.[S]	ARID2	Q68CP9-1 [248-255]	1xCarboxyethyl (CEL/CEA) [R253]
[R].HHPEHFSGRPR.[E]	FN1	P02751 [1392-1402]	1xCarboxyethyl (CEL/CEA) [R1400]
[K].HALFIFGPFNSIRSLAIR.[V]	SCN11A	Q9UI33-1 [107-124]	1xPhospho [S117]; 1xCarboxyethyl (CEL/CEA) [R119]
[R].SESIRSLQSVRR.[S]	GPR87	Q9BY21 [335-346]	1xCarboxyethyl (CEL/CEA) [R339]
[K].RLFVIRPSR.[F]	NDUFB5	O43674-1 [53-61]	1xCarboxyethyl (CEL/CEA) [R53]; 1xTHP [R58]
[K].RILALAR.[K]	PRKCE	Q02156 [458-464]	1xCarboxyethyl (CEL/CEA) [R458]
[K].LAAVDATVNQVLASRYGIR.[G]	PDIA6	Q15084-1 [217-235]	1xCarboxyethyl (CEL/CEA) [R231]; 1xMGH [R]
[R].LSNQGSQESSLRK.[T]	NT5C1B	Q96P26-2 [37-49]	2xPhospho [S42; S45]; 1xCarboxyethyl (CEL/CEA) [R48]
[R].EDSARPGAHAKVK.[K]	HNRNPA0	Q13151 [86-98]	1xCarboxyethyl (CEL/CEA) [R90]
[K].DSLLGIYGRR.[N]	TENM1	Q9UKZ4 [439-448]	1xCarboxyethyl (CEL/CEA) [R447]
[WR].AVLGSVRTGGAGSK.[W]	AFDN-DT	Q9Y6Z5-1 [116-129]; [164-177]	1xCarboxyethyl (CEL/CEA) [R122]; 1xCarboxyethyl (CEL/CEA) [R170]
[R].EQLQMLRERELER.[E]	RBSN	Q9H1K0 [520-532]	1xCarboxyethyl (CEL/CEA) [R526]; 1xMGH [R528]
[K].NVFFILAERARDPSAK.[K]	MRO	Q9BYG7 [48-63]	1xCarboxyethyl (CEL/CEA) [R56]
[R].IFVGGIDFKTNESDLRK.[F]	BOLL	Q8N9W6-1 [35-51]	1xCarboxyethyl (CEL/CEA) [R50]
[K].GERLRLPPWLK.[T]	LIAS	O43766-1 [71-81]	1xCarboxyethyl (CEL/CEA) [R73]; 1xAPY [R75]
[K].SILNERR.[K]	KIF9	Q9HAQ2-1 [601-607]	1xCarboxyethyl (CEL/CEA) [R606]; 1xTHP [R]
[K].RQTVALELLESER.[K]	ARHGEF33	A8MVX0-1 [266-278]	1xCarboxyethyl (CEL/CEA) [R266]
[R].QPDRSLRPEEIEELREAFR.[E]	CABP1	Q9NZU7-1 [74-92]	1xCarboxyethyl (CEL/CEA) [R77]
[R].RGNMPQRGGGGGGSGGIGYPYPR.[A]	HNRNPU	Q00839-2 [714-736]; Q00839 [733-755]	Q00839-2 1xCarboxyethyl (CEL/CEA) [R714]; Q00839 1xCarboxyethyl (CEL/CEA) [R733]
[R].VWIPDPDEVWRSAELTK.[D]	MYO5B	Q9ULV0 [13-29]	1xCarboxyethyl (CEL/CEA) [R23]
[R].EDSARPGAHAKVKK.[L]	HNRNPA0	Q13151 [86-99]	1xCarboxyethyl (CEL/CEA) [R90]
[K].LVRLPGLIDVHVHLREPGGTHK.[E]	CAD	P27708 [1461-1482]	1xCarboxyethyl (CEL/CEA) [R1475]; 1x MGH [1463]
[R].ADTLDPALLRPGRLDRK.[I]	PSMC4	P43686 [314-330]	1xCarboxyethyl (CEL/CEA) [R326]; 1xAPY [R323]; 1xTHP [R329]
[R].VSGPGVRRDTLTEQLR.[W]	PLCH2	O75038 [1289-1304]	1xCarboxyethyl (CEL/CEA) [R1295]; 1xTHP [R1296]
[R].EHEREVLQK.[A]	STMN2	Q93045 [111-119]	1xCarboxyethyl (CEL/CEA) [R114]
[R].VNRSQSFAGVLGSHER.[G]	RIPOR1	Q6ZS17 [17-32]	1xCarboxyethyl (CEL/CEA) [R19]
[R].TGLEVKPFITNPRAVKK.[C]	ASPA	P45381 [44-60]	1xCarboxyethyl (CEL/CEA) [R56]
[R].LRSLVLPPACVRLLPGGFSK.[T]	DGKQ	P52824 [239-258]	1xCarboxyethyl (CEL/CEA) [R240]; 1xMGH [R250]
[R].RPEATAAPLTPRGR.[E]	TOP6BL	Q8N6T0 [521-534]	2xPhospho [T525; T530]; 1xCarboxyethyl (CEL/CEA) [R521]
[K].RDADASK.[A]	ZNF638	Q14966-1 [776-782]	1xCarboxyethyl (CEL/CEA) [R776]
[R].LAENFCVCHLATGDMLRAMVASGSELGK.[K]	AK2	P54819 [35-62]	1xCarboxyethyl (CEL/CEA) [R51]
[K].VGLLYRLLQASILAYLVVWVFLIK.[K]	P2RX5	Q93086-1 [29-52]	2xPhospho [Y33; S39]; 1xCarboxyethyl (CEL/CEA) [R34]
[K].EAALICLAPSVPPILTVKSWDTMQLRAAR.[S]	NTRK1	P04629-3 [3-31]	1xCarboxyethyl (CEL/CEA) [R28]
[K].ASGGGAGALSSAPHRLGR.[A]	FAM149A	A5PLN7 [576-593]	1xPhospho [S585]; 1xCarboxyethyl (CEL/CEA) [R]
[K].NFPFERLYDLNHNEIGELIRMPK.[M]	SNRNP200	O75643-1 [1147-1169]	1xCarboxyethyl (CEL/CEA) [R1166]; 1xAPY [R1152]
[R].WNITSQRR.[K]	MARVELD3	Q96A59-3 [121-128]	1xPhospho [S125]; 1xCarboxyethyl (CEL/CEA) [R127]; 1xAPY [R]
[K].REYGNLELK.[K]	ZNF90	Q03938 [106-114]	1xCarboxyethyl (CEL/CEA) [R106]
[R].ARRHSDGTFTSELSR.[L]	SCT	P09683 [25-39]	2xCarboxyethyl (CEL/CEA) [R26; R27]; 1xTHP [R]
[R].ETLLARLVDSIK.[D]	DYNC2H1	Q8NCM8-1 [442-453]	1xCarboxyethyl (CEL/CEA) [R447]
[K].FLGTALRR.[T]	ABCA11	Q4W5N1 [141-148]	1xCarboxyethyl (CEL/CEA) [R147]; 1xAPY [R]
[R].EPPSRARPPPPLAARPAPAPAAPRPRSPAEAEAR.[G]	CLEC2L	P0C7M8 [6-39]	2xPhospho [S9; S32]; 1xCarboxyethyl (CEL/CEA) [R10]
[R].SPRKPVCPILGGTVMPNK.[T]	IHO1	Q8IYA8 [507-524]	1xCarboxyethyl (CEL/CEA) [R509]
[K].RFIYRQDLYK.[H]	ZNF225	Q9UK10 [352-361]	1xCarboxyethyl (CEL/CEA) [R352]; 1xMGH [R356]
[R].LARPNISSVIRSSLGK.[Y]	MRPL43	Q8N983-6 [215-230]	1xCarboxyethyl (CEL/CEA) [R217]; 1xTHP [R225]
[R].DLQFSEIRETSAK.[V]	TNXB	P22105 [3759-3771]	1xCarboxyethyl (CEL/CEA) [R3766]

Table 6.4. CEA/MGH-DH-modified Peptides Observed in Proteomic Analysis. After data processing, we observed a list of 47 CEA/MGH-DH-modified peptides.

Annotated Sequence	Gene	Positions in Master Proteins	Modifications in Master Proteins
[R].RVTQVVR.[D]	PADI3	Q9ULW8 [441-447]	1xTHP [R441]
[K].RHFNAPSHIRR.[K]	RPL26	P61254 [17-27]	1xTHP [R26]; 1xMGH [R17]
[K].LVLRIPNRGIDLLK.[K]	MATR3	P43243 [575-588]	1xTHP [R578]
[K].RLDYLNLK.[G]	FBXO39	Q8N4B4 [163-170]	1xTHP [R163]
[R].RIRVDYSITK.[R]	TRA2A	Q13595-1 [189-198]	1xCarboxyethyl (CEL/CEA) [R189]; 1xTHP [R191]
[K].KRLVELLK.[D]	FSIP1	Q8NA03 [277-284]	1xTHP [R278]
[R].EFDNMARVEDKR.[R]	TCEAL2	Q9H3H9 [170-181]	1xTHP [R176]
[K].ETAVFINISRYPR.[A]	GRHPR	Q9UBQ7-2 [93-105]	1xTHP [R102]
[K].QSISIGRGTRK.[R]	DNAI1	Q9UI46 [16-26]	1xTHP [R22]
[K].HIAMHYSNPRPK.[F]	RBM5	P52756 [170-181]	1xPhospho [Y175]; 1xTHP [R179]
[K].RLFVIRPSR.[F]	NDUFB5	O43674-1 [53-61]	1xCarboxyethyl (CEL/CEA) [R53]; 1xTHP [R58]
[M].FPAGPPSHSLLRLPLLQLLLLVVQAVGR.[G]	FKBP10	Q96AY3 [2-29]	1xPhospho [S8]; 1xTHP [R13]
[K].LRDEINLAK.[Q]	STIM1	Q13586 [286-294]	1xTHP [R287]
[K].QDSLDIYNERDLFK.[T]	STRIP2	Q9ULQ0-1 [352-365]	1xTHP [R361]
[K].ESDIRPSK.[L]	MICAL2	O94851 [514-521]	1xTHP [R518]
[K].EKLCYVALDFEQEMVRAAASSSPER.[S]	ACTBL2	Q562R1 [215-239]	1xAPY [R239]; 1xTHP[R230]
[K].RLNIRVISGQQLPK.[V]	PLCD1	P51178-1 [630-643]	1xAPY [R634]; 1xTHP [R630]
[K].AVADAIRTSLGPK.[G]	CCT4	P50991 [43-55]	1xTHP [R49]
[R].VTRYPLIIK.[N]	ITSN1	Q15811 [1382-1390]	2xPhospho [T1383; Y1385]; 1xTHP [R1384]
[K].RPPILECLEKLEK.[S]	RSF1	Q96T23 [578-590]	1xTHP [R578]
[K].KIIVLTGAGVSVSCGIPDFRSR.[D]	SIRT1	Q96EB6 [255-276]	1xAPY [R276]; 1xTHP [R274]
[K].SILNERR.[K]	KIF9	Q9HAQ2-1 [601-607]	1xCarboxyethyl (CEL/CEA) [R606]; 1xTHP [R]
[R].RSPRSSDGK.[L]	KCNE1	P15382 [33-41]	1xPhospho [S37]; 1xTHP [R36]
[K].EDSLTASQRK.[Q]	SERF1A; SERF1B	O75920-1 [28-37]	1xTHP [R36]
[R].ADTLDPALLRPGRLDRK.[I]	PSMC4	P43686 [314-330]	1xCarboxyethyl (CEL/CEA) [R326]; 1xAPY [R323]; 1xTHP [R329]
[R].VSGPGVRRDTLTEQLR.[W]	PLCH2	O75038 [1289-1304]	1xCarboxyethyl (CEL/CEA) [R1295]; 1xTHP [R1296]
[R].RTEQEEDEELLSESR.[K]	SMARCA1	P28370-1 [148-162]	1xTHP [R]; 1xMGH [R]
[R].IQEELSALRAEHQQDSEDLFKK.[I]	SUN2	Q9UH99 [355-376]	1xTHP [R363]
[R].EPCNLALRRAEEYLILEK.[Y]	TXK	P42681 [97-114]	1xPhospho [Y109]; 1xTHP [R105]; 1xMGH [R104]
[R].NFILDQTNVSAAAQRR.[K]	HNRNPU	Q00839-2 [557-572]; Q00839 [576-591]	Q00839-2 1xTHP [R571]; Q00839 1xTHP [R590]
[R].RLNENLK.[A]	NEK1	Q96PY6-1 [715-721]	1xTHP [R715]
[R].SLKASERETIK.[M]	CCDC40	Q4G0X9 [871-881]	2xPhospho [S871; T879]; 1xTHP [R877]
[K].LRQENMVLK.[L]	SREBF2	Q12772 [387-395]	1xTHP [R388]
[R].ALMTAVCYSAIIFETPLRVDVAVLK.[A]	EIF4G1	Q04637-8 [1482-1506]	1xPhospho [Y1489]; 1xTHP [R1499]
[K].RDILVAFK.[G]	PSAPL1	Q6NUJ1 [417-424]	1xTHP [R417]
[K].RESELLLFTERLTSK.[N]	CCDC186	Q7Z3E2 [584-598]	1xPhospho [S586]; 1xTHP [R594]; 1xMGH [R584]
[K].ITLRSGAVHRLYTLEGK.[L]	DCDC2	Q9UHG0 [177-193]	2xTHP [R180; R186]
[R].RQQPPLGPSSSLLSLPGLK.[S]	TBC1D10B	Q4KMP7 [648-666]	1xPhospho [S656]; 1xTHP [R648]
[K].DREIPVPLMER.[Q]	FGD1	P98174 [352-362]	1xTHP [R353]
[K].RLDALLSEPIPIHGRGNFPTLSVQPR.[Q]	TENT5B	Q96A09 [59-84]	2xTHP [R; R]; 1xMGH [R73]
[R].ARRHSDGTFTSELSR.[L]	SCT	P09683 [25-39]	2xCarboxyethyl (CEL/CEA) [R26; R27]; 1xTHP [R]
[K].DIRPRSARAACK.[G]	NDUFA6	P56556 [4-15]	1xAPY [R6]; 1xTHP [R8]
[K].DFQEPSISGGRK.[F]	IGFN1	Q86VF2-5 [726-737]	1xTHP [R736]
[R].RPASLAQRAR.[R]	REM1	O75628 [260-269]	1xTHP [R260]
[R].VFDMIRR.[R]	EIF4A3	P38919 [167-173]	1xTHP [R172]
[K].LGEAAVLEIVERLTKLIR.[E]	SMPDL3B	Q92485-1 [103-120]	1xTHP [R114]
[R].AFGDIVRALKK.[S]	FADS2B	A8MWK0 [461-471]	1xTHP [R467]
[R].RKSEEIQK.[R]	MCM10	Q7L590-1 [575-582]	1xTHP [R575]
[R].RELSLGRK.[K]	SCARF2	Q96GP6-1 [480-487]	1xAPY [R486]; 1xTHP[R480]
[K].VARSATARVR.[S]	MRPS31	Q92665 [210-219]	1xPhospho [S213]; 1xTHP [R212]
[R].TDPNGDYIRR.[Y]	CRY1	Q16526 [422-431]	1xTHP [R430]
[K].LRRGAKPEGK.[A]	NCAPD2	Q15021 [1270-1279]	2xTHP [R1271; R1272]
[R].LARPNISSVIRSSLGK.[Y]	MRPL43	Q8N983-6 [215-230]	1xCarboxyethyl (CEL/CEA) [R217]; 1xTHP [R225]

Table 6.5. [M+144]-modified Peptides Observed in Proteomic Analysis. After data processing, we observed a list of 53 [M+144]-modified peptides.

Enrichment Score: 3.19	**Count**	**P_Value**	**Fold Change**	**Benjamini**	**negLOG(p.adjust)**
RRM_dom	6	3.90E-04	9.50E+00	6.90E-02	1.16
DOMAIN:RRM	6	4.70E-04	9.10E+00	1.40E-01	0.85
RBD_domain_sf	6	6.90E-04	8.30E+00	6.90E-02	1.16
Nucleotide-bd_a/b_plait_sf	6	7.50E-04	8.20E+00	6.90E-02	1.16
RRM	6	1.30E-03	7.20E+00	8.00E-02	1.10
Enrichment Score: 2.43	**Count**	**P_Value**	**Fold Change**	**Benjamini**	**negLOG(p.adjust)**
ATP-binding	12	1.30E-03	2.60E+00	2.00E-02	1.70
ATP binding	12	3.30E-03	2.70E+00	2.10E-01	0.68
Nucleotide-binding	12	1.20E-02	2.00E+00	8.90E-02	1.05
Enrichment Score: 2.4	**Count**	**P_Value**	**Fold Change**	**Benjamini**	**negLOG(p.adjust)**
RRM_dom_euk	3	2.10E-03	4.30E+01	1.50E-01	0.82
mRNA 3'-UTR AU-rich region binding	3	3.20E-03	3.50E+01	2.10E-01	0.68
RRM_1	3	4.20E-03	3.00E+01	1.30E-01	0.89
DOMAIN:RRM 3	3	8.40E-03	2.10E+01	6.10E-01	0.21
Enrichment Score: 2.03	**Count**	**P_Value**	**Fold Change**	**Benjamini**	**negLOG(p.adjust)**
actin filament binding	5	3.20E-03	8.10E+00	2.10E-01	0.68
Actin-binding	5	1.50E-02	5.10E+00	2.30E-01	0.64
actin binding	5	1.60E-02	5.00E+00	2.50E-01	0.60
Enrichment Score: 2.02	**Count**	**P_Value**	**Fold Change**	**Benjamini**	**negLOG(p.adjust)**
protein serine/threonine kinase activity	6	4.30E-03	5.50E+00	2.10E-01	0.68
Serine/threonine-protein kinase	6	9.10E-03	4.50E+00	2.30E-01	0.64
Prot_kinase_dom	6	1.00E-02	4.50E+00	3.50E-01	0.46
S_TKc	6	1.10E-02	4.30E+00	2.30E-01	0.64
DOMAIN:Protein kinase	6	1.20E-02	4.30E+00	7.20E-01	0.14
Kinase-like_dom_sf	6	1.40E-02	4.10E+00	3.90E-01	0.41
Enrichment Score: 1.48	**Count**	**P_Value**	**Fold Change**	**Benjamini**	**negLOG(p.adjust)**
histone H2AS1 kinase activity	4	3.30E-02	5.60E+00	2.50E-01	0.60
histone H2BS14 kinase activity	4	3.30E-02	5.60E+00	2.50E-01	0.60
histone H3T3 kinase activity	4	3.30E-02	5.60E+00	2.50E-01	0.60
histone H2AS121 kinase activity	4	3.30E-02	5.60E+00	2.50E-01	0.60
Rho-dependent protein serine/threonine kinase activity	4	3.30E-02	5.60E+00	2.50E-01	0.60
histone H2BS36 kinase activity	4	3.30E-02	5.60E+00	2.50E-01	0.60
histone H3S57 kinase activity	4	3.30E-02	5.60E+00	2.50E-01	0.60
histone H2AT120 kinase activity	4	3.30E-02	5.60E+00	2.50E-01	0.60
3-phosphoinositide-dependent protein kinase activity	4	3.30E-02	5.60E+00	2.50E-01	0.60
eukaryotic translation initiation factor 2alpha kinase activity	4	3.30E-02	5.60E+00	2.50E-01	0.60
ribosomal protein S6 kinase activity	4	3.30E-02	5.60E+00	2.50E-01	0.60
histone H3S10 kinase activity	4	3.30E-02	5.60E+00	2.50E-01	0.60
histone H2AXS139 kinase activity	4	3.30E-02	5.60E+00	2.50E-01	0.60
histone H3S28 kinase activity	4	3.30E-02	5.60E+00	2.50E-01	0.60
histone H4S1 kinase activity	4	3.30E-02	5.60E+00	2.50E-01	0.60
histone H3T45 kinase activity	4	3.30E-02	5.60E+00	2.50E-01	0.60
DNA-dependent protein kinase activity	4	3.30E-02	5.60E+00	2.50E-01	0.60
histone H3T11 kinase activity	4	3.40E-02	5.60E+00	2.50E-01	0.60
histone H3T6 kinase activity	4	3.40E-02	5.60E+00	2.50E-01	0.60
AMP-activated protein kinase activity	4	3.40E-02	5.50E+00	2.50E-01	0.60

Table 6.6. DAVID Functional Annotation Clustering Analysis for APY Hits. This analysis was performed with the following settings: Classification stringency: highest; Kappa Similarity: Similarity term overlap: 3, Similarity threshold: 1.00; Classification: Initial group membership: 3, Final group membership: 3, Multiple linkage threshold: 0.50; Enrichment thresholds: EASE: 0.05.

References

(1) Martin, M. S.; Jacob-Dolan, J. W.; Pham, V. T. T.; Sjoblom, N. M.; Scheck, R. A. The Chemical Language of Protein Glycation. *Nat Chem Biol* **2025**, *21* (3), 324–336. https://doi.org/10.1038/s41589-024-01644-y.

(2) Li, Z.; Li, S.; Luo, M.; Jhong, J.-H.; Li, W.; Yao, L.; Pang, Y.; Wang, Z.; Wang, R.; Ma, R.; Yu, J.; Huang, Y.; Zhu, X.; Cheng, Q.; Feng, H.; Zhang, J.; Wang, C.; Hsu, J. B.-K.; Chang, W.-C.; Wei, F.-X.; Huang, H.-D.; Lee, T.-Y. dbPTM in 2022: An Updated Database for Exploring Regulatory Networks and Functional Associations of Protein Post-Translational Modifications. *Nucleic Acids Research* **2022**, *50* (D1), D471–D479. https://doi.org/10.1093/nar/gkab1017.

(3) Baldensperger, T.; Preissler, M.; Becker, C. F. W. Non-Enzymatic Posttranslational Protein Modifications in Protein Aggregation and Neurodegenerative Diseases. *RSC Chem. Biol.* **2025**, *6* (2), 129–149. https://doi.org/10.1039/D4CB00221K.

(4) Lee, J. M.; Hammarén, H. M.; Savitski, M. M.; Baek, S. H. Control of Protein Stability by Post-Translational Modifications. *Nat Commun* **2023**, *14* (1), 201. https://doi.org/10.1038/s41467-023-35795-8.

(5) Trujillo, M. N.; Galligan, J. J. Reconsidering the Role of Protein Glycation in Disease. *Nat Chem Biol* **2023**, *19* (8), 922–927. https://doi.org/10.1038/s41589-023-01382-7.

(6) Amadori, M. Products of Condensation between Glucose and P-Phenetidine I. *Atti Accad. Lincei 2* **1925**, 337–342.

(7) Heyns, V. K.; Koch, W. Über Die Bildung Eines Aminozuckers Aus D-Fructose Und Ammoniak. *Zeitschrift für Naturforschung B* **1952**, *7* (8), 486–488. https://doi.org/10.1515/znb-1952-0812.

(8) Hodge, J. E. Dehydrated Foods, Chemistry of Browning Reactions in Model Systems. *J. Agric. Food Chem.* **1953**, *1* (15), 928–943. https://doi.org/10.1021/jf60015a004.

(9) Kulkarni, R. A.; Bak, D. W.; Wei, D.; Bergholtz, S. E.; Briney, C. A.; Shrimp, J. H.; Alpsoy, A.; Thorpe, A. L.; Bavari, A. E.; Crooks, D. R.; Levy, M.; Florens, L.; Washburn, M. P.; Frizzell, N.; Dykhuizen, E. C.; Weerapana, E.; Linehan, W. M.; Meier, J. L. A Chemoproteomic Portrait of the Oncometabolite Fumarate. *Nat Chem Biol* **2019**, *15* (4), 391–400. https://doi.org/10.1038/s41589-018-0217-y.

(10) Wagner, G. R.; Bhatt, D. P.; O'Connell, T. M.; Thompson, J. W.; Dubois, L. G.; Backos, D. S.; Yang, H.; Mitchell, G. A.; Ilkayeva, O. R.; Stevens, R. D.; Grimsrud, P. A.; Hirschey, M. D. A Class of Reactive Acyl-CoA Species Reveals the Non-Enzymatic Origins of Protein Acylation. *Cell Metabolism* **2017**, *25* (4), 823-837.e8. https://doi.org/10.1016/j.cmet.2017.03.006.

(11) Jacob-Dolan, J. W.; Sterling, A. C.; Brutus, M. E.; Hansel, S. M.; Scheck, R. A. Discovery of Glycation-Derived Cross-Links at Arginine. *J. Am. Chem. Soc.* **2026**, jacs.5c12902. https://doi.org/10.1021/jacs.5c12902.

(12) Maillard, L. C. Action of Amino Acids on Sugars. Formation of Melanoidins in a Methodical Way. *Compte-rendu de l'academie des sciences* **66-68**, *154*, 1912.

(13) Maillard, L. C. General Reaction of Amino Acids on Sugars: Its Biological Consequences. *CR Séances Soc. Biol. Ses. Fil* **1912**, *72*, 599–601.

(14) Oya, T.; Hattori, N.; Mizuno, Y.; Miyata, S.; Maeda, S.; Osawa, T.; Uchida, K. Methylglyoxal Modification of Protein. *Journal of Biological Chemistry* **1999**, *274* (26), 18492–18502. https://doi.org/10.1074/jbc.274.26.18492.

(15) Ahmed, N.; Thornalley, P. J.; Dawczynski, J.; Franke, S.; Strobel, J.; Stein, G.; Haik, G. M. Methylglyoxal-Derived Hydroimidazolone Advanced Glycation End-Products of Human Lens Proteins. *Invest. Ophthalmol. Vis. Sci.* **2003**, *44* (12), 5287. https://doi.org/10.1167/iovs.03-0573.
(16) Thornalley, P. J.; Battah, S.; Ahmed, N.; Karachalias, N.; Agalou, S.; Babaei-Jadidi, R.; Dawnay, A. Quantitative Screening of Advanced Glycation Endproducts in Cellular and Extracellular Proteins by Tandem Mass Spectrometry. *Biochemical Journal* **2003**, *375* (3), 581–592. https://doi.org/10.1042/bj20030763.
(17) Biemel, K. M.; Friedl, D. A.; Lederer, M. O. Identification and Quantification of Major Maillard Cross-Links in Human Serum Albumin and Lens Protein. *Journal of Biological Chemistry* **2002**, *277* (28), 24907–24915. https://doi.org/10.1074/jbc.M202681200.
(18) Shipanova, I. N.; Glomb, M. A.; Nagaraj, R. H. Protein Modification by Methylglyoxal: Chemical Nature and Synthetic Mechanism of a Major Fluorescent Adduct. *Archives of Biochemistry and Biophysics* **1997**, *344* (1), 29–36. https://doi.org/10.1006/abbi.1997.0195.
(19) McEwen, J. M.; Fraser, S.; Guir, A. L. S.; Dave, J.; Scheck, R. A. Synergistic Sequence Contributions Bias Glycation Outcomes. *Nat Commun* **2021**, *12* (1), 3316. https://doi.org/10.1038/s41467-021-23625-8.
(20) Bollong, M. J.; Lee, G.; Coukos, J. S.; Yun, H.; Zambaldo, C.; Chang, J. W.; Chin, E. N.; Ahmad, I.; Chatterjee, A. K.; Lairson, L. L.; Schultz, P. G.; Moellering, R. E. A Metabolite-Derived Protein Modification Integrates Glycolysis with KEAP1–NRF2 Signalling. *Nature* **2018**, *562* (7728), 600–604. https://doi.org/10.1038/s41586-018-0622-0.
(21) Thornalley, P. J. PROTEIN AND NUCLEOTIDE DAMAGE BY GLYOXAL AND METHYLGLYOXAL IN PHYSIOLOGICAL SYSTEMS - ROLE IN AGEING AND DISEASE. *Drug Metabolism and Drug Interactions* **2008**, *23* (1–2), 125–150. https://doi.org/10.1515/DMDI.2008.23.1-2.125.
(22) Bunn, H. F.; Higgins, P. J. Reaction of Monosaccharides with Proteins: Possible Evolutionary Significance. *Science* **1981**, *213* (4504), 222–224. https://doi.org/10.1126/science.12192669.
(23) Rabbani, N.; Thornalley, P. J. Methylglyoxal, Glyoxalase 1 and the Dicarbonyl Proteome. *Amino Acids* **2012**, *42* (4), 1133–1142. https://doi.org/10.1007/s00726-010-0783-0.
(24) Phillips, S. A.; Thornalley, P. J. The Formation of Methylglyoxal from Triose Phosphates: Investigation Using a Specific Assay for Methylglyoxal. *European Journal of Biochemistry* **1993**, *212* (1), 101–105. https://doi.org/10.1111/j.1432-1033.1993.tb17638.x.
(25) Richard, J. P. Mechanism for the Formation of Methylglyoxal from Triosephosphates. *Biochemical Society Transactions* **1993**, *21* (2), 549–553. https://doi.org/10.1042/bst0210549.
(26) Wang, T.; Douglass, E. F.; Fitzgerald, K. J.; Spiegel, D. A. A "Turn-On" Fluorescent Sensor for Methylglyoxal. *J. Am. Chem. Soc.* **2013**, *135* (33), 12429–12433. https://doi.org/10.1021/ja406077j.
(27) Shaheen, F.; Shmygol, A.; Rabbani, N.; Thornalley, P. J. A Fluorogenic Assay for Methylglyoxal. *Biochemical Society Transactions* **2014**, *42* (2), 548–555. https://doi.org/10.1042/BST20140028.

(28) Chaplen, F. W. R.; Fahl, W. E.; Cameron, D. C. Evidence of High Levels of Methylglyoxal in Cultured Chinese Hamster Ovary Cells. *Proc. Natl. Acad. Sci. U.S.A.* **1998**, *95* (10), 5533–5538. https://doi.org/10.1073/pnas.95.10.5533.
(29) Jacob-Dolan, J. W.; Sterling, A. C.; Brutus, M. E.; Hansel, S. M.; Scheck, R. A. Discovery of Glycation-Derived Crosslinks at Arginine. July 31, 2025. https://doi.org/10.1101/2025.07.28.667285.
(30) Lederer, M. O.; Klaiber, R. G. Cross-Linking of Proteins by Maillard Processes: Characterization and Detection of Lysine–Arginine Cross-Links Derived from Glyoxal and Methylglyoxal. *Bioorganic & Medicinal Chemistry* **1999**, *7* (11), 2499–2507. https://doi.org/10.1016/S0968-0896(99)00212-6.
(31) Sjoblom, N. M.; Kelsey, M. M. G.; Scheck, R. A. A Systematic Study of Selective Protein Glycation. *Angew Chem Int Ed* **2018**, *57* (49), 16077–16082. https://doi.org/10.1002/anie.201810037.
(32) Ahmed, N.; Dobler, D.; Dean, M.; Thornalley, P. J. Peptide Mapping Identifies Hotspot Site of Modification in Human Serum Albumin by Methylglyoxal Involved in Ligand Binding and Esterase Activity. *Journal of Biological Chemistry* **2005**, *280* (7), 5724–5732. https://doi.org/10.1074/jbc.M410973200.
(33) Henning, C.; Glomb, M. A. Pathways of the Maillard Reaction under Physiological Conditions. *Glycoconj J* **2016**, *33* (4), 499–512. https://doi.org/10.1007/s10719-016-9694-y.
(34) Wang, T.; Kartika, R.; Spiegel, D. A. Exploring Post-Translational Arginine Modification Using Chemically Synthesized Methylglyoxal Hydroimidazolones. *J. Am. Chem. Soc.* **2012**, *134* (21), 8958–8967. https://doi.org/10.1021/ja301994d.
(35) deRamon, E. A.; Sabbasani, V. R.; Streeter, M. D.; Liu, Y.; Newhouse, T. R.; McDonald, D. M.; Spiegel, D. A. Pentosinane, a Post-Translational Modification of Human Proteins with Underappreciated Stability. *J. Am. Chem. Soc.* **2022**, *144* (48), 21843–21847. https://doi.org/10.1021/jacs.2c09626.
(36) Ahmed, N.; Argirov, O. K.; Minhas, H. S.; Cordeiro, C. A. A.; Thornalley, P. J. Assay of Advanced Glycation Endproducts (AGEs): Surveying AGEs by Chromatographic Assay with Derivatization by 6-Aminoquinolyl-N-Hydroxysuccinimidyl-Carbamate and Application to N∈-Carboxymethyl-Lysine- and N∈-(1-Carboxyethyl)Lysine-Modified Albumin. *Biochemical Journal* **2002**, *364* (1), 1–14. https://doi.org/10.1042/bj3640001.
(37) Klöpfer, A.; Spanneberg, R.; Glomb, M. A. Formation of Arginine Modifications in a Model System of N^{α} - *Tert* -Butoxycarbonyl (Boc)-Arginine with Methylglyoxal. *J. Agric. Food Chem.* **2011**, *59* (1), 394–401. https://doi.org/10.1021/jf103116c.
(38) Arakawa, S.; Suzuki, R.; Kurosaka, D.; Ikeda, R.; Hayashi, H.; Kayama, T.; Ohno, R.; Nagai, R.; Marumo, K.; Saito, M. Mass Spectrometric Quantitation of AGEs and Enzymatic Crosslinks in Human Cancellous Bone. *Sci Rep* **2020**, *10* (1), 18774. https://doi.org/10.1038/s41598-020-75923-8.
(39) Galligan, J. J.; Wepy, J. A.; Streeter, M. D.; Kingsley, P. J.; Mitchener, M. M.; Wauchope, O. R.; Beavers, W. N.; Rose, K. L.; Wang, T.; Spiegel, D. A.; Marnett, L. J. Methylglyoxal-Derived Posttranslational Arginine Modifications Are Abundant Histone Marks. *Proc. Natl. Acad. Sci. U.S.A.* **2018**, *115* (37), 9228–9233. https://doi.org/10.1073/pnas.1802901115.

(40) Sjöberg, J. S.; Bulterijs, S. Characteristics, Formation, and Pathophysiology of Glucosepane: A Major Protein Cross-Link. *Rejuvenation Research* **2009**, *12* (2), 137–148. https://doi.org/10.1089/rej.2009.0846.
(41) Allen, D. W.; Schroeder, W. A.; Balog, J. Observations on the Chromatographic Heterogeneity of Normal Adult and Fetal Human Hemoglobin: A Study of the Effects of Crystallization and Chromatography on the Heterogeneity and Isoleucine Content. *J. Am. Chem. Soc.* **1958**, *80* (7), 1628–1634. https://doi.org/10.1021/ja01540a030.
(42) Uchiki, T.; Weikel, K. A.; Jiao, W.; Shang, F.; Caceres, A.; Pawlak, D.; Handa, J. T.; Brownlee, M.; Nagaraj, R.; Taylor, A. Glycation-altered Proteolysis as a Pathobiologic Mechanism That Links Dietary Glycemic Index, Aging, and Age-related Disease (in Nondiabetics). *Aging Cell* **2012**, *11* (1), 1–13. https://doi.org/10.1111/j.1474-9726.2011.00752.x.
(43) Monnier, V. M.; Cerami, A. Nonenzymatic Browning in Vivo: Possible Process for Aging of Long-Lived Proteins. *Science* **1981**, *211* (4481), 491–493. https://doi.org/10.1126/science.6779377.
(44) Rowan, S.; Jiang, S.; Korem, T.; Szymanski, J.; Chang, M.-L.; Szelog, J.; Cassalman, C.; Dasuri, K.; McGuire, C.; Nagai, R.; Du, X.-L.; Brownlee, M.; Rabbani, N.; Thornalley, P. J.; Baleja, J. D.; Deik, A. A.; Pierce, K. A.; Scott, J. M.; Clish, C. B.; Smith, D. E.; Weinberger, A.; Avnit-Sagi, T.; Lotan-Pompan, M.; Segal, E.; Taylor, A. Involvement of a Gut–Retina Axis in Protection against Dietary Glycemia-Induced Age-Related Macular Degeneration. *Proc. Natl. Acad. Sci. U.S.A.* **2017**, *114* (22). https://doi.org/10.1073/pnas.1702302114.
(45) Antognelli, C.; Mezzasoma, L.; Fettucciari, K.; Talesa, V. N. A Novel Mechanism of Methylglyoxal Cytotoxicity in Prostate Cancer Cells. *The International Journal of Biochemistry & Cell Biology* **2013**, *45* (4), 836–844. https://doi.org/10.1016/j.biocel.2013.01.003.
(46) Van Heijst, J. W. J.; Niessen, H. W. M.; Hoekman, K.; Schalkwijk, C. G. Advanced Glycation End Products in Human Cancer Tissues: Detection of N^{ε}-(Carboxymethyl)Lysine and Argpyrimidine. *Annals of the New York Academy of Sciences* **2005**, *1043* (1), 725–733. https://doi.org/10.1196/annals.1333.084.
(47) Kim, J.; Kim, O. S.; Kim, C.-S.; Sohn, E.; Jo, K.; Kim, J. S. Accumulation of Argpyrimidine, a Methylglyoxal-Derived Advanced Glycation End Product, Increases Apoptosis of Lens Epithelial Cells Both *in Vitro* and *in Vivo*. *Exp Mol Med* **2012**, *44* (2), 167. https://doi.org/10.3858/emm.2012.44.2.012.
(48) Padayatti, P. S.; Ng, A. S.; Uchida, K.; Glomb, M. A.; Nagaraj, R. H. Argpyrimidine, a Blue Fluorophore in Human Lens Proteins: High Levels in Brunescent Cataractous Lenses. *Invest Ophthalmol Vis Sci* **2001**, *42* (6), 1299–1304.
(49) Basta, G. Advanced Glycation End Products and Vascular Inflammation: Implications for Accelerated Atherosclerosis in Diabetes. *Cardiovascular Research* **2004**, *63* (4), 582–592. https://doi.org/10.1016/j.cardiores.2004.05.001.
(50) Antognelli, C.; Gambelunghe, A.; Muzi, G.; Talesa, V. N. Peroxynitrite-Mediated Glyoxalase I Epigenetic Inhibition Drives Apoptosis in Airway Epithelial Cells Exposed to Crystalline Silica via a Novel Mechanism Involving Argpyrimidine-Modified Hsp70, JNK, and NF-κB. *Free Radical Biology and Medicine* **2015**, *84*, 128–141. https://doi.org/10.1016/j.freeradbiomed.2015.03.026.

(51) Matveenko, M.; Cichero, E.; Fossa, P.; Becker, C. F. W. Impaired Chaperone Activity of Human Heat Shock Protein Hsp27 Site-Specifically Modified with Argpyrimidine. *Angew Chem Int Ed* **2016**, *55* (38), 11397–11402. https://doi.org/10.1002/anie.201605366.
(52) Naito, Y.; Takagi, T.; Oya-Ito, T.; Okada, H.; Suzuki, T.; Hirata, I.; Hirai, M.; Uchiyama, K.; Handa, O.; Uchida, K.; Yoshikawa, T. Impaired Gastric Ulcer Healing in Diabetic Mice: Role of Methylglyoxal. *J Physiol Pharmacol* **2009**, *60 Suppl 7*, 123–130.
(53) Sakamoto, H.; Mashima, T.; Yamamoto, K.; Tsuruo, T. Modulation of Heat-Shock Protein 27 (Hsp27) Anti-Apoptotic Activity by Methylglyoxal Modification. *Journal of Biological Chemistry* **2002**, *277* (48), 45770–45775. https://doi.org/10.1074/jbc.M207485200.
(54) Bair, W. B.; Cabello, C. M.; Uchida, K.; Bause, A. S.; Wondrak, G. T. GLO1 Overexpression in Human Malignant Melanoma. *Melanoma Research* **2010**, *20* (2), 85–96. https://doi.org/10.1097/CMR.0b013e3283364903.
(55) Jaisson, S.; Gillery, P. Evaluation of Nonenzymatic Posttranslational Modification–Derived Products as Biomarkers of Molecular Aging of Proteins. *Clinical Chemistry* **2010**, *56* (9), 1401–1412. https://doi.org/10.1373/clinchem.2010.145201.
(56) Gao, Y.; Wang, Y. Site-Selective Modifications of Arginine Residues in Human Hemoglobin Induced by Methylglyoxal. *Biochemistry* **2006**, *45* (51), 15654–15660. https://doi.org/10.1021/bi061410o.
(57) Shapiro, R.; McManus, M. J.; Zalut, C.; Bunn, H. F. Sites of Nonenzymatic Glycosylation of Human Hemoglobin A. *Journal of Biological Chemistry* **1980**, *255* (7), 3120–3127. https://doi.org/10.1016/S0021-9258(19)85860-X.
(58) Iberg, N.; Flückiger, R. Nonenzymatic Glycosylation of Albumin in Vivo. Identification of Multiple Glycosylated Sites. *Journal of Biological Chemistry* **1986**, *261* (29), 13542–13545. https://doi.org/10.1016/S0021-9258(18)67052-8.
(59) Walton, D. J.; Shilton, B. H. Site Specificity of Protein Glycation. *Amino Acids* **1991**, *1* (2), 199–203. https://doi.org/10.1007/BF00806917.
(60) Sahoo, R.; Ghosh, P.; Chorev, M.; Halperin, J. A. A Distinctive Histidine Residue Is Essential for in Vivo Glycation-inactivation of Human CD59 Transgenically Expressed in Mice Erythrocytes: Implications for Human Diabetes Complications. *American J Hematol* **2017**, *92* (11), 1198–1203. https://doi.org/10.1002/ajh.24886.
(61) Zhang, B.; Yang, Y.; Yuk, I.; Pai, R.; McKay, P.; Eigenbrot, C.; Dennis, M.; Katta, V.; Francissen, K. C. Unveiling a Glycation Hot Spot in a Recombinant Humanized Monoclonal Antibody. *Anal. Chem.* **2008**, *80* (7), 2379–2390. https://doi.org/10.1021/ac701810q.
(62) Bilova, T.; Paudel, G.; Shilyaev, N.; Schmidt, R.; Brauch, D.; Tarakhovskaya, E.; Milrud, S.; Smolikova, G.; Tissier, A.; Vogt, T.; Sinz, A.; Brandt, W.; Birkemeyer, C.; Wessjohann, L. A.; Frolov, A. Global Proteomic Analysis of Advanced Glycation End Products in the Arabidopsis Proteome Provides Evidence for Age-Related Glycation Hot Spots. *Journal of Biological Chemistry* **2017**, *292* (38), 15758–15776. https://doi.org/10.1074/jbc.M117.794537.
(63) Dong, H.; Zhang, Y.; Huang, Y.; Deng, H. Pathophysiology of RAGE in Inflammatory Diseases. *Front. Immunol.* **2022**, *13*, 931473. https://doi.org/10.3389/fimmu.2022.931473.
(64) Guvatova, Z. G.; Vakhrusheva, A.; Moskalev, A. A Receptor for Glycation End Products (RAGE) Is a Key Transmitter between Garb-Aging and Inflammaging. *Ageing Research Reviews* **2026**, *113*, 102919. https://doi.org/10.1016/j.arr.2025.102919.

(65) Kierdorf, K.; Fritz, G. RAGE Regulation and Signaling in Inflammation and Beyond. *Journal of Leukocyte Biology* **2013**, *94* (1), 55–68. https://doi.org/10.1189/jlb.1012519.
(66) Taguchi, A.; Blood, D. C.; Del Toro, G.; Canet, A.; Lee, D. C.; Qu, W.; Tanji, N.; Lu, Y.; Lalla, E.; Fu, C.; Hofmann, M. A.; Kislinger, T.; Ingram, M.; Lu, A.; Tanaka, H.; Hori, O.; Ogawa, S.; Stern, D. M.; Schmidt, A. M. Blockade of RAGE–Amphoterin Signalling Suppresses Tumour Growth and Metastases. *Nature* **2000**, *405* (6784), 354–360. https://doi.org/10.1038/35012626.
(67) Zheng, Q.; Omans, N. D.; Leicher, R.; Osunsade, A.; Agustinus, A. S.; Finkin-Groner, E.; D'Ambrosio, H.; Liu, B.; Chandarlapaty, S.; Liu, S.; David, Y. Reversible Histone Glycation Is Associated with Disease-Related Changes in Chromatin Architecture. *Nat Commun* **2019**, *10* (1), 1289. https://doi.org/10.1038/s41467-019-09192-z.
(68) Kalapos, M. P. Methylglyoxal in Living Organisms. *Toxicology Letters* **1999**, *110* (3), 145–175. https://doi.org/10.1016/S0378-4274(99)00160-5.
(69) Szwergold, B. S.; Howell, S.; Beisswenger, P. J. Human Fructosamine-3-Kinase. *Diabetes* **2001**, *50* (9), 2139–2147. https://doi.org/10.2337/diabetes.50.9.2139.
(70) Kim, N. Y.; Goddard, T. N.; Sohn, S.; Spiegel, D. A.; Crawford, J. M. Biocatalytic Reversal of Advanced Glycation End Product Modification. *ChemBioChem* **2019**, *20* (18), 2402–2410. https://doi.org/10.1002/cbic.201900158.
(71) Wu, X.; Palfey, B. A.; Mossine, V. V.; Monnier, V. M. Kinetic Studies, Mechanism, and Substrate Specificity of Amadoriase I from *Aspergillus Sp* . *Biochemistry* **2001**, *40* (43), 12886–12895. https://doi.org/10.1021/bi011244e.
(72) Richarme, G.; Mihoub, M.; Dairou, J.; Bui, L. C.; Leger, T.; Lamouri, A. Parkinsonism-Associated Protein DJ-1/Park7 Is a Major Protein Deglycase That Repairs Methylglyoxal- and Glyoxal-Glycated Cysteine, Arginine, and Lysine Residues. *Journal of Biological Chemistry* **2015**, *290* (3), 1885–1897. https://doi.org/10.1074/jbc.M114.597815.
(73) Sharma, N.; Rao, S. P.; Kalivendi, S. V. The Deglycase Activity of DJ-1 Mitigates α-Synuclein Glycation and Aggregation in Dopaminergic Cells: Role of Oxidative Stress Mediated Downregulation of DJ-1 in Parkinson's Disease. *Free Radical Biology and Medicine* **2019**, *135*, 28–37. https://doi.org/10.1016/j.freeradbiomed.2019.02.014.
(74) Andreeva, A.; Bekkhozhin, Z.; Omertassova, N.; Baizhumanov, T.; Yeltay, G.; Akhmetali, M.; Toibazar, D.; Utepbergenov, D. The Apparent Deglycase Activity of DJ-1 Results from the Conversion of Free Methylglyoxal Present in Fast Equilibrium with Hemithioacetals and Hemiaminals. *Journal of Biological Chemistry* **2019**, *294* (49), 18863–18872. https://doi.org/10.1074/jbc.RA119.011237.
(75) Mazza, M. C.; Shuck, S. C.; Lin, J.; Moxley, M. A.; Termini, J.; Cookson, M. R.; Wilson, M. A. DJ -1 Is Not a Deglycase and Makes a Modest Contribution to Cellular Defense against Methylglyoxal Damage in Neurons. *Journal of Neurochemistry* **2022**, *162* (3), 245–261. https://doi.org/10.1111/jnc.15656.
(76) Choi, J.; Tak, S.; Jung, H.; Cha, S.; Hwang, E.; Lee, D.; Lee, J.; Ryu, K.; Park, C. Kinetic Evidence in Favor of Glyoxalase III and against Deglycase Activity of DJ -1. *Protein Science* **2023**, *32* (5), e4641. https://doi.org/10.1002/pro.4641.
(77) Gao, Q.; Jacob-Dolan, J. W.; Scheck, R. A. Parkinsonism-Associated Protein DJ-1 Is an Antagonist, Not an Eraser, for Protein Glycation. *Biochemistry* **2023**, *62* (6), 1181–1190. https://doi.org/10.1021/acs.biochem.3c00028.

(78) Zheng, Q.; Osunsade, A.; David, Y. Protein Arginine Deiminase 4 Antagonizes Methylglyoxal-Induced Histone Glycation. *Nat Commun* **2020**, *11* (1), 3241. https://doi.org/10.1038/s41467-020-17066-y.
(79) Akıllıoğlu, H. G.; Lund, M. N. Quantification of Advanced Glycation End Products and Amino Acid Cross-Links in Foods by High-Resolution Mass Spectrometry: Applicability of Acid Hydrolysis. *Food Chemistry* **2022**, *366*, 130601. https://doi.org/10.1016/j.foodchem.2021.130601.
(80) Scheijen, J. L. J. M.; Clevers, E.; Engelen, L.; Dagnelie, P. C.; Brouns, F.; Stehouwer, C. D. A.; Schalkwijk, C. G. Analysis of Advanced Glycation Endproducts in Selected Food Items by Ultra-Performance Liquid Chromatography Tandem Mass Spectrometry: Presentation of a Dietary AGE Database. *Food Chemistry* **2016**, *190*, 1145–1150. https://doi.org/10.1016/j.foodchem.2015.06.049.
(81) Glomb, M. A.; Lang, G. Isolation and Characterization of Glyoxal−Arginine Modifications. *J. Agric. Food Chem.* **2001**, *49* (3), 1493–1501. https://doi.org/10.1021/jf001082d.
(82) Njoroge, F. G.; Fernandes, A. A.; Monnier, V. M. Mechanism of Formation of the Putative Advanced Glycosylation End Product and Protein Cross-Link 2-(2-Furoyl)-4(5)-(2-Furanyl)-1H-Imidazole. *Journal of Biological Chemistry* **1988**, *263* (22), 10646–10652. https://doi.org/10.1016/S0021-9258(18)38020-7.
(83) Hellwig, M.; Humpf, H.-U.; Hengstler, J.; Mally, A.; Vieths, S.; Henle, T. Quality Criteria for Studies on Dietary Glycation Compounds and Human Health: Opinion of the Senate Commission on Food Safety (SKLM) of the German Research Foundation (DFG). *J. Agric. Food Chem.* **2019**, *67* (41), 11307–11311. https://doi.org/10.1021/acs.jafc.9b04172.
(84) Lee, J. S.; Chung, Y.-S.; Chang, S. Y.; Jung, Y.-S.; Kim, S. H. Simple Quantification of Pentosidine in Human Urine and Plasma by High-Performance Liquid Chromatography. *International Journal of Analytical Chemistry* **2017**, *2017*, 1–6. https://doi.org/10.1155/2017/1389807.
(85) Hurben, A. K.; Zhang, Q.; Galligan, J. J.; Tretyakova, N.; Erber, L. Endogenous Cellular Metabolite Methylglyoxal Induces DNA–Protein Cross-Links in Living Cells. *ACS Chem. Biol.* **2024**, *19* (6), 1291–1302. https://doi.org/10.1021/acschembio.4c00100.
(86) Li, S.; Yang, D.; Gao, X.; Yao, S.; Wang, S.; Zhu, J.; Shu, J. Argpyrimidine Bonded to RAGE Regulates Autophagy and Cell Cycle to Cause Periodontal Destruction. *Journal Cellular Physiology* **2022**, *237* (12), 4460–4476. https://doi.org/10.1002/jcp.30886.
(87) Mukherjee, S.; Vogl, D. P.; Becker, C. F. W. Site-Specific Glycation of Human Heat Shock Protein (Hsp27) Enhances Its Chaperone Activity. *ACS Chem. Biol.* **2023**, *18* (8), 1760–1771. https://doi.org/10.1021/acschembio.3c00214.
(88) Gomes, R.; Sousa Silva, M.; Quintas, A.; Cordeiro, C.; Freire, A.; Pereira, P.; Martins, A.; Monteiro, E.; Barroso, E.; Ponces Freire, A. Argpyrimidine, a Methylglyoxal-Derived Advanced Glycation End-Product in Familial Amyloidotic Polyneuropathy. *Biochemical Journal* **2005**, *385* (2), 339–345. https://doi.org/10.1042/BJ20040833.
(89) Sudnitsyna, M. V.; Gusev, N. B. Is the Small Heat Shock Protein HspB1 (Hsp27) a Real and Predominant Target of Methylglyoxal Modification? *Cell Stress and Chaperones* **2019**, *24* (2), 419–426. https://doi.org/10.1007/s12192-019-00975-3.
(90) Wang, T.; Streeter, M. D.; Spiegel, D. A. Generation and Characterization of Antibodies against Arginine-Derived Advanced Glycation Endproducts. *Bioorganic & Medicinal Chemistry Letters* **2015**, *25* (21), 4881–4886. https://doi.org/10.1016/j.bmcl.2015.06.013.

(91) Streeter, M. D.; Rowan, S.; Ray, J.; McDonald, D. M.; Volkin, J.; Clark, J.; Taylor, A.; Spiegel, D. A. Generation and Characterization of Anti-Glucosepane Antibodies Enabling Direct Detection of Glucosepane in Retinal Tissue. *ACS Chem. Biol.* **2020**, *15* (10), 2655–2661. https://doi.org/10.1021/acschembio.0c00093.
(92) Zhang, Q.; Tang, N.; Brock, J. W. C.; Mottaz, H. M.; Ames, J. M.; Baynes, J. W.; Smith, R. D.; Metz, T. O. Enrichment and Analysis of Nonenzymatically Glycated Peptides: Boronate Affinity Chromatography Coupled with Electron-Transfer Dissociation Mass Spectrometry. *J. Proteome Res.* **2007**, *6* (6), 2323–2330. https://doi.org/10.1021/pr070112q.
(93) Frolov, A.; Hoffmann, R. *Analysis of Amadori Peptides Enriched by Boronic Acid Affinity Chromatography*. *Annals of the New York Academy of Sciences* **2008**, *1126* (1), 253–256. https://doi.org/10.1196/annals.1433.060.
(94) Maksimovic, I.; Zheng, Q.; Trujillo, M. N.; Galligan, J. J.; David, Y. An Azidoribose Probe to Track Ketoamine Adducts in Histone Ribose Glycation. *J. Am. Chem. Soc.* **2020**, *142* (22), 9999–10007. https://doi.org/10.1021/jacs.0c01325.
(95) Sibbersen, C.; Palmfeldt, J.; Hansen, J.; Gregersen, N.; Jørgensen, K. A.; Johannsen, M. Development of a Chemical Probe for Identifying Protein Targets of α-Oxoaldehydes. *Chem. Commun.* **2013**, *49* (38), 4012. https://doi.org/10.1039/c3cc41099d.
(96) Sibbersen, C.; Schou Oxvig, A.-M.; Bisgaard Olesen, S.; Nielsen, C. B.; Galligan, J. J.; Jørgensen, K. A.; Palmfeldt, J.; Johannsen, M. Profiling of Methylglyoxal Blood Metabolism and Advanced Glycation End-Product Proteome Using a Chemical Probe. *ACS Chem. Biol.* **2018**, *13* (12), 3294–3305. https://doi.org/10.1021/acschembio.8b00732.
(97) Coukos, J. S.; Lee, C. W.; Pillai, K. S.; Liu, K. J.; Moellering, R. E. Widespread, Reversible Cysteine Modification by Methylglyoxal Regulates Metabolic Enzyme Function. *ACS Chem. Biol.* **2023**, *18* (1), 91–101. https://doi.org/10.1021/acschembio.2c00727.
(98) Chen, X.; Liu, Y.; Kong, L.; Wen, Z.; Wang, W.; Wang, C. Quantitative Chemoproteomic Profiling of Protein Cross-Links Induced by Methylglyoxal. *ACS Chem. Biol.* **2022**, *17* (8), 2010–2017. https://doi.org/10.1021/acschembio.2c00017.
(99) Gangadhariah, M. H.; Wang, B.; Linetsky, M.; Henning, C.; Spanneberg, R.; Glomb, M. A.; Nagaraj, R. H. Hydroimidazolone Modification of Human αA-Crystallin: Effect on the Chaperone Function and Protein Refolding Ability. *Biochimica et Biophysica Acta (BBA) - Molecular Basis of Disease* **2010**, *1802* (4), 432–441. https://doi.org/10.1016/j.bbadis.2010.01.010.
(100) Ahmed, N.; Argirov, O. K.; Minhas, H. S.; Cordeiro, C. A. A.; Thornalley, P. J. Assay of Advanced Glycation Endproducts (AGEs): Surveying AGEs by Chromatographic Assay with Derivatization by 6-Aminoquinolyl-N-Hydroxysuccinimidyl-Carbamate and Application to N∈-Carboxymethyl-Lysine- and N∈-(1-Carboxyethyl)Lysine-Modified Albumin. *Biochemical Journal* **2002**, *364* (1), 1–14. https://doi.org/10.1042/bj3640001.
(101) Di Sanzo, S.; Spengler, K.; Leheis, A.; Kirkpatrick, J. M.; Rändler, T. L.; Baldensperger, T.; Dau, T.; Henning, C.; Parca, L.; Marx, C.; Wang, Z.-Q.; Glomb, M. A.; Ori, A.; Heller, R. Mapping Protein Carboxymethylation Sites Provides Insights into Their Role in Proteostasis and Cell Proliferation. *Nat Commun* **2021**, *12* (1), 6743. https://doi.org/10.1038/s41467-021-26982-6.
(102) Greifenhagen, U.; Frolov, A.; Blüher, M.; Hoffmann, R. Site-Specific Analysis of Advanced Glycation End Products in Plasma Proteins of Type 2 Diabetes Mellitus

Patients. *Anal Bioanal Chem* **2016**, *408* (20), 5557–5566. https://doi.org/10.1007/s00216-016-9651-4.
(103) Zhang, Q.; Monroe, M. E.; Schepmoes, A. A.; Clauss, T. R. W.; Gritsenko, M. A.; Meng, D.; Petyuk, V. A.; Smith, R. D.; Metz, T. O. Comprehensive Identification of Glycated Peptides and Their Glycation Motifs in Plasma and Erythrocytes of Control and Diabetic Subjects. *J. Proteome Res.* **2011**, *10* (7), 3076–3088. https://doi.org/10.1021/pr200040j.
(104) Gomes, R. A.; Miranda, H. V.; Silva, M. S.; Graça, G.; Coelho, A. V.; Ferreira, A. E.; Cordeiro, C.; Freire, A. P. Yeast Protein Glycation *in Vivo* by Methylglyoxal: Molecular Modification of Glycolytic Enzymes and Heat Shock Proteins. *The FEBS Journal* **2006**, *273* (23), 5273–5287. https://doi.org/10.1111/j.1742-4658.2006.05520.x.
(105) Bilova, T.; Lukasheva, E.; Brauch, D.; Greifenhagen, U.; Paudel, G.; Tarakhovskaya, E.; Frolova, N.; Mittasch, J.; Balcke, G. U.; Tissier, A.; Osmolovskaya, N.; Vogt, T.; Wessjohann, L. A.; Birkemeyer, C.; Milkowski, C.; Frolov, A. A Snapshot of the Plant Glycated Proteome. *Journal of Biological Chemistry* **2016**, *291* (14), 7621–7636. https://doi.org/10.1074/jbc.M115.678581.
(106) Johansen, M. B.; Kiemer, L.; Brunak, S. Analysis and Prediction of Mammalian Protein Glycation. *Glycobiology* **2006**, *16* (9), 844–853. https://doi.org/10.1093/glycob/cwl009.
(107) Venkatraman, J.; Aggarwal, K.; Balaram, P. Helical Peptide Models for Protein Glycation: Proximity Effects in Catalysis of the Amadori Rearrangement. *Chemistry & Biology* **2001**, *8* (7), 611–625. https://doi.org/10.1016/S1074-5521(01)00036-9.
(108) Ito, S.; Nakahari, T.; Yamamoto, D. The Structural Feature Surrounding Glycated Lysine Residues in Human Hemoglobin. *Biomed. Res.* **2011**, *32* (3), 217–223. https://doi.org/10.2220/biomedres.32.217.
(109) Martin, M. S.; Bayaraa, N.; Fox, B. T.; Lin, Y.; Scheck, R. A. Predictable Modulation of a Spontaneous Post-translational Modification in Living Cells. *Angew Chem Int Ed* **2025**, *64* (39), e202512415. https://doi.org/10.1002/anie.202512415.
(110) Alt, N.; Schieberle, P. Model Studies on the Influence of High Hydrostatic Pressure on the Formation of Glycated Arginine Modifications at Elevated Temperatures. *J. Agric. Food Chem.* **2005**, *53* (14), 5789–5797. https://doi.org/10.1021/jf050615l.
(111) Martins, S. I. F. S.; Van Boekel, M. A. J. S. A Kinetic Model for the Glucose/Glycine Maillard Reaction Pathways. *Food Chemistry* **2005**, *90* (1–2), 257–269. https://doi.org/10.1016/j.foodchem.2004.04.006.
(112) Ronau, J. A.; Beckmann, J. F.; Hochstrasser, M. Substrate Specificity of the Ubiquitin and Ubl Proteases. *Cell Res* **2016**, *26* (4), 441–456. https://doi.org/10.1038/cr.2016.38.
(113) Renatus, M.; Parrado, S. G.; D'Arcy, A.; Eidhoff, U.; Gerhartz, B.; Hassiepen, U.; Pierrat, B.; Riedl, R.; Vinzenz, D.; Worpenberg, S.; Kroemer, M. Structural Basis of Ubiquitin Recognition by the Deubiquitinating Protease USP2. *Structure* **2006**, *14* (8), 1293–1302. https://doi.org/10.1016/j.str.2006.06.012.
(114) Burch, T. J.; Haas, A. L. Site-Directed Mutagenesis of Ubiquitin. Differential Roles for Arginine in the Interaction with Ubiquitin-Activating Enzyme. *Biochemistry* **1994**, *33* (23), 7300–7308. https://doi.org/10.1021/bi00189a035.
(115) Kozlov, G.; Nguyen, L.; Lin, T.; De Crescenzo, G.; Park, M.; Gehring, K. Structural Basis of Ubiquitin Recognition by the Ubiquitin-Associated (UBA) Domain of the Ubiquitin Ligase EDD. *Journal of Biological Chemistry* **2007**, *282* (49), 35787–35795. https://doi.org/10.1074/jbc.M705655200.

(116) Van Heijst, J. W. J.; Niessen, H. W. M.; Hoekman, K.; Schalkwijk, C. G. Advanced Glycation End Products in Human Cancer Tissues: Detection of N^{ε} -(Carboxymethyl)Lysine and Argpyrimidine. *Annals of the New York Academy of Sciences* **2005**, *1043* (1), 725–733. https://doi.org/10.1196/annals.1333.084.
(117) Nokin, M.-J.; Durieux, F.; Peixoto, P.; Chiavarina, B.; Peulen, O.; Blomme, A.; Turtoi, A.; Costanza, B.; Smargiasso, N.; Baiwir, D.; Scheijen, J. L.; Schalkwijk, C. G.; Leenders, J.; De Tullio, P.; Bianchi, E.; Thiry, M.; Uchida, K.; Spiegel, D. A.; Cochrane, J. R.; Hutton, C. A.; De Pauw, E.; Delvenne, P.; Belpomme, D.; Castronovo, V.; Bellahcène, A. Methylglyoxal, a Glycolysis Side-Product, Induces Hsp90 Glycation and YAP-Mediated Tumor Growth and Metastasis. *eLife* **2016**, *5*, e19375. https://doi.org/10.7554/eLife.19375.
(118) Kessel, L.; Kalinin, S.; Nagaraj, R. H.; Larsen, M.; Johansson, L. B.-Å. Time-Resolved and Steady-State Fluorescence Spectroscopic Studies of the Human Lens with Comparison to Argpyrimidine, Pentosidine and 3-OH-Kynurenine¶. *Photochem Photobiol* **2002**, *76* (5), 549. https://doi.org/10.1562/0031-8655(2002)076<0549:TRASSF>2.0.CO;2.
(119) Gakamsky, A.; Duncan, R. R.; Howarth, N. M.; Dhillon, B.; Buttenschön, K. K.; Daly, D. J.; Gakamsky, D. Tryptophan and Non-Tryptophan Fluorescence of the Eye Lens Proteins Provides Diagnostics of Cataract at the Molecular Level. *Sci Rep* **2017**, *7* (1), 40375. https://doi.org/10.1038/srep40375.
(120) Bhattacherjee, A.; Dhara, K.; Chakraborti, A. S. Argpyrimidine-Tagged Rutin-Encapsulated Biocompatible (Ethylene Glycol Dimers) Nanoparticles: Synthesis, Characterization and Evaluation for Targeted Drug Delivery. *International Journal of Pharmaceutics* **2016**, *509* (1–2), 507–517. https://doi.org/10.1016/j.ijpharm.2016.05.042.
(121) Sarkisyan, K. S.; Goryashchenko, A. S.; Lidsky, P. V.; Gorbachev, D. A.; Bozhanova, N. G.; Gorokhovatsky, A. Yu.; Pereverzeva, A. R.; Ryumina, A. P.; Zherdeva, V. V.; Savitsky, A. P.; Solntsev, K. M.; Bommarius, A. S.; Sharonov, G. V.; Lindquist, J. R.; Drobizhev, M.; Hughes, T. E.; Rebane, A.; Lukyanov, K. A.; Mishin, A. S. Green Fluorescent Protein with Anionic Tryptophan-Based Chromophore and Long Fluorescence Lifetime. *Biophysical Journal* **2015**, *109* (2), 380–389. https://doi.org/10.1016/j.bpj.2015.06.018.
(122) Alhujaily, M.; Abbas, H.; Xue, M.; De La Fuente, A.; Rabbani, N.; Thornalley, P. J. Studies of Glyoxalase 1-Linked Multidrug Resistance Reveal Glycolysis-Derived Reactive Metabolite, Methylglyoxal, Is a Common Contributor in Cancer Chemotherapy Targeting the Spliceosome. *Front. Oncol.* **2021**, *11*, 748698. https://doi.org/10.3389/fonc.2021.748698.
(123) Bierhaus, A.; Fleming, T.; Stoyanov, S.; Leffler, A.; Babes, A.; Neacsu, C.; Sauer, S. K.; Eberhardt, M.; Schnölzer, M.; Lasitschka, F.; Neuhuber, W. L.; Kichko, T. I.; Konrade, I.; Elvert, R.; Mier, W.; Pirags, V.; Lukic, I. K.; Morcos, M.; Dehmer, T.; Rabbani, N.; Thornalley, P. J.; Edelstein, D.; Nau, C.; Forbes, J.; Humpert, P. M.; Schwaninger, M.; Ziegler, D.; Stern, D. M.; Cooper, M. E.; Haberkorn, U.; Brownlee, M.; Reeh, P. W.; Nawroth, P. P. Methylglyoxal Modification of Nav1.8 Facilitates Nociceptive Neuron Firing and Causes Hyperalgesia in Diabetic Neuropathy. *Nat Med* **2012**, *18* (6), 926–933. https://doi.org/10.1038/nm.2750.
(124) Kim, J.; Kim, N. H.; Sohn, E.; Kim, C.-S.; Kim, J. S. Methylglyoxal Induces Cellular Damage by Increasing Argpyrimidine Accumulation and Oxidative DNA Damage in Human Lens Epithelial Cells. *Biochemical and Biophysical Research Communications* **2010**, *391* (1), 346–351. https://doi.org/10.1016/j.bbrc.2009.11.061.

(125) Antognelli, C.; Mezzasoma, L.; Mearini, E.; Talesa, V. N. Glyoxalase 1−419C>A Variant Is Associated with Oxidative Stress: Implications in Prostate Cancer Progression. *PLoS ONE* **2013**, *8* (9), e74014. https://doi.org/10.1371/journal.pone.0074014.
(126) Renard, B.-L.; Boucherle, B.; Maurin, B.; Molina, M.-C.; Norez, C.; Becq, F.; Décout, J.-L. An Expeditious Access to 5-Pyrimidinol Derivatives from Cyclic Methylglyoxal Diadducts, Formation of Argpyrimidines under Physiological Conditions and Discovery of New CFTR Inhibitors. *European Journal of Medicinal Chemistry* **2011**, *46* (5), 1935–1941. https://doi.org/10.1016/j.ejmech.2011.02.037.
(127) Kinoshita, S.; Mera, K.; Ichikawa, H.; Shimasaki, S.; Nagai, M.; Taga, Y.; Iijima, K.; Hattori, S.; Fujiwara, Y.; Shirakawa, J.; Nagai, R. N^{ω} -(Carboxymethyl)Arginine Is One of the Dominant Advanced Glycation End Products in Glycated Collagens and Mouse Tissues. *Oxidative Medicine and Cellular Longevity* **2019**, *2019*, 1–14. https://doi.org/10.1155/2019/9073451.
(128) Nagai, R.; Matsumoto, K.; Ling, X.; Suzuki, H.; Araki, T.; Horiuchi, S. Glycolaldehyde, a Reactive Intermediate for Advanced Glycation End Products, Plays an Important Role in the Generation of an Active Ligand for the Macrophage Scavenger Receptor. *Diabetes* **2000**, *49* (10), 1714–1723. https://doi.org/10.2337/diabetes.49.10.1714.
(129) Nemet, I.; Vikić-Topić, D.; Varga-Defterdarović, L. Spectroscopic Studies of Methylglyoxal in Water and Dimethylsulfoxide. *Bioorganic Chemistry* **2004**, *32* (6), 560–570. https://doi.org/10.1016/j.bioorg.2004.05.008.
(130) Riley, H. L.; Morley, J. F.; Friend, N. A. C. 255. Selenium Dioxide, a New Oxidising Agent. Part I. Its Reaction with Aldehydes and Ketones. *J. Chem. Soc.* **1932**, 1875. https://doi.org/10.1039/jr9320001875.
(131) Cannon, T. M.; Lagarto, J. L.; Dyer, B. T.; Garcia, E.; Kelly, D. J.; Peters, N. S.; Lyon, A. R.; French, P. M. W.; Dunsby, C. Characterization of NADH Fluorescence Properties under One-Photon Excitation with Respect to Temperature, pH, and Binding to Lactate Dehydrogenase. *OSA Continuum* **2021**, *4* (5), 1610. https://doi.org/10.1364/OSAC.423082.
(132) Oktaviani, N. A.; Pool, T. J.; Kamikubo, H.; Slager, J.; Scheek, R. M.; Kataoka, M.; Mulder, F. A. A. Comprehensive Determination of Protein Tyrosine pKa Values for Photoactive Yellow Protein Using Indirect 13C NMR Spectroscopy. *Biophysical Journal* **2012**, *102* (3), 579–586. https://doi.org/10.1016/j.bpj.2011.12.024.
(133) Harris, T. K.; Turner, G. J. Structural Basis of Perturbed pKa Values of Catalytic Groups in Enzyme Active Sites. *IUBMB Life* **2002**, *53* (2), 85–98. https://doi.org/10.1080/15216540211468.
(134) Aktaş, A. H.; Sanli, N.; Pekcan, G. Spectrometric Determination of pKa Values for Some Phenolic Compounds in Acetonitrile-Water Mixtures. *Acta Chimica Slovenica* **2006**, *53*, 214–218.
(135) Seyedsayamdost, M. R.; Reece, S. Y.; Nocera, D. G.; Stubbe, J. Mono-, Di-, Tri-, and Tetra-Substituted Fluorotyrosines: New Probes for Enzymes That Use Tyrosyl Radicals in Catalysis. *J. Am. Chem. Soc.* **2006**, *128* (5), 1569–1579. https://doi.org/10.1021/ja055926r.
(136) Wojciechowski, M.; Grycuk, T.; Antosiewicz, J. M.; Lesyng, B. Prediction of Secondary Ionization of the Phosphate Group in Phosphotyrosine Peptides. *Biophysical Journal* **2003**, *84* (2), 750–756. https://doi.org/10.1016/S0006-3495(03)74894-2.

(137) Martin, M. S.; Bayaraa, N.; Fox, B. T.; Lin, Y.-S.; Scheck, R. A. Predictable Modulation of a Spontaneous Post-Translational Modification in Living Cells. *Angew. Chem. Int. Ed.* **2025**. https://doi.org/10.1002/anie.202512415.
(138) Voigt, M.; Smuda, M.; Pfahler, C.; Glomb, M. A. Oxygen-Dependent Fragmentation Reactions during the Degradation of 1-Deoxy-d-Erythro-Hexo-2,3-Diulose. *J. Agric. Food Chem.* **2010**, *58* (9), 5685–5691. https://doi.org/10.1021/jf100140h.
(139) Glomb, M. A.; Henning, C. Formation of Reactive Fragmentation Products during the Maillard Degradation of Reducing Sugars − A Review. In *ACS Symposium Series*; Granvogl, M., Peterson, D., Schieberle, P., Eds.; American Chemical Society: Washington, DC, 2016; Vol. 1237, pp 117–131. https://doi.org/10.1021/bk-2016-1237.ch009.
(140) Thornalley, P. J.; Langborg, A.; Minhas, H. S. Formation of Glyoxal, Methylglyoxal and 3-Deoxyglucosone in the Glycation of Proteins by Glucose. *Biochem J* **1999**, *344 Pt 1* (Pt 1), 109–116.
(141) Jiang, L.; Althoff, E. A.; Clemente, F. R.; Doyle, L.; Röthlisberger, D.; Zanghellini, A.; Gallaher, J. L.; Betker, J. L.; Tanaka, F.; Barbas, C. F.; Hilvert, D.; Houk, K. N.; Stoddard, B. L.; Baker, D. De Novo Computational Design of Retro-Aldol Enzymes. *Science* **2008**, *319* (5868), 1387–1391. https://doi.org/10.1126/science.1152692.
(142) Romero-Rivera, A.; Garcia-Borràs, M.; Osuna, S. Role of Conformational Dynamics in the Evolution of Retro-Aldolase Activity. *ACS Catal.* **2017**, *7* (12), 8524–8532. https://doi.org/10.1021/acscatal.7b02954.
(143) De Raffele, D.; Martí, S.; Moliner, V. Understanding the Directed Evolution of De Novo Retro-Aldolases from QM/MM Studies. *ACS Catal.* **2020**, *10* (14), 7871–7883. https://doi.org/10.1021/acscatal.0c01165.
(144) Coukos, J. S.; Lee, C. W.; Pillai, K. S.; Shah, H.; Moellering, R. E. PARK7 Catalyzes Stereospecific Detoxification of Methylglyoxal Consistent with Glyoxalase and Not Deglycase Function. *Biochemistry* **2023**, *62* (21), 3126–3133. https://doi.org/10.1021/acs.biochem.3c00325.
(145) Chari, R. V.; Kozarich, J. W. Deuterium Isotope Effects on the Product Partitioning of Fluoromethylglyoxal by Glyoxalase I. Proof of a Proton Transfer Mechanism. *Journal of Biological Chemistry* **1981**, *256* (19), 9785–9788. https://doi.org/10.1016/S0021-9258(19)68690-4.
(146) Hall, S. S.; Doweyko, A. M.; Jordan, F. Glyoxalase I Enzyme Studies. 4. General Base Catalyzed Enediol Proton Transfer Rearrangement of Methyl- and Phenylglyoxalglutathionylhemithiol Acetal to S-Lactoyl- and S-Mandeloylglutathione Followed by Hydrolysis. A Model for the Glyoxalase Enzyme System. *J. Am. Chem. Soc.* **1978**, *100* (18), 5934–5939. https://doi.org/10.1021/ja00486a054.
(147) Ducker, G. S.; Rabinowitz, J. D. One-Carbon Metabolism in Health and Disease. *Cell Metabolism* **2017**, *25* (1), 27–42. https://doi.org/10.1016/j.cmet.2016.08.009.
(148) Pietzke, M.; Meiser, J.; Vazquez, A. Formate Metabolism in Health and Disease. *Molecular Metabolism* **2020**, *33*, 23–37. https://doi.org/10.1016/j.molmet.2019.05.012.
(149) Crossley, S. W. M.; Tenney, L.; Pham, V. N.; Xie, X.; Zhao, M. W.; Chang, C. J. A Transfer Hydrogenation Approach to Activity-Based Sensing of Formate in Living Cells. *J. Am. Chem. Soc.* **2024**, *146* (13), 8865–8876. https://doi.org/10.1021/jacs.3c09735.
(150) Koizumi, K.; Nakayama, M.; Zhu, W.-J.; Ito, S. Characteristic Effects of Methylglyoxal and Its Degraded Product Formate on Viability of Human Histiocytes: A Possible

Detoxification Pathway of Methylglyoxal. *Biochemical and Biophysical Research Communications* **2011**, *407* (2), 426–431. https://doi.org/10.1016/j.bbrc.2011.03.041.
(151) Kitamura, Y.; Kawase, M.; Ohmori, S. Formate Excretion in Urine of Rats Fed Dimethylaminoazobenzene-Rich Diets: The Possibility of Formate Formation from D-Lactate. Okayama University Medical School June 2008. https://doi.org/10.18926/AMO/30975.
(152) Nukaya, H.; Inaoka, Y.; Ishida, H.; Tsuji, K.; Suwa, Y.; Wakabayashi, K.; Kosuge, T. Modification of the Amino Group of Guanosine by Methylglyoxal and Other .ALPHA.-Ketoaldehydes in the Presence of Hydrogen Peroxide. *Chem. Pharm. Bull.* **1993**, *41* (4), 649–653. https://doi.org/10.1248/cpb.41.649.
(153) Nakayama, M.; Saito, K.; Sato, E.; Nakayama, K.; Terawaki, H.; Ito, S.; Kohno, M. Radical Generation by the Non-Enzymatic Reaction of Methylglyoxal and Hydrogen Peroxide. *Redox Report* **2007**, *12* (3), 125–133. https://doi.org/10.1179/135100007X200182.
(154) Argilés, J. M. The Oxidation of Methylglyoxal by Mammalian Pyruvate Dehydrogenase. *Archives of Biochemistry and Biophysics* **1989**, *273* (1), 238–244. https://doi.org/10.1016/0003-9861(89)90184-7.
(155) Watkins, N. G.; Neglia-Fisher, C. I.; Dyer, D. G.; Thorpe, S. R.; Baynes, J. W. Effect of Phosphate on the Kinetics and Specificity of Glycation of Protein. *Journal of Biological Chemistry* **1987**, *262* (15), 7207–7212. https://doi.org/10.1016/S0021-9258(18)48224-5.
(156) Li, X.-H.; Xie, J.-Z.; Jiang, X.; Lv, B.-L.; Cheng, X.-S.; Du, L.-L.; Zhang, J.-Y.; Wang, J.-Z.; Zhou, X.-W. Methylglyoxal Induces Tau Hyperphosphorylation via Promoting AGEs Formation. *Neuromol Med* **2012**, *14* (4), 338–348. https://doi.org/10.1007/s12017-012-8191-0.
(157) Patil, G.; Kulsange, S.; Kazi, R.; Chirmade, T.; Kale, V.; Mote, C.; Aswar, M.; Koratkar, S.; Agawane, S.; Kulkarni, M. Behavioral and Proteomic Studies Reveal Methylglyoxal Activate Pathways Associated with Alzheimer's Disease. *ACS Pharmacol. Transl. Sci.* **2023**, *6* (1), 65–75. https://doi.org/10.1021/acsptsci.2c00143.
(158) Miyata, S.; Miyazaki, H.; Liu, B.-F.; Fukunaga, M.; Hamada, Y.; Ueyama, S.; Muramoto, O.; Jiang, Q. Y.; Kusunoki, H.; Uriuhara, A.; Hirota, Y.; Kasuga, M. Activation of MAP Kinase Superfamily Signaling Pathways by Methylglyoxal. *International Congress Series* **2002**, *1245*, 87–89. https://doi.org/10.1016/S0531-5131(02)00913-5.
(159) Dafre, A. L.; Schmitz, A. E.; Maher, P. Methylglyoxal-Induced AMPK Activation Leads to Autophagic Degradation of Thioredoxin 1 and Glyoxalase 2 in HT22 Nerve Cells. *Free Radical Biology and Medicine* **2017**, *108*, 270–279. https://doi.org/10.1016/j.freeradbiomed.2017.03.028.
(160) Thornalley, P. J.; Yurek-George, A.; Argirov, O. K. Kinetics and Mechanism of the Reaction of Aminoguanidine with the α-Oxoaldehydes Glyoxal, Methylglyoxal, and 3-Deoxyglucosone under Physiological Conditions. *Biochemical Pharmacology* **2000**, *60* (1), 55–65. https://doi.org/10.1016/S0006-2952(00)00287-2.
(161) McLellan, A. C.; Thornalley, P. J. Synthesis and Chromatography of 1,2-Diamino-4,5-Dimethoxybenzene, 6,7-Dimethoxy-2-Methylquinoxaline and 6,7-Dimethoxy-2,3-Dimethylquinoxaline for Use in a Liquid Chromatographic Fluorimetric Assay of Methylglyoxal. *Analytica Chimica Acta* **1992**, *263* (1–2), 137–142. https://doi.org/10.1016/0003-2670(92)85435-9.

(162) Senavirathna, L.; Hasapes, C.; Chen, R.; Pan, S. Accumulation of Intracellular Protein Advanced Glycation End Products Alters Cellular Homeostasis for Protein Clearance in Pancreatic Ductal Epithelial Cells. *Biochemistry* **2024**, *63* (14), 1723–1729. https://doi.org/10.1021/acs.biochem.4c00250.
(163) Takata, T.; Sakasai-Sakai, A.; Ueda, T.; Takeuchi, M. Intracellular Toxic Advanced Glycation End-Products in Cardiomyocytes May Cause Cardiovascular Disease. *Sci Rep* **2019**, *9* (1), 2121. https://doi.org/10.1038/s41598-019-39202-5.
(164) Jeong, S.-R.; Lee, K.-W. Methylglyoxal-Derived Advanced Glycation End Product (AGE4)-Induced Apoptosis Leads to Mitochondrial Dysfunction and Endoplasmic Reticulum Stress through the RAGE/JNK Pathway in Kidney Cells. *IJMS* **2021**, *22* (12), 6530. https://doi.org/10.3390/ijms22126530.
(165) Fournet, M.; Bonté, F.; Desmoulière, A. Glycation Damage: A Possible Hub for Major Pathophysiological Disorders and Aging. *Aging and disease* **2018**, *9* (5), 880. https://doi.org/10.14336/AD.2017.1121.
(166) Zheng, L.; Boeren, S.; Liu, C.; Bakker, W.; Wang, H.; Rietjens, I. M. C. M.; Saccenti, E. Proteomics-Based Identification of Biomarkers Reflecting Endogenous and Exogenous Exposure to the Advanced Glycation End Product Precursor Methylglyoxal in SH-SY5Y Human Neuroblastoma Cells. *International Journal of Biological Macromolecules* **2024**, *272*, 132859. https://doi.org/10.1016/j.ijbiomac.2024.132859.
(167) Donnellan, L.; Young, C.; Simpson, B. S.; Acland, M.; Dhillon, V. S.; Costabile, M.; Fenech, M.; Hoffmann, P.; Deo, P. Proteomic Analysis of Methylglyoxal Modifications Reveals Susceptibility of Glycolytic Enzymes to Dicarbonyl Stress. *IJMS* **2022**, *23* (7), 3689. https://doi.org/10.3390/ijms23073689.
(168) Merigan, T. C.; Dreyer, W. J.; Berger, A. A Technique for the Specific Cleavage of Arginyl Bonds by Trypsin. *Biochimica et Biophysica Acta* **1962**, *62* (1), 122–131. https://doi.org/10.1016/0006-3002(62)90497-3.
(169) Huang, D. W.; Sherman, B. T.; Tan, Q.; Collins, J. R.; Alvord, W. G.; Roayaei, J.; Stephens, R.; Baseler, M. W.; Lane, H. C.; Lempicki, R. A. The DAVID Gene Functional Classification Tool: A Novel Biological Module-Centric Algorithm to Functionally Analyze Large Gene Lists. *Genome Biol* **2007**, *8* (9), R183. https://doi.org/10.1186/gb-2007-8-9-r183.
(170) Aguilan, J. T.; Kulej, K.; Sidoli, S. Guide for Protein Fold Change and *p* -Value Calculation for Non-Experts in Proteomics. *Mol. Omics* **2020**, *16* (6), 573–582. https://doi.org/10.1039/D0MO00087F.
(171) PhosphoSitePlus®. http://www.phosphosite.org/.
(172) Chang, W.; Gruber, D.; Chari, S.; Kitazawa, H.; Hamazumi, Y.; Hisanaga, S.; Bulinski, J. C. Phosphorylation of MAP4 Affects Microtubule Properties and Cell Cycle Progression. *Journal of Cell Science* **2001**, *114* (15), 2879–2887. https://doi.org/10.1242/jcs.114.15.2879.
(173) Chang, J.-K.; Ni, Y.; Han, L.; Sinnett-Smith, J.; Jacamo, R.; Rey, O.; Young, S. H.; Rozengurt, E. Protein Kinase D1 (PKD1) Phosphorylation on Ser203 by Type I P21-Activated Kinase (PAK) Regulates PKD1 Localization. *Journal of Biological Chemistry* **2017**, *292* (23), 9523–9539. https://doi.org/10.1074/jbc.M116.771394.
(174) Osma-Garcia, I. C.; Mouysset, M.; Capitan-Sobrino, D.; Aubert, Y.; Turner, M.; Diaz-Muñoz, M. D. The RNA Binding Proteins TIA1 and TIAL1 Promote Mcl1 mRNA

Translation to Protect Germinal Center Responses from Apoptosis. *Cell Mol Immunol* **2023**, *20* (9), 1063–1076. https://doi.org/10.1038/s41423-023-01063-4.
(175) Gu, L.; Fu, Y.; Li, X. Roles of Post-Translational Modifications of UHRF1 in Cancer. *Epigenetics & Chromatin* **2024**, *17* (1), 15. https://doi.org/10.1186/s13072-024-00540-y.
(176) Fu, Y.; Cao, T.; Zou, X.; Ye, Y.; Liu, Y.; Peng, Y.; Deng, T.; Yin, L.; Li, X. AKT1 Regulates UHRF1 Protein Stability and Promotes the Resistance to Abiraterone in Prostate Cancer. *Oncogenesis* **2023**, *12* (1), 1. https://doi.org/10.1038/s41389-022-00446-y.
(177) Geng, L.; Burrow, C. R.; Li, H.-P.; Wilson, P. D. Modification of the Composition of Polycystin-1 Multiprotein Complexes by Calcium and Tyrosine Phosphorylation. *Biochimica et Biophysica Acta (BBA) - Molecular Basis of Disease* **2000**, *1535* (1), 21–35. https://doi.org/10.1016/S0925-4439(00)00079-X.
(178) Li, H.-P.; Geng, L.; Burrow, C. R.; Wilson, P. D. Identification of Phosphorylation Sites in the PKD1-Encoded Protein C-Terminal Domain. *Biochemical and Biophysical Research Communications* **1999**, *259* (2), 356–363. https://doi.org/10.1006/bbrc.1999.0780.
(179) Streets, A.; Ong, A. Post-Translational Modifications of the Polycystin Proteins. *Cellular Signalling* **2020**, *72*, 109644. https://doi.org/10.1016/j.cellsig.2020.109644.
(180) Renzone, G.; Arena, S.; Scaloni, A. Proteomic Characterization of Intermediate and Advanced Glycation End-Products in Commercial Milk Samples. *Journal of Proteomics* **2015**, *117*, 12–23. https://doi.org/10.1016/j.jprot.2014.12.021.
(181) Mendes, N. P.; De Souza, E. C. G.; Juvanhol, L. L.; De Oliveira, L. L.; Alfenas, R. D. C. G. Fluorescent Advanced Glycation End Products Contents in Foods and Culinary Preparations. *Food and Humanity* **2025**, *4*, 100620. https://doi.org/10.1016/j.foohum.2025.100620.
(182) Liu, R.; Zhang, M.; Xu, L.; Liu, J.; Yang, P.; Li, M.; Qin, J. Fluorescent Advanced Glycation End Products in Type 2 Diabetes and Its Association with Diabetes Duration, Hemoglobin A1c, and Diabetic Complications. *Front. Nutr.* **2022**, *9*, 1083872. https://doi.org/10.3389/fnut.2022.1083872.
(183) Monnier, V. M.; Vishwanath, V.; Frank, K. E.; Elmets, C. A.; Dauchot, P.; Kohn, R. R. Relation between Complications of Type I Diabetes Mellitus and Collagen-Linked Fluorescence. *N Engl J Med* **1986**, *314* (7), 403–408. https://doi.org/10.1056/NEJM198602133140702.
(184) Cho, H.; Hong, N.-K.; Yong, I.; Kwon, H.-Y.; Kang, N.-Y.; Ciaramicoli, L. M.; Kim, P.; Chang, Y.-T. Development of a Specific Fluorescent Probe to Detect Advanced Glycation End Products (AGEs). *J. Mater. Chem. B* **2024**, *12* (25), 6155–6163. https://doi.org/10.1039/D4TB00590B.
(185) Wen, J.; Zhang, Q.; Zhou, L. Fluorescent Probes for Sensing and Visualizing Methylglyoxal: Progress, Challenges, and Perspectives. *RSC Adv.* **2024**, *14* (52), 38757–38777. https://doi.org/10.1039/D4RA07512A.
(186) Xu, H.; Liu, X.-R.; Cai, Z.-H.; Zheng, J.; Wang, Y.-W.; Peng, Y. Rapid Sensing and Imaging of Methylglyoxal in Living Cells Enabled by a Near-Infrared Fluorescent Probe. *Org. Biomol. Chem.* **2022**, *20* (23), 4782–4786. https://doi.org/10.1039/D2OB00698G.
(187) Wilker, S. C.; Chellan, P.; Arnold, B. M.; Nagaraj, R. H. Chromatographic Quantification of Argpyrimidine, a Methylglyoxal-Derived Product in Tissue Proteins: Comparison with Pentosidine. *Analytical Biochemistry* **2001**, *290* (2), 353–358. https://doi.org/10.1006/abio.2001.4992.

(188) Ross, J. A.; Jameson, D. M. Time-Resolved Methods in Biophysics. 8. Frequency Domain Fluorometry: Applications to Intrinsic Protein Fluorescence. *Photochem Photobiol Sci* **2008**, *7* (11), 1301–1312. https://doi.org/10.1039/b804450n.
(189) Fossum, C. J.; Johnson, B. O. V.; Golde, S. T.; Kielman, A. J.; Finke, B.; Smith, M. A.; Lowater, H. R.; Laatsch, B. F.; Bhattacharyya, S.; Hati, S. Insights into the Mechanism of Tryptophan Fluorescence Quenching Due to Synthetic Crowding Agents: A Combined Experimental and Computational Study. *ACS Omega* **2023**, *8* (47), 44820–44830. https://doi.org/10.1021/acsomega.3c06006.
(190) Yang, H.; Xiao, X.; Zhao, X.; Wu, Y. Intrinsic Fluorescence Spectra of Tryptophan, Tyrosine and Phenyloalanine; Lv, Y., Le, J., Chen, H., Wang, J., Shao, J., Eds.; Jinhua, Suzhou, Chengdu, Xi'an, Wuxi, China, 2017; p 102554M. https://doi.org/10.1117/12.2268397.
(191) Ishida, Y. I.; Kayama, T.; Kibune, Y.; Nishimoto, S.; Koike, S.; Suzuki, T.; Horiuchi, Y.; Miyashita, M.; Itokawa, M.; Arai, M.; Ogasawara, Y. Identification of an Argpyrimidine-Modified Protein in Human Red Blood Cells from Schizophrenic Patients: A Possible Biomarker for Diseases Involving Carbonyl Stress. *Biochemical and Biophysical Research Communications* **2017**, *493* (1), 573–577. https://doi.org/10.1016/j.bbrc.2017.08.150.
(192) Melhuish, W. H. QUANTUM EFFICIENCIES OF FLUORESCENCE OF ORGANIC SUBSTANCES: EFFECT OF SOLVENT AND CONCENTRATION OF THE FLUORESCENT SOLUTE[1]. *J. Phys. Chem.* **1961**, *65* (2), 229–235. https://doi.org/10.1021/j100820a009.
(193) A Guide to Recording Fluorescence Quantum Yields. https://static.horiba.com/fileadmin/Horiba/Application/Materials/Material_Research/Quantum_Dots/quantumyieldstrad.pdf (accessed 2026-02-19).